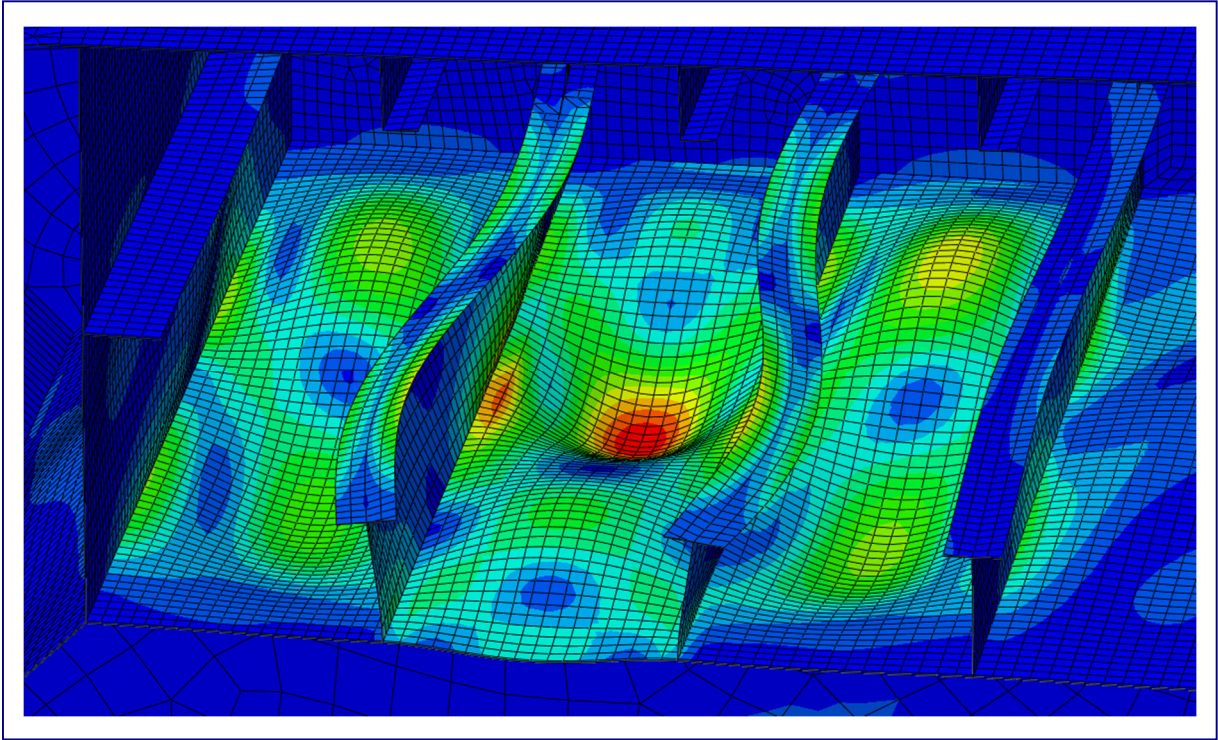# CHALMERS

Sloshing Impact Response in LNG Membrane Carriers

A response analysis of the hull structure supporting the membrane tanks

Master's Thesis in the International Master's Programme Naval Architecture and Ocean Engineering

ANDRÉ LILJEGREN AND OLA LINDAHL

Department of Shipping and Marine Technology
Division of Marine Technology
CHALMERS UNIVERSITY OF TECHNOLOGY
Gothenburg, Sweden 2015
Master's thesis 2015:X-15/329

MASTER'S THESIS IN THE INTERNATIONAL MASTER'S PROGRAMME IN
NAVAL ARCHITECTURE AND OCEAN ENGINEERING

Sloshing Impact Response in LNG Membrane Carriers

A response analysis of the hull structure supporting the membrane tanks

ANDRÉ LILJEGREN AND OLA LINDAHL

Department of Shipping and Marine Technology
Division of Marine Technology
CHALMERS UNIVERSITY OF TECHNOLOGY
Gothenburg, Sweden 2015

Sloshing Impact Response in LNG Membrane Carriers -

A response analysis of the hull structure supporting the membrane tanks
ANDRÉ LILJEGREN AND OLA LINDAHL

Cover:
Torsional deflection mode of the stiffeners in the inner deck structure giving rise to high dynamic amplification in response.

Sloshing Impact Response in LNG Membrane Carriers -
A response analysis of the hull structure supporting the membrane tanks
Master's Thesis in the International Master's Programme in Naval Architecture and
Ocean Engineering

ANDRÉ LILJEGREN AND OLA LINDAHL
Department of Shipping and Marine Technology
Division of Marine Technology
Chalmers University of Technology

ABSTRACT

The growing environmental awareness during recent years has led to a significant increase in the use of natural gas as a green energy supply. This, in turn, has increased the demand for transportation of *liquefied natural gas* (LNG) and therefore LNG carriers are growing in both size and numbers.

This master's thesis deals with a challenging design issue for LNG carriers with membrane type cargo tanks; the determination of structural response due to sloshing impact loads. These loads are characterized by very short durations and are thus likely to inflict a dynamic amplification in the response of the hull.

This thesis covers a study consisting of FE analyses performed on a model representing parts of an LNG membrane tank. The main objective was to find and quantify the *dynamic amplification factor* (DAF) for the structural response towards sloshing impact pressures. The influence of variations in the load characteristics such as load duration, extent of the loaded area, load location as well as the influence of the insulation system was evaluated. The analyses were performed using an explicit calculation scheme in the commercial finite element software ABAQUS.

The study shows that the response in the studied region of the hull structure experiences significant levels of dynamic amplification during impact loads with specific durations. This has been found especially pronounced for certain load locations due to their excitation of structural members in the inner deck structure. The outcome of the response sensitivity analysis also shows that the insulation system (MARK III type) used for containing the cargo has a large effect on the dynamic behaviour of the hull structure. It has been found to alter the magnitude of the stress and deflection response for key structural members. It also changes the load time durations for which the maximum dynamic amplification occurs and increases the magnitude of the corresponding response DAF.

It has been found that dynamic response, such as torsional deflection modes of the stiffeners and amplification effects from the insulation system, gives DAF values of up to 2. The effects have been found to be present for temporal load characteristics commonly occurring in sloshing model tests and full-scale measurements and are therefore likely to occur for a vessel in operation.

Key words: ABAQUS explicit, DAF, Dynamic amplification, Dynamic response, Impact loads, LNG membrane carriers, MARK III, Sloshing

Strukturrespons från impulslaster genererade av vätskan i LNG lastfartyg -
En responsanalys över den bärande skrovstrukturen i membrantankarna
Examensarbete inom mastersprogrammet Naval Architecture and Ocean Engineering

ANDRÉ LILJEGREN OCH OLA LINDAHL
Institutionen för Sjöfart och marin teknik
Avdelningen för Marin teknik
Chalmers tekniska högskola

SAMMANFATTNING

De senaste årens växande miljömedvetenhet har lett till en betydande ökning av användningen av natur gas bland annat för energi produktion. Detta har i sin tur ökat efterfrågan på transporter av *natur gas i flytande form* (LNG) och tankfartyg för LNG växer i både storlek och antal.

Detta examensarbete handlar om ett utmanande designproblem för LNG-fartyg utrustade med membrantankar; beräkning av strukturresponsen på grund av impulslaster som kan uppstå när den fria vätskeytan slår emot den omgivande tankstrukturen. Dessa laster är karaktäriserade av mycket kort tidsvarighet och kan därför ge upphov till dynamisk förstärkning av responsen i skrovstrukturen.

Avhandlingen presenterar en studie bestående av FE-analyser utförda på en modell som representerar delar av en LNG-membrantank. Huvudmålet var att hitta och kvantifiera den dynamiska förstärkningsfaktorn i skrovrespons mot impulstrycklaster. Påverkan av variationer i lastegenskaper såsom, varaktighet, storlek på lastområdet och positionen av den pålagda lasten samt påverkan från isolationssystemet är utvärderade. Analyserna har utförts med explicit beräkningsmetod i den kommersiella mjukvaran ABAQUS.

Studien påvisar att responsen i den studerade skrovstrukturen upplever en betydande nivå av dynamisk amplifikation då den utsätts för impulslaster med vissa specifika pulslängder. Detta har noterats som speciellt framträdande för specifika lastpositioner som har visat sig ge upphov till excitation av strukturelement i den inre däckstruckturen. Studien av responskänsligheten visar också att isolationssystemet (av typ MARK III) i tanken har en stor påverkan på det dynamiska beteendet för skrovstrukturen. Det har observerats att storleken på spänningar och deflektioner i de studerade strukturelementen ändras vid introduktionen av isolationssystemet. De tidsintervall som gett upphov till de maximala dynamiska förstärkningarna i dessa strukturvar ändras också. Vidare ökar även storleken på den dynamiska förstärkningsfaktorn.

Slutsatsen från analyserna är att dynamiska fenomen så som vridning av longitudinella styvare och förstärkning av struktursvaret i skrovet från isolationssystemet kan ge upphov till en dynamisk förstärkningsfaktor av magnitud 2. Dessa effekter har visat sig inträffa för last-tidsvarigheter vanligt förekommande i modellförsök och fullskalemätningar och kommer därför även troligen uppkomma för fartyg i användning.

Nyckelord: ABAQUS Explicit, Dynamisk förstärkning, Dynamisk förstärkningsfaktor Dynamisk respons, Impulslaster, LNG-membranfartyg, MARK III, Vätskelaster

Contents

Preface

This thesis is a part of the requirements for the master's degree in Naval Architecture at Chalmers University of Technology, Gothenburg, and has been carried out at the Division of Marine Technology, Department of Shipping and Marine Technology, Chalmers University of Technology in cooperation with DNV GL, Division of Tanker and Dry Cargo, in Høvik, Norway.

We would like to acknowledge all the people around us that have contributed with support, guidance and effort in order to make this thesis possible. We would especially like to thank the following persons:

Carl-Johan Åkerström for helping us in establishing a contact with DNV GL and for taking good care of us during our stay in Oslo;

Sverre Olav Bergli for allowing us to conduct our thesis at the department hull approval, tanker and dry cargo, within DNV GL. We would also like to express our gratitude for the financial support for accommodation, which was highly appreciated:

our supervisor at DNV GL, Magnus Lindgren, for his dedication to the project, his technical expertise, and his guidance throughout the whole project;

our co-supervisor at DNV GL, Tom Klungseth Østvold, for important input and his knowledge within the topic, which has been very helpful in the project;

our supervisor and examiner, Professor Jonas Ringsberg, for his excellent guidance and support during the project and for taking on the responsibility as supervisor.

Gothenburg, June, 2015

André Liljegren and Ola Lindahl

Due to confidentiality, references to drawings used in the thesis and absolute values of stresses and displacement cannot be displayed. Questions regarding this information can be answered by Magnus Lindgren at DNV GL Høvik, Norway. Contact information as per below:

Email: Magnus.Lindgren@dnvgl.com

Phone: +47 67579900

Abbreviations

CCS   Cargo Containment System
DAF   Dynamic Amplification Factor
FE   Finite Element
FLNG   Floating Liquefied Natural Gas facility
GM   Metacentric height
LC   Load case
LNG   Liquefied Natural Gas
RAO   Response Amplitude Operator

Company names

DNV GL   DNV GL classification society
GTT   Gaztranport et Technigaz

1 Introduction

This chapter presents the background and objectives of the thesis. A brief overview of the methodology and limitations of the work are also presented followed by the outline of the thesis.

1.1 Background and motivation of work

Due to an increased environmental awareness together with more stringent regulations regarding emissions the use of alternative energy solutions and fuels are gaining ground. Natural gas has become one of the most prominent of such energy sources and the need for transporting it has steadily increased during recent years. To meet this demand a large number of *liquefied natural gas* (LNG) carriers have been built, mainly with membrane-type cargo tanks. This vessel type will be gone through more extensively in Chapter 2.1. One of the challenging design issues for these systems is related to the determination of sloshing impact loads in the tanks and its relation to the structural response of the hull. The reason for this is that these loads are dependent on many different physical effects, giving them a stochastic nature. The work of Malencia and Kwon (2013) points out that gas cushion, liquid compressibility, gas boil-off and hydroelasticity are examples of such effects.

It has become more and more important to get an accurate estimation of sloshing impact loads and their effect on the hull structure. This is due to the fact that the ships being built are growing in size and that their operational requirements are becoming increasingly demanding (Pastoor et al., 2005). Previously, the typical LNG carrier was in the size of 140 000 m^3, while in later years sizes up to 260 000 m^3 have been built. Furthermore, restrictions have previously limited the allowable filling levels in the cargo tanks to be either close to full or close to empty. The relocations of loading and discharging sites to more weather exposed locations are increasing and the coming use of *floating liquefied natural gas facilities* (FLNG) is contributing to a growing need to operate with partial filling levels. This may introduce very violent sloshing phenomena inducing high loads on both the *cargo containment system* (CCS) and the supporting ship structure (Malencia and Kwon, 2013). Therefore, the industry has increased its focus on sloshing impact loads and the issues connected to it.

The current design methods are to a large extent dependent on input from model tests (DNV, 2014). Tanks in model scale are subjected to motions in order to induce the sloshing that is expected for the full-scale tank in operation. Pressure sensors are arranged in clusters inside the model tanks in locations where sloshing loads are considered as frequently occurring. The measured loads are then recorded and used for setting up long-term load distributions, which in turn form the base for calculating design loads with extreme prediction methods (DNV, 2014). The test procedures are highly advanced and aim at ensuring that the experienced loads are within the limit of the strength of the CCS. They are a result of extensive development and are today the most reliable input in terms of estimating the loads, which is why they are utilized as input for hull design loads as well.

To compensate for the model scale the measured pressures needs scaling to be representative for the full-scale design. Within the used scaling methods there are, however, some uncertainties. These originate from the random nature of sloshing loads and natural limitations in the experimental setup. One of these natural limitations is that LNG is not feasible to conduct model tests with and therefore water is most commonly used instead. Another example is that the local effects, such as the

formation of entrapped gas pockets, have been found troublesome to scale in an accurate manner, which is described by Lafeber et al. (2012) and Bogaert et al. (2010a). Furthermore, the model tanks used can be considered rigid, making the hydroelastic effects that are expected in a real cargo tank hard to account for (Malencia and Kwon, 2013). Finally, it should be noted that the characteristics of the full-scale sloshing loads are highly dependent on the density ratio between liquid and gas in the tank. Expected load durations have been found especially affected by this factor, which is pointed out by Lee et al. (2006). The differences in liquid media used in the model tests compared to LNG do thus add uncertainties to the loads acquired from these tests.

Another issue with being reliant on model tests for the hull design is that this approach requires a significant engineering effort and is very time-consuming. This gives rise to the need for simplifying the design criteria currently in use. DNV GL is a large actor in the work of developing procedures more easy to use for the designers, based on acquired knowledge from model tests, full-scale measurements and other analyses. This thesis is thought to provide support for this process.

The stochastic nature of measured loads and the uncertainty of measurements demands further investigation of how sensitive the structures subjected to sloshing loads are to load parameter variations. Extensive investigations regarding the structural response of the insulation system in membrane tanks and how it is influenced by such load variations have been made. The strength of the insulation is lot less than that of its supporting structural members and thus considered the primary structural issue when it comes to local response. Local effects on the hull structure will nevertheless be present (Graczyk, 2008). Therefore, the hull structure's sensitivity towards the temporal and spatial variations that are connected to sloshing loads should be taken into consideration when designing the hull. This is the major underlying motivation for the work presented in this thesis.

Sloshing impact loads are highly dynamic scenarios with very short load durations. Structures exposed to dynamic loadings with load durations that are in the order of the structure's natural period are likely to experience a dynamic amplification in the structural response depending on the characteristics of the load (Graczyk, 2008). Such amplifications from a dynamic load can lead to significant increases, up to a theoretical factor of a maximum of two, in the structural response compared to a corresponding static load (Biggs, 1964). This amplification factor in response due to dynamic loads is denoted *dynamic amplification factor* (DAF). Previously performed dynamic analyses of stiffened steel plate structures are made by Tavakoli and Kiakojouri (2013). The structure analysed in their work is similar to the ones commonly used in ship deck structures and it was found that the structure's natural periods were in the order of a few milliseconds. These natural periods coincide fairly well with the most commonly occurring load durations of sloshing impacts based on model tests (Graczyk and Moan, 2008; DNV GL, 2015). This gives reasons to believe that impact loadings from sloshing occurrences may induce dynamic amplification in the supporting hull structure, which possibly could be of significance for its design. A large focus in this thesis has therefore been put into how the response of the supporting hull structure is affected by temporal variations in impact loadings.

1.2 Objectives and scope of work

The main objective is to quantify the dynamic amplification factors, of the structural response in the hull, which are expected to occur due to sloshing impact loads in cargo tanks on LNG membrane carriers. This is to be done by numerically evaluating the response sensitivity against temporal and spatial variations in impact load characteristics for a reference vessel.

The scope of work consists of the following:

- Developing a model representing parts of a LNG membrane tank, where sloshing impacts are likely to occur. The model will be based on realistic ship design with basis in a 175 000 m^3 LNG membrane carrier.
- Identifying critical structural members of the hull structure with regard to structural response in terms of stress and deflection, when subjected to representative sloshing impact loads.
- Evaluating the stress and deflection sensitivity towards temporal and spatial properties of impact loadings for the identified structural members.
  - o Determining the influence from load location for a range of relevant load durations.
  - o Determining the influence from load extent for a range of relevant load durations.
  - o Determining the influence from the cargo containment system for a range of relevant load durations.

1.3 Methodology

The *finite element* (FE) software ABAQUS (Dassault systèmes, 2014) is utilized to numerically asses the structural response towards dynamic impact loads. The methodology used in this numerical study can be illustrated by the workflow presented in Figure 1.1. The analyses are based on a discretised FE model representing the geometrical and structural properties corresponding to parts of the hull structure supporting the membrane tanks. Loads are determined and applied to the model for each set of analyses. The desired output data from the FE analyses is extracted through post processing in order to evaluate the results. The method utilized for each of the presented analyses steps is described in the following.
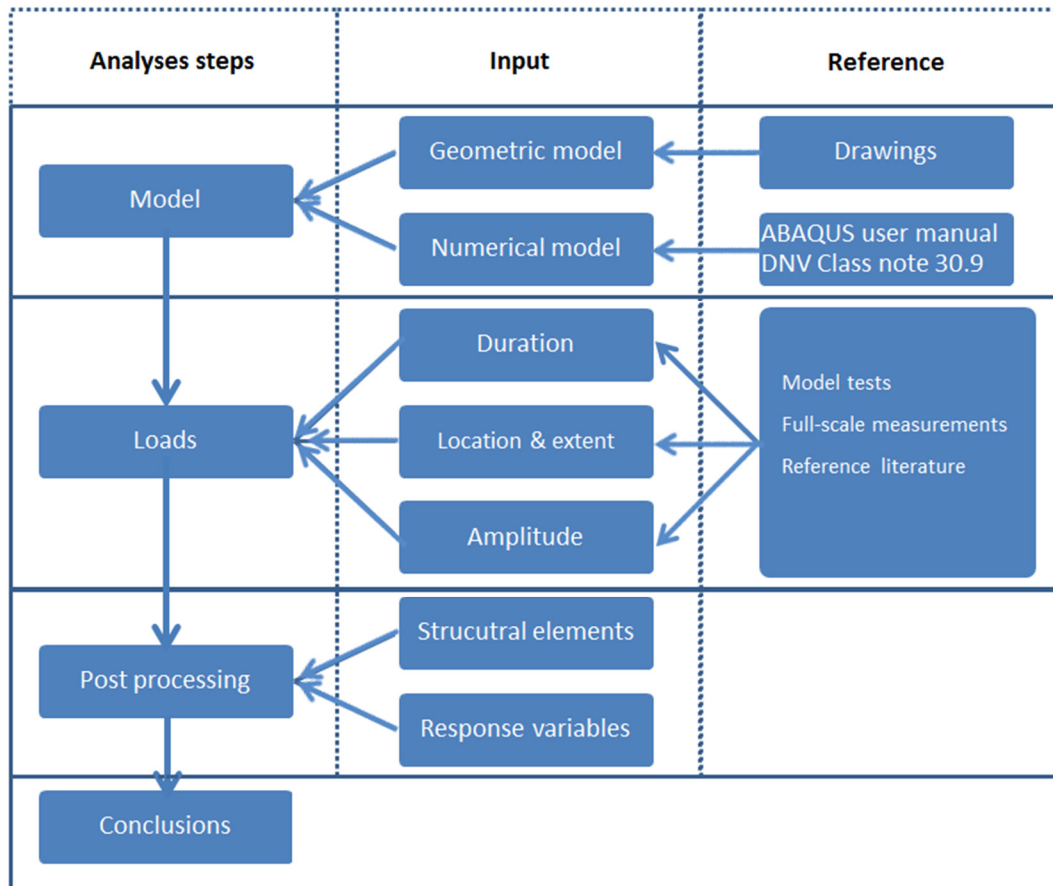

Figure 1.1   Schematic workflow.

Drawings from a classification approval of a typical LNG membrane carrier with a cargo capacity of approximately 175 000 m^3 form the basis of the FE model geometry. The geometry under consideration represents a section of the hull structure supporting a cargo hold, at a location prone to sloshing impact. DNV class note 30.9 is used as support in the modelling (DNV, 2014).

A series of explicit, linear dynamic FE-analyses for different load cases is performed using the FE model. The studied load cases correspond to a variety of impulse pressure loads with different combinations of load duration, location and extent. Experimental data is used as reference for the choice of the considered load parameters. The experimental data under consideration is mainly acquired from the documentations of sloshing model tests performed by the company *Gaztranport et Technigaz* (GTT). Report material from full-scale sloshing measurements on an LNG carrier performed by DNV GL and other actors is also considered (DNV GL, 2015).

The maximum structural response for each of the studied load cases is extracted from the FE output data in the post processing. The structural responses that are considered correspond to von Mises stress and deflection components in the stiffened inner deck structure. The dynamic response behaviour is also visually studied in the ABAQUS graphical interface.

1.4 Limitations

The limitations of the scope of this master's thesis are as follows:

- Only one ship-specific design of the hull structure supporting the membrane tank is evaluated.
- The structural response assessment is limited to one tank location in the aftmost located tank of a studied reference vessel. The studied region represents a location especially prone to experiencing sloshing impacts. The aftmost located tank also has a design that is relatively consistent among similar vessels.
- Structural details such as welds and cut-outs are not included in the FE models.
- Only linear elastic material behaviour is considered throughout the study; material plasticity and effects like strain hardening are not accounted for.
- Geometric nonlinearity and non-linear contact formulations are not considered in the numerical analyses.
- Only local loadings from sloshing impacts are addressed. Global loads such as hull girder bending moments and hydrostatic pressures within the tanks are not taken into consideration.
- The choice of load location and area extent is based on documentation from previously performed sloshing model tests and full-scale measurements held by DNV GL. Due to the confidentiality of these reports only limited data can be published in this thesis.

1.5 Outline of thesis

Chapter 2 presents a brief summary of sloshing in LNG membrane carriers. In Chapter 3 the specifics regarding the FE model for the load parameter study is presented, followed by Chapter 4 with the specifics regarding the FE model for the cargo containment system influence study. The achieved results are subsequently presented and discussed in Chapter 5. Conclusions and recommendations for future work are presented in in Chapters 6 and 7, respectively.

2 Sloshing of LNG-cargo

This chapter provides a summary of sloshing loads and why LNG membrane carriers are especially prone to experiencing these loads compared to vessels carrying other liquids. It introduces the fundamentals regarding the problem at hand and provides an overview of the complex nature of the sloshing phenomena.

2.1 LNG membrane carriers

There are different types of LNG carriers in use, the one under consideration in this master's thesis is the type with membrane cargo tanks. The most common design of these vessels has 4 cargo compartments over the length, which is illustrated in Figure 2.1. The cargo tanks are separated by two transverse bulkheads and a cofferdam in between.
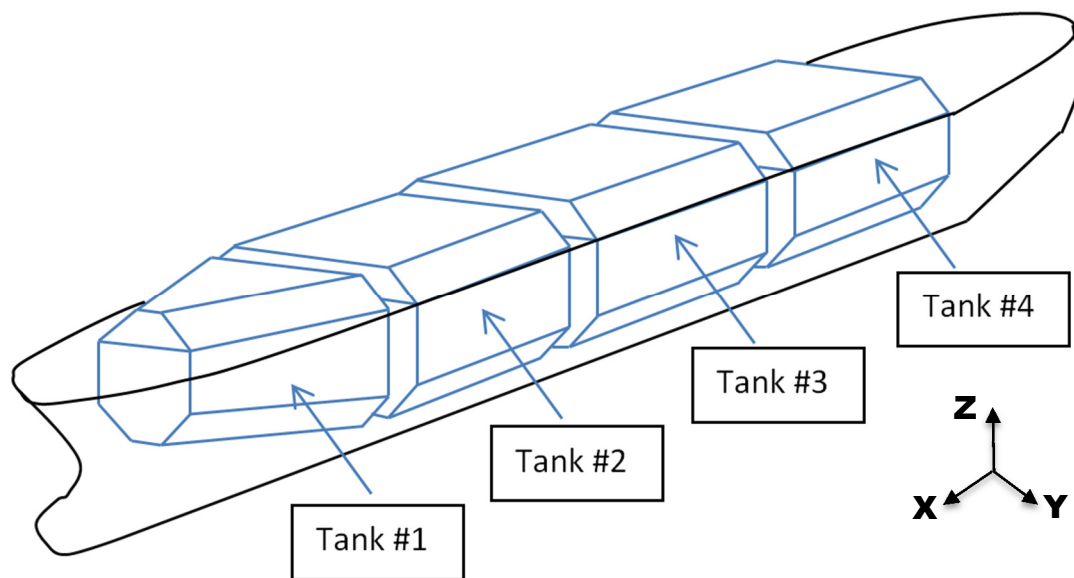

Figure 2.1   Tank arrangement and numbering of a typical LNG membrane tank carrier.

An example of a 4 tank LNG membrane carrier is presented in Figure 2.2. The upper parts of the tanks are visible in the figure, rising above the main deck.

Figure 2.2   Typical LNG membrane carrier, courtesy of DNV GL.

The tanks usually span over the greater part of the breadth of the vessel and have chamfered side structures at the top and bottom, see Figure 2.3. Typical dimensions are 40 m wide, 40-50 m long and 30 m high. Tank number 1 or the forward tank is typically smaller and has a different cross section compared to the other tanks.
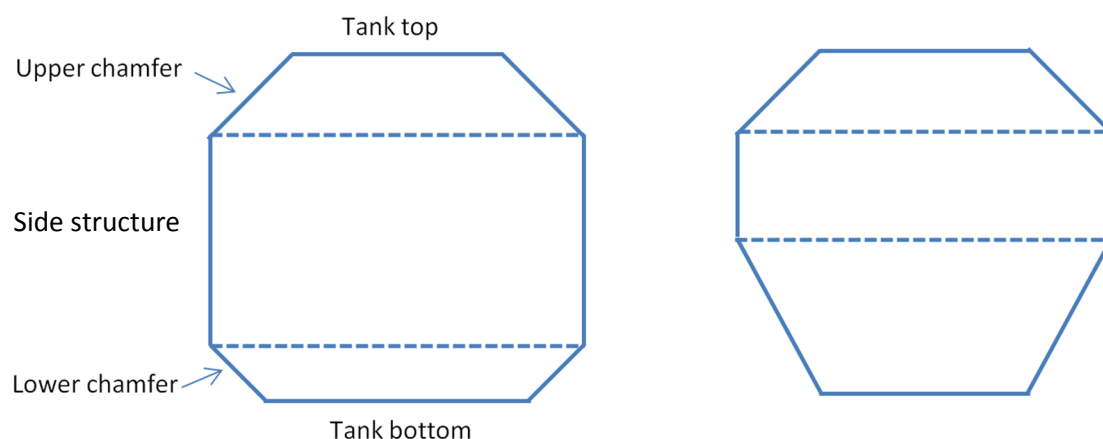

Figure 2.3   Principle outlines of typical LNG membrane tank cross sections. The left cross section is typical for tank number 2-4 and the right- hand tank cross section is typical for tank number 1.

The boiling temperature of natural gas is -163° Celsius. To maintain the gas temperature below the boiling point and thereby keeping the gas in its liquefied state, the compartments have to be heat insulated. This is done by different kinds of insulation panels that limit the gas boil-off and avoids the hull structure to be cooled down by the cargo. The reason that contact between the cargo and the hull is undesired is that the steel hull will become very brittle and experience thermal stresses if exposed to low temperatures. The membranes serve as barriers and isolate the liquid from the hull. The membranes and insulation panels make up the so-called *cargo containment system*, which hereafter is referred to as the CCS.

The two most common types of CCS are the Mark III and NO96 systems, both of which are designed and manufactured by GTT. Mark III consists of a primary

membrane made out of corrugated plates in stainless steel and a secondary membrane made of a composite laminated material. The membranes are separated from each other and the hull by loadbearing insulation panels made of reinforced polyurethane foam (GTT, 2012a). NO96 is built up somewhat differently and consists of two identical invar (nickel-steel alloy) membranes. The membrane closest to the cargo acts as the primary barrier and the outer one is fitted for redundancy reasons. They are composed of non-corrugated and continuous strakes giving a flat inner surface with the exception of the sheet joints. The membranes are separated from each other and the hull by loadbearing plywood boxes. In the NO96 the insulation boxes are filled with thermally insulating expanded perlite (GTT, 2012b).

As stated in Chapter 1.1 a major design issue for the LNG membrane vessels and their CCS are sloshing loads. These loads are not unique to LNG carriers but are more or less evident for most vessels transporting cargo in liquid form. However, for the greater part of other liquid cargo carriers there are more means of limiting the sloshing phenomena. An example is the tanks in oil carriers, where there usually are wash bulkheads fitted limiting the free surface motion. A higher degree of cargo compartmentalization and pressure-filled holds are other ways of reducing or eliminating the sloshing effects. For the membrane type LNG carriers the properties of the design and cargo puts restrictions on such possibilities. The structural composition of the tank wall does not allow for any internal bulkheads to be fitted. This is partly because the CCS is too weak to support such structural members and partly because any non-isolated connections to the hull would lead to significant heat conduction and large stresses form temperature gradients. Due to the complex and costly CCS and increased cargo capacity, fewer compartments are economically advantageous; see Graczyk (2008). Since the cargo will unavoidably suffer from continues gas boil-off, a free liquid surface will always be present in the tank. All in all, the resulting large free liquid surfaces in LNG membrane tanks make them prone to experiencing severe sloshing phenomena.

A parametric analysis aimed at investigating potential relations between sloshing design pressures acquired from model test and ship specifics parameters of LNG membrane carriers has been performed as part of the project. The study and the conclusions drawn are presented in Appendix A of this thesis.

2.2 Sloshing loads

Sloshing loads is a common term for the loads occurring in enclosed compartments containing liquids as a result of the relative motions between the free surface of the liquid and the corresponding tank. This chapter provides a summary of these loads and their characteristics.

2.2.1 Load types and load locations

There are several types of sloshing scenarios with very different load characteristics. DNV GL categorises the design loads from the moving liquids in tanks into sloshing pressures and impact pressures, respectively; see DNV (2015). A common factor for all types of sloshing occurrences is that they are dependent on the filling level of the tank together with the vessel's motions.

The sloshing pressures are dynamic pressure loads that arise from standing waves in the cargo tanks (DNV, 2014). Depending on elevation of the wave these loads can be treated as more or less global, effecting large portions of the tank. The load period is represented by the period of the standing wave and is thus governed by the resonance

behaviour of the liquid surface. This means that a partially filled tank that is put into motion will continually be exposed to these loads. The resonance period depends on the tank geometry and filling level and is normally in the order of several seconds. The pressures exerted on the containment system are approximately in the same magnitude as the hydrostatic pressures based on the instantaneous wave elevation (DNV, 2014).

The impact pressures are caused by the fluid surface impacting on the containment system at high velocities (DNV, 2014). This means that load duration for each event is very short, usually in the order of a few milliseconds (Graczyk and Moan, 2008; DNV GL, 2015). Contrary to sloshing pressures, the impact loads are also in many cases localized phenomena. This means that the affected area during a sloshing impact event is rather limited in extent. The violent nature of the event can, however, produce very high pressure peaks on the containment system (DNV GL, 2015). The severity of these loads depends on numerous factors, such as impact angle, impact velocity, the formation of gas pockets etc. (Malencia and Kwon, 2013). Therefore severe sloshing impacts can only be expected to occur on an occasional basis.

Different types of impacts can occur depending on the filling level and motion of the vessel. A couple of different cases can be identified as typically severe. For higher levels of filling in combination with quartering to head seas, the tank roof will be likely to frequently suffer from sloshing impacts. This is due to diagonal resonance of waves in the cargo impacting on the area around the corner where the transverse bulkhead, tank top and the chamfer meet, see Figure 2.4. For filling levels below 90 % down to the lower termination of the upper chamfer, sloshing will typically occur in the region where the upper chamfer meets the roof and the vertical part of the tank side. In conditions with low filling levels the impacts are most likely to occur as breaking waves impacting on the structure. A very severe case of this phenomenon is called hydraulic jump or travelling bore and can affect large portions of the tank. This is characterized by a change in free surface level travelling at high speed and hitting the longitudinal or transverse bulkhead (DNV, 2014), see Figure 2.5.
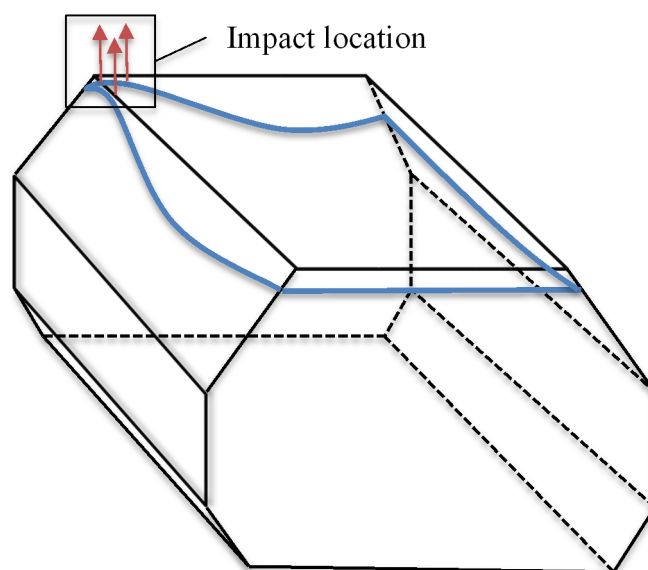

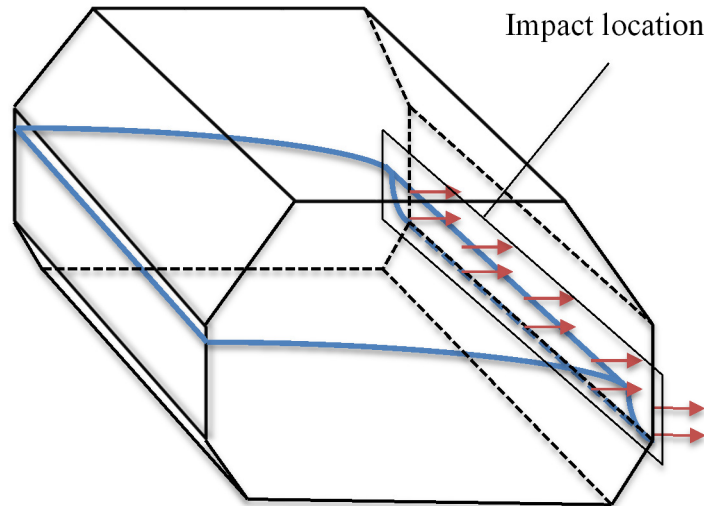*Figure 2.4   Schematic illustration of a typical sloshing event at high filling levels.*

Figure 2.5   Schematic illustration of a hydraulic jump or travelling bore hitting the side structure.

2.2.2 Characteristics for sloshing impacts at high filling levels

As mentioned in Chapter 1.1, the properties of sloshing impacts depend on many physical phenomena giving them a very stochastic nature. So far, the most utilized method for the determination of these loads in LNG membrane tanks is by using model tests. Some full-scale tests and measurements have also been conducted. In the following, findings regarding the load characteristics for sloshing impacts are presented. The focus lies on the sloshing impacts occurring at high filling levels.

A common issue for sloshing model tests and full-scale measurements is that the possibility to pinpoint the exact pressure distribution is rather limited since the pressure sensors have a finite spacing (ABS, 2006; DNV 2014). This makes the measurable footprints of the pressure distribution limited to interpolation between measurement points. A clear trend in the relationship between the averaged pressure magnitude and the extent of the tank that the load acts upon can, however, be found (DNV GL, 2015). For impacts occurring in the corners of the tank roof the averaged magnitudes decrease quickly with the load extent. This indicates that the highest registered pressure peaks are very limited in size. For this reason, CCS design pressures acquired from model are usually presented as average pressures over a range of area extents (DNV, 2014).

Sloshing impacts are characterized by load pulses with very short load durations. Their temporal characteristics are usually described in terms of rise times. The rise time is a measure of the time it takes for the pressure pulse to reach its peak from the point of exceeding a threshold pressure, see Figure 2.6. Model tests for determining the design pressures regarding the CCS have shown that frequently occurring rise times for sloshing impacts range between approximately 0.5-3.5 ms (DNV GL, 2015). The work done by Graczyk and Moan (2008) has also shown that the most commonly occurring impact rise time is approximately 1 ms.
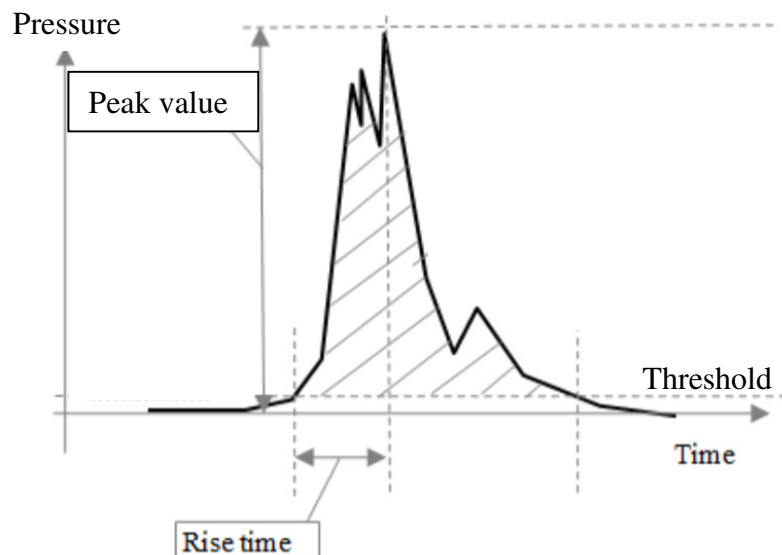
Figure 2.6   Schematic illustration of a typical sloshing impact pulse, retrieved and modified with permission from DNV (2014).

The ratio between rise time and total load duration for sloshing impacts varies a lot due to the stochastic nature of sloshing impacts. The formation of air pockets during impacts is a phenomenon that greatly contributes to the large spread. Boagert et al. (2010b) have found this phenomenon to be very pronounced for containment systems of the Mark III type, due to their dense corrugations of the primary membranes. Experimental model tests have, however, shown that the load rise time is less than half the duration for most of the severe sloshing impact occurrences giving a skewed load pulse with a shorter rise time than decay time (Graczyk et al., 2007).

The magnitude of the sloshing impact pressures tends to vary greatly depending on the location of the impact. Closer to the transverse bulkhead and the chamfer the impact is more violent and generates high pressures with a rapidly decreasing magnitude the further away from the vertical boundaries of the tank they act (Graczyk and Moan, 2008). This claim has been strengthened by both sloshing model tests and full-scale measurements of a vessel in operation. In the full-scale measurements pressure peaks of approximately 1 MPa where found to occur close to the corner of the tank ceiling and 0.2 MPa at a slight distance away from the corner (DNV GL, 2015).

3 FE model for load parameter influence study

As described in Chapter 1.2 this thesis aims at investigating the dynamic response in the supporting hull structure of an LNG membrane tank due to sloshing impact loads. The sensitivity towards changes in load parameters are analysed numerically with an FE model representing a local part of the tank structure. The tank under investigation is tank number 4 in an LNG membrane carrier. Tank number 4 has shown to be one of the most sloshing-exposed tanks and has a geometry that is similar among existing ships (DNV GL, 2015).

Previous studies have shown that a region frequently exposed to sloshing impacts is the upper corners where the chamfer meets the tank top (DNV, 2014). An example of the sloshing impacts in this region is presented in Chapter 2.2.1, Figure 2.4. Therefore, the model is chosen to represent this region.

3.1 Geometric extent

The model used in this sensitivity study represents a part of the hull structure surrounding the membrane tank. The modelled part is located in a region corresponding to the forward, upper parts of the tank. In the transverse direction the model is limited to the port side only. The span in the longitudinal direction is taken from the aft transverse bulkhead at the border of tank number 3 to the fourth web frame from the forward bulkhead in tank number 4. The full longitudinal span of the cofferdam and the transverse bulkheads of tanks 3 and 4 are included in the model. An overview of the global position of the model and the extent is illustrated in Figure 3.1.
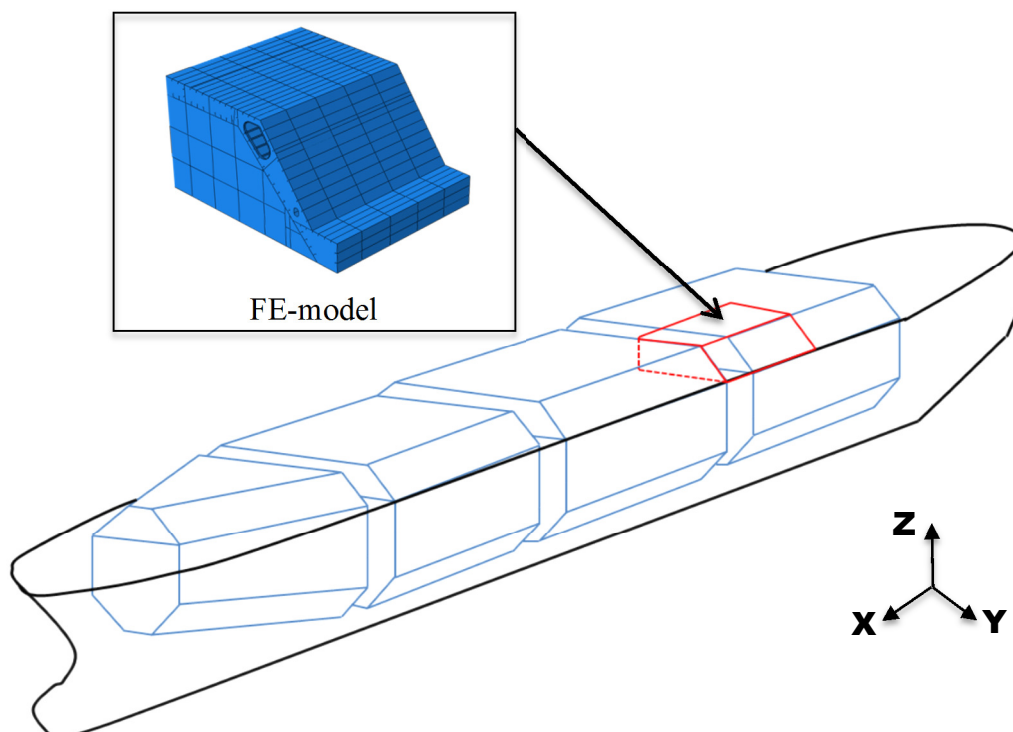

Figure 3.1   Principle outline illustrating the tank arrangement in a 4 tank LNG membrane carrier that outlines the location and extent of the studied part of the tank.

A more detailed overview of the structural extent of the modelled part of the tank is presented in Figure 3.2. Here the modelled part of the transverse bulkhead is outlined by the dashed red lines. Longitudinal elements and web frame sections under consideration are outlined with continuous red lines.
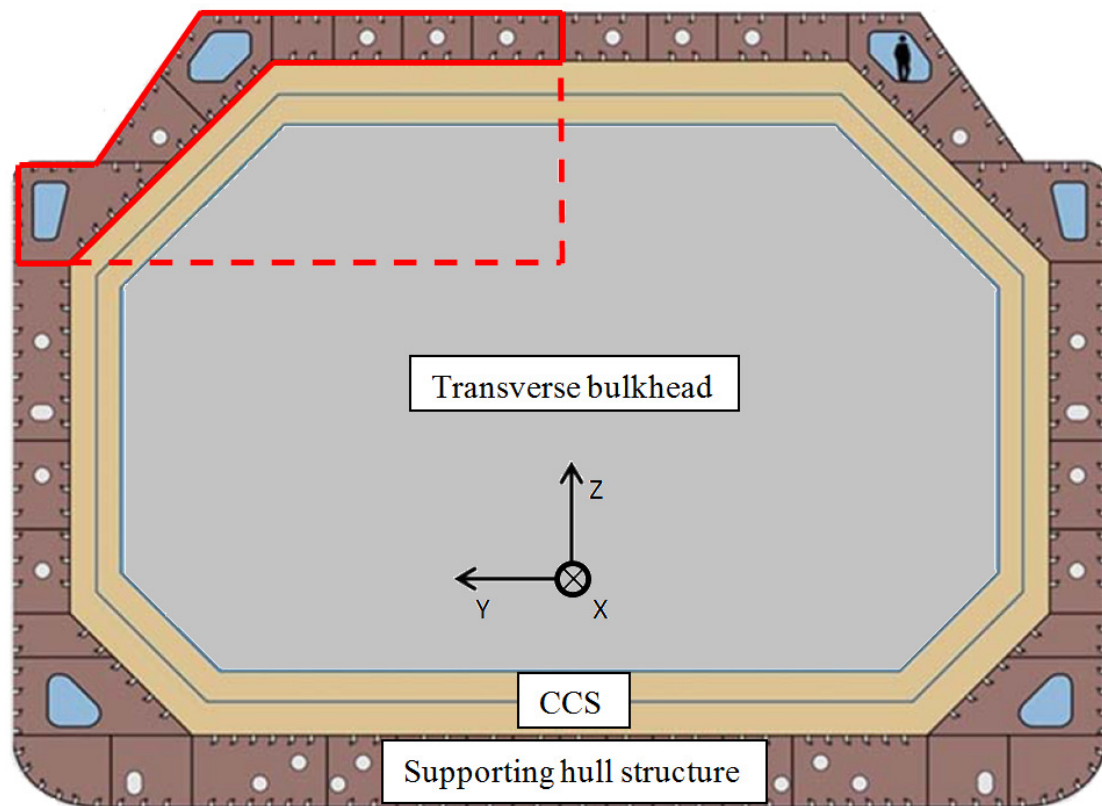

Figure 3.2   *Principle illustration of an LNG membrane carrier's midships section that outlines the transverse extent of the considered supporting hull structure, retrieved and modified with permission from DNV (2011).*

As discussed in Chapter 2.2, sloshing impacts in the tank top are usually highly localized. This implies that any load representation in the model becomes very small compared to the tank dimensions. Only the maximum responses of the structural members under consideration are of interest for the study and they occur in a region close to the applied load. The use of a local FE model is therefore assumed to be justified. The choice is also supported from a performed size-dependency study where the structural response, due to impact loadings, is compared between models of different extent. Results from this study show that the maximum response differs negligibly between the studied models for the same load case. The details regarding the size-dependency analysis can be found in Appendix B.

The model is based on drawings from a classification approval of the studied vessel and is presented in Figure 3.3. As discussed in the preface, these drawings are confidential documents and can therefore not be disclosed in this thesis.
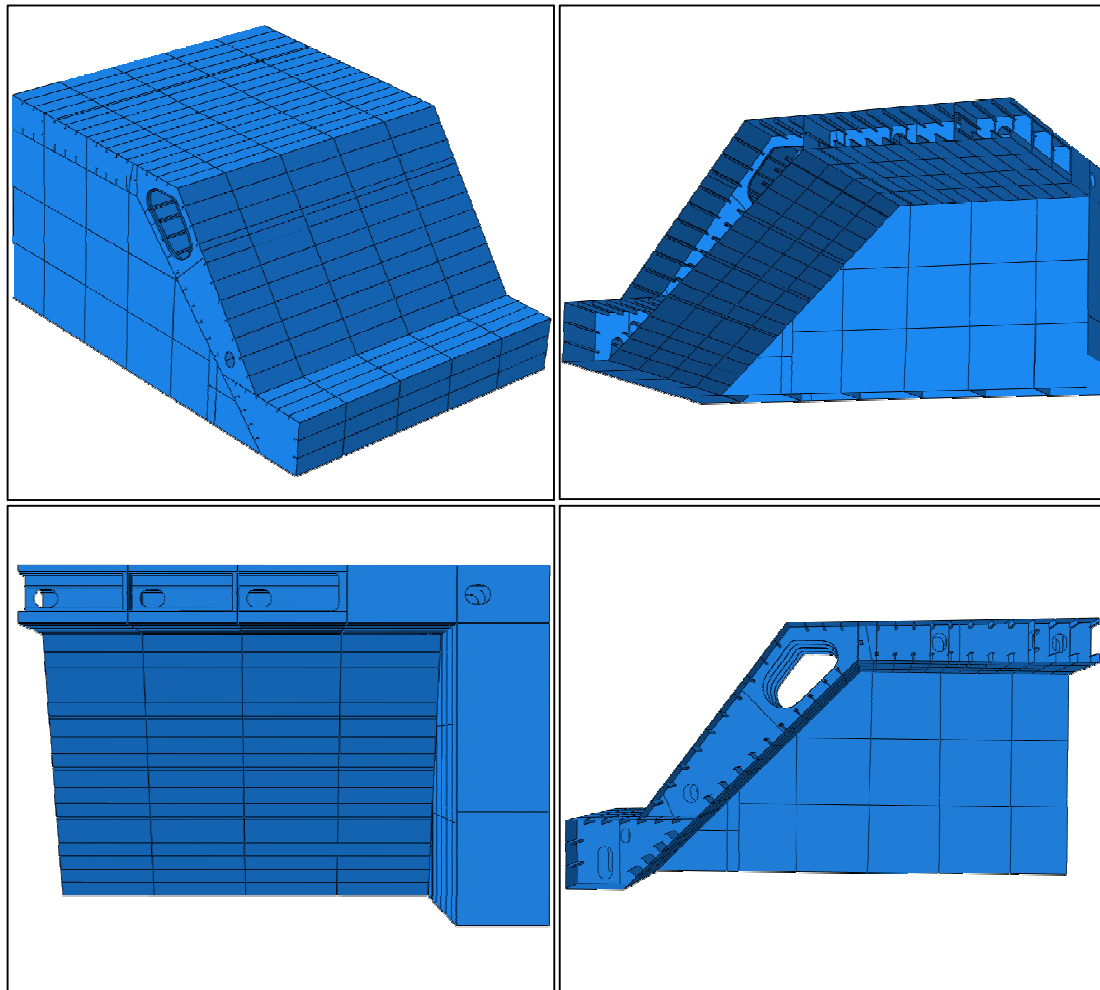

Figure 3.3   Overview of used FE model.

3.2 Boundary conditions

Figure 3.4 illustrates the faces and edges of the model subjected to applied boundary conditions (highlighted in red). The corresponding nodes in all of these boundaries are pinned against translation in all directions. In the size dependency study presented in Appendix B, two sets of boundary conditions for the FE model were also compared in terms of structural response behaviour of the model. This comparison showed that the choice of boundary conditions have a negligible influence of the structural response relevant for the response analyses intended for the FE model.
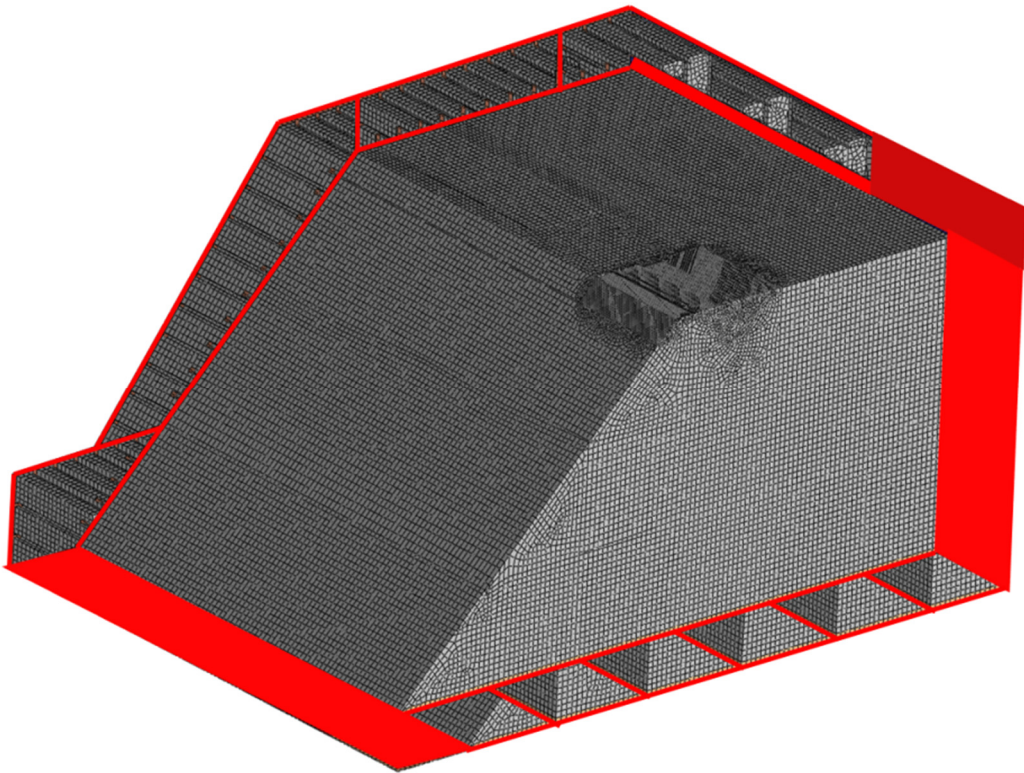

Figure 3.4   Faces and edges where boundary conditions are applied (highlighted in red).

3.3 Mesh

The FE model is discretized using small-strain shell elements under the assumption that the deformations due to the investigated impact loads will remain small. This is justified by the fact that only linear elastic behaviour of the structural response is considered in this study. The default small-strain element of this type in ABAQUS Explicit is the four-node S4R element. These are, however, known to perform poorly when applied to problems where warping is present, such as twisting beams (Dassault Systemes, 2014b). This shortcoming is eliminated in the S4RSW element by the introduction of additional terms to the strain-displacement equations. The added terms couples the curvatures for warped elements to the nodal translations as described by Belytschko (1991). Depending on the location of the intended loads it is natural to assume that the structural elements, especially the stiffeners, will experience some degree of warping. Therefore, the more comprehensive S4RSW element is used in the analyses.

The global mesh is generated by implementing ABAQUS default settings for mesh density. It is dominated by quadrilateral elements and has an average element side length of approximately 170 mm. A local mesh density refinement is made in order to achieve a model that is mesh-independent in terms of the structural response relevant for the dynamic response study. Figure 3.5 illustrates the structural members that have been discretized with the finer mesh. The chosen mesh density in this refined region is a result of a preformed mesh dependency study. Details regarding this study are presented in Appendix C. A local mesh density corresponding to an averaged element side length of approximately 40-50 mm depending on the meshed geometry was found to be sufficient. This gives a model that is computationally efficient yet capable of giving acceptable solutions for the intended analyses.
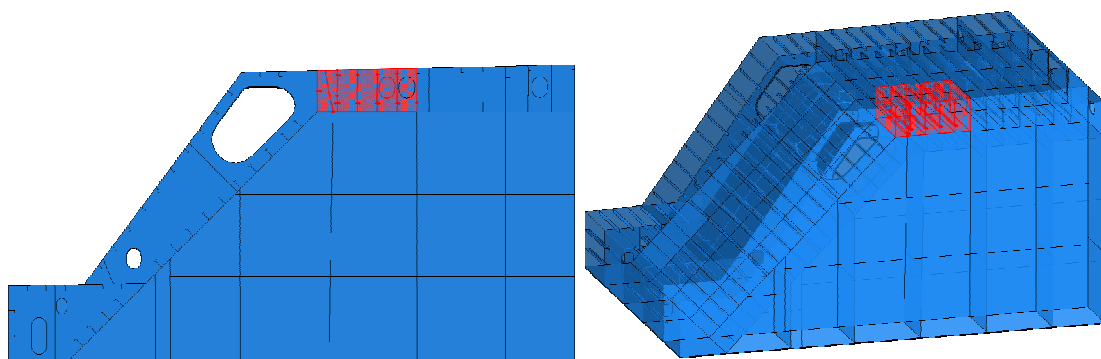

Figure 3.5   Illustration of the tank region subjected to mesh refinement (highlighted in red).

3.4 Load cases

In order to reach the desired outcome of the dynamic response study, a significant amount of data regarding the structural response is needed for a variety of load cases. This data is acquired through FE analyses.

A structure's dynamic response is closely connected to the dynamic characteristics of the loadings it is subjected to. The load duration is one of the most obvious of such features and is one of the key factors for dynamic amplification in structural response (Graczyk, 2008). A number of different rise times are thus considered for the applied loads, and these are presented in Table 3.1. The ratio between rise time and total load duration is set to 1/3 for the analyses. This goes in line with what is mentioned in Chapter 2.2.2. An example of the used load shape is given in Figure 3.6. The load duration is introduced into ABAQUS Explicit as a tabulated load history. The motivation to the chosen rise times comes from a number of sources. Model tests have shown that rise times around 1 ms frequently occur; see Graczyk and Moan (2008). Another reason for choosing these rise times is that the dynamic amplification decreases for rise times above 10 ms for the structure under consideration, which has been found in previously conducted numerical studies of similar ship structures (DNV GL, 2015).

Table 3.1   Rise times under consideration.

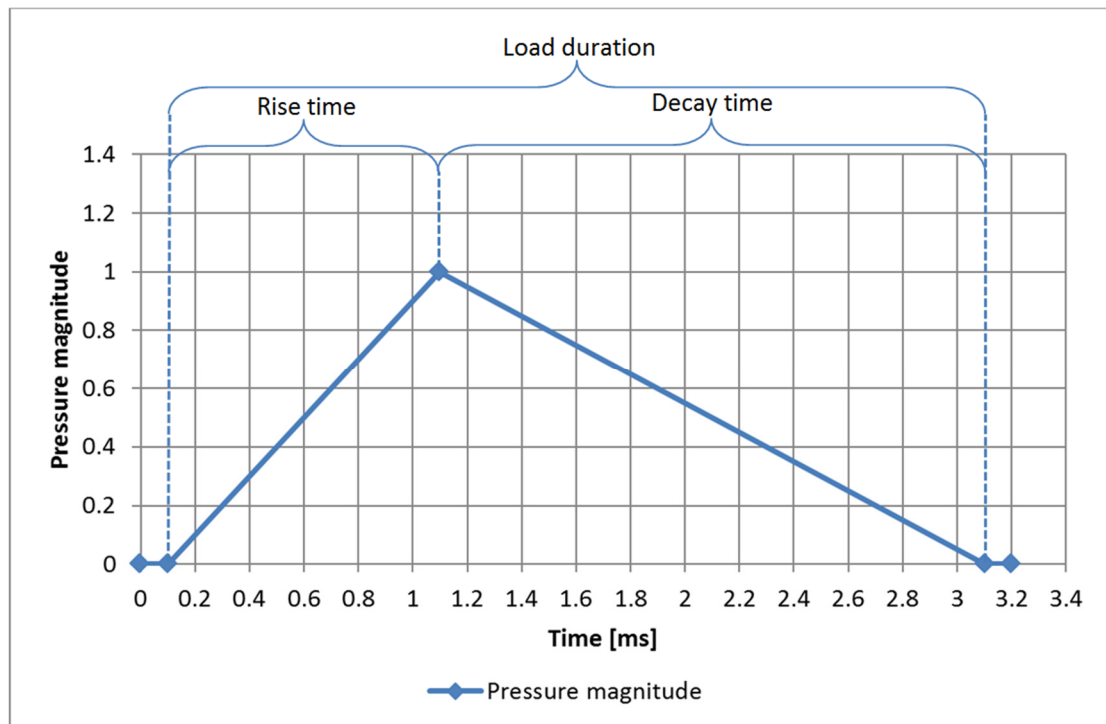| Rise Time [ms]	Decay time [ms]	Total load duration [ms]
0.1	0.2	0.3
0.3	0.6	0.9
0.5	1	1.5
0.7	1.4	2.1
1	2	3
1.5	3	4.5
2	4	6
3	6	9
5	10	15
7	14	21
10	20	30
20	40	60

*Figure 3.6   Principle illustration of pulse shape for the applied impact pressures, 1 ms rise time.*

It is very difficult to determine the exact dependency between load extent and structural response and also between load location and structural response since each and every load case induces very different dynamics into the system. Instead, a broader approach is undertaken, which aims at giving some guidance into which combination of area size and location that gives the largest dynamic amplifications in the hull structure. The studied tank region where loads are applied is the part of the inner deck that is subjected to mesh refinement as discussed in Chapter 3.3. The motivation for this load location is due to the fact that severe sloshing impacts are strongly present in the corner area close to the bulkhead and chamfer, see Chapter 2.2.1.

In general, the classification rules state required properties of the stiffening elements like plate and stiffeners for dimensioning against sloshing impact loads (DNV, 2013). Therefore, the load cases are determined with this in mind. The loaded areas under consideration for the studied load cases are located centred under the first longitudinal stiffener from the chamfer and in the middle of an adjacent plate away from the chamfer, see Table 3.2. The reason for not selecting the plate segment closest to the chamfer is that it contains a structural inconsistency in terms of plate thickness. Both loads are located at a distance of 300 mm from the transverse bulkhead in order to account for the non-modelled *cargo containment system* (CCS). For each of the two locations three different sizes of the area are to be analysed. The areas under consideration are presented in Table 3.2. The loads are applied in between two stiffeners and underneath one stiffener, respectively, because these locations represent extreme cases in terms of structural arrangement. This gives the possibility to quantify how the key structural members are affected by a change in load location. The two cases represent the largest possible difference in load location within the spacing of two adjacent plate fields.
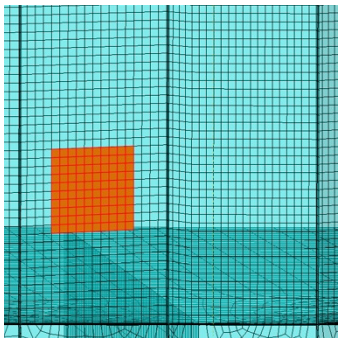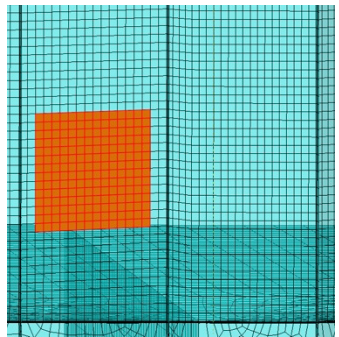
For all six load cases presented in Table 3.2, the applied load has a rectangular shape and the load is applied uniformly over the whole loaded area. The motivation to use the rectangular shape is that it has been used in previously conducted numerical studies of sloshing impact loads (DNV GL, 2015). The uniform distribution of the pressure is motivated by the fact that the study aims at investigating the pure influence of the load parameter variations under consideration. If the load intensity differs within the load footprint this could influence the dynamic behaviour. As discussed in Chapter 2.2.2 model tests usually present the pressure loads as an average pressure for a specific area extent and therefore the reference pressure magnitudes are based on uniform pressures. The peak magnitude of the applied load is 1 MPa, which is in the range of the highest magnitudes measured in full-scale measurements. This corresponds to a force of 160 kN on the smallest load surface of 400×400 mm to put it into perspective.
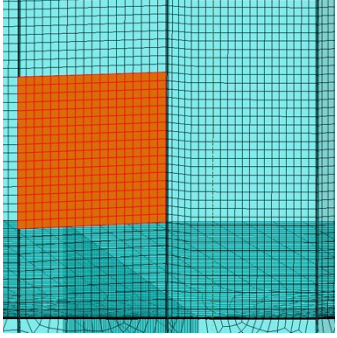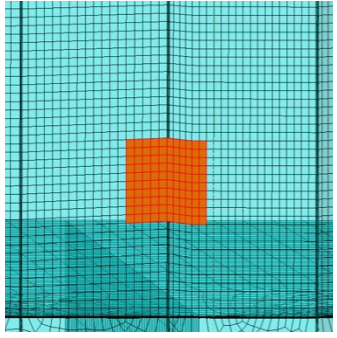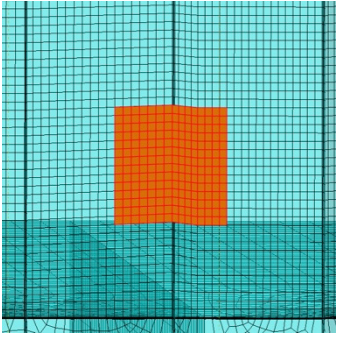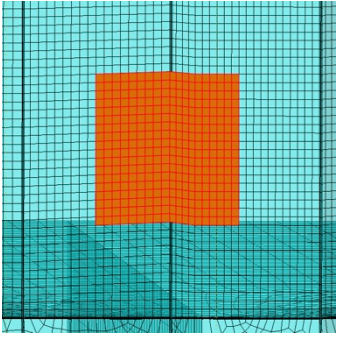
In order to calculate the non-dimensional *dynamic amplification factor* (DAF) for the studied responses, a static reference value of the studied responses is needed. Therefore, additional static analyses are also performed using ABAQUS standard for all load cases with regards to load location and area.

Table 3.2   Description of the load cases under consideration for the FE model.
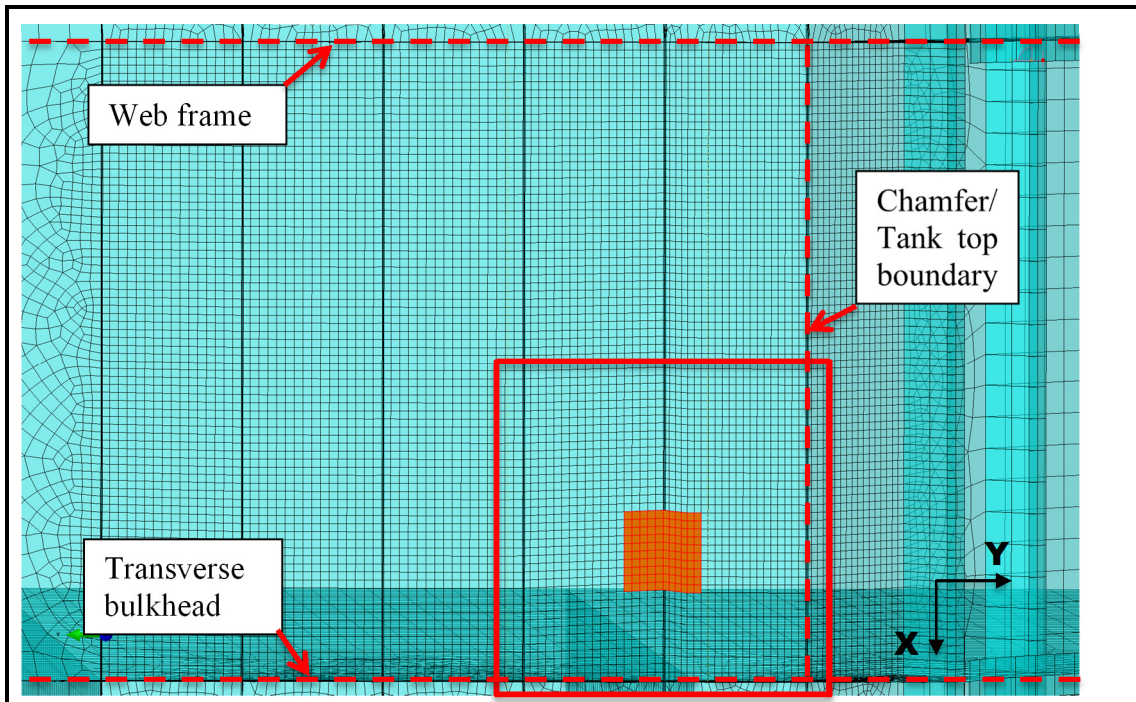
The loads are applied on the inner deck plate in the corner outlined by the transverse bulkhead and the upper chamfer. The red rectangle outlines the zoomed-in sections displayed below. The three first ones are applied in between two stiffeners and the last three are applied underneath one of the stiffeners. All load cases are evaluated for load rise times of 0.1 to 20 ms and also for a static load.

Load case name	Load extent approximately [mm×mm]	Load location	Illustration
LC Plate 400	400×400	In between stiffeners	
LC Plate 600	600×600	In between stiffeners	

LC Plate 800	800×800	In between stiffeners	
LC Stiffener 400	400×400	Underneath stiffener	
LC Stiffener 600	600×600	Underneath stiffener	
LC Stiffener 800	800×800	Underneath stiffener	

4 FE-model for CCS influence study

The loads applied on the model described in Chapter 3 are uniformly distributed impact pressure loads with a rectangular area. They are applied directly on the inner deck. A real sloshing impact event will, however, inflict a local pressure pulse on the primary membrane and then translate through the *cargo containment system* (CCS) to the underlying steel hull structure. The CCS can thus be seen as a load filter. Furthermore, the physical properties of the CCS will evidently affect the dynamic behaviour of the supporting hull structure. In order to get a measure of how large an influence the CCS has on the dynamic response of the hull, a separate smaller FE model is set up. The model is presented in Figure 4.1 and represents a part of the supporting hull structure together with parts of the CCS. In the following, this FE model is referred to as the small model whilst the FE-model presented in Chapter 3 is referred to as the full model.
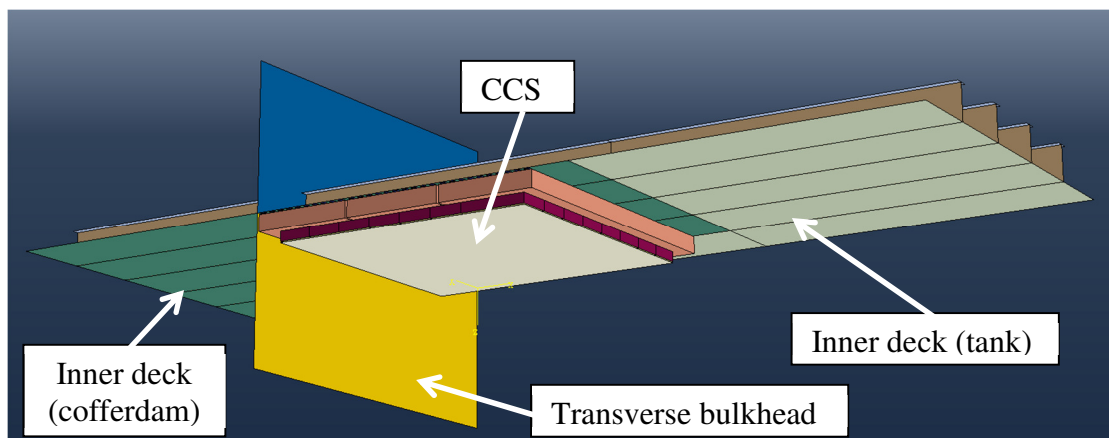

Figure 4.1   Illustration of the small model including a part of the CCS.

Figure 4.2 illustrates which part of the hull structure in the full model that is included in the small model. It covers the region of interest with regard to previously described analyses, though only including the inner deck structure and plating of the transverse bulkhead closest to the tank under consideration. In order to maintain most of the dynamic behaviour in the structural members under consideration the modelled part of the inner deck structure is extended longitudinally in both directions from the corner plate field. It thus spans from the forward transverse bulkhead to the second tank web frame.
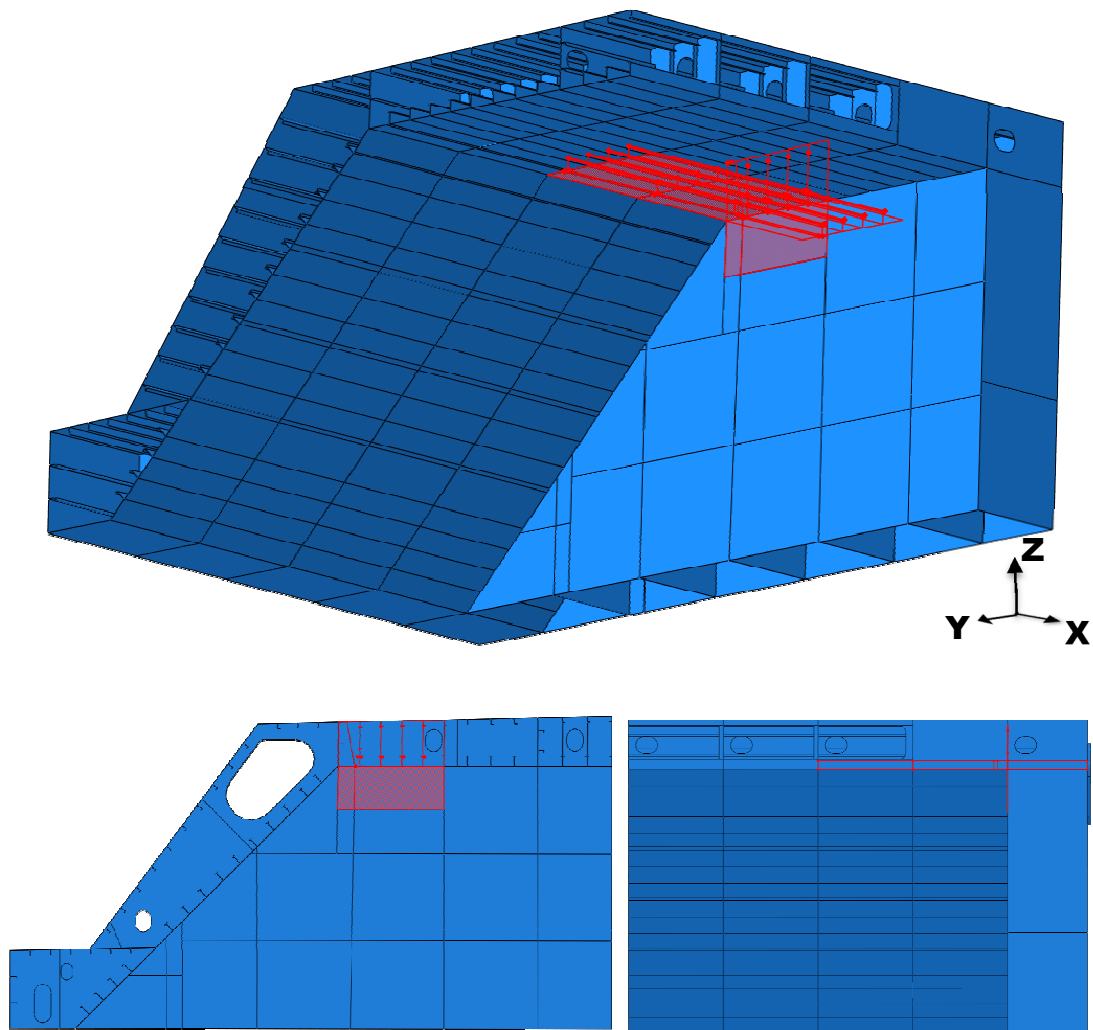
Figure 4.2   Location of the small model within the full model.

Considering the results from the size-dependency study described in Appendix B the limited extent of this model is not to be considered sufficient for accurately representing the actual hull response. It is, however, assumed as being adequate for quantifying the influence that the CCS has on the hull response during an impact event.

4.1 Cargo containment system

The CCS used in this study is a simplified version of the Mark III system described in Chapter 2.1. The modelled part of the insulation system approximately covers a 3 m × 3 m surface of the inner deck. The extent of the modelled CCS is chosen so as to cover most of the stiffened plate field closest to the transverse bulkhead. This is to assure that the area of interest with regards to load application and response extraction is assigned with the properties of the CCS in order to make a fair judgement of the containment system's influence on the hull response. To save computational effort, the extent is limited to three secondary insulation panels, each 3×1 m.

In the boundaries where the inner deck meets the transvers bulkhead and the chamfer, respectively, the Mark III system shows a more complex composition than in the flat areas. In order to simplify the modelling procedure these parts are excluded from the

small model. The contact connection between the corner panel and the flat panels in the tank roof are limited in terms of load transfer. Therefore the influence of this simplification is assumed to be very small in terms of response in the hull structure. Furthermore, the secondary triplex membrane is omitted from the model as well due to its small contribution to the global stiffness and mass (DNV, 2014).

The modelled CCS is built up in layers by a number of separate parts tied together at surfaces in the normal direction. Both solid, shell and membrane elements are used for representing the different layers. The complete composition of the stack-up is illustrated in Figure 4.3. The figure also presents the dimensions of the separate parts in each layer together with their corresponding general element type.
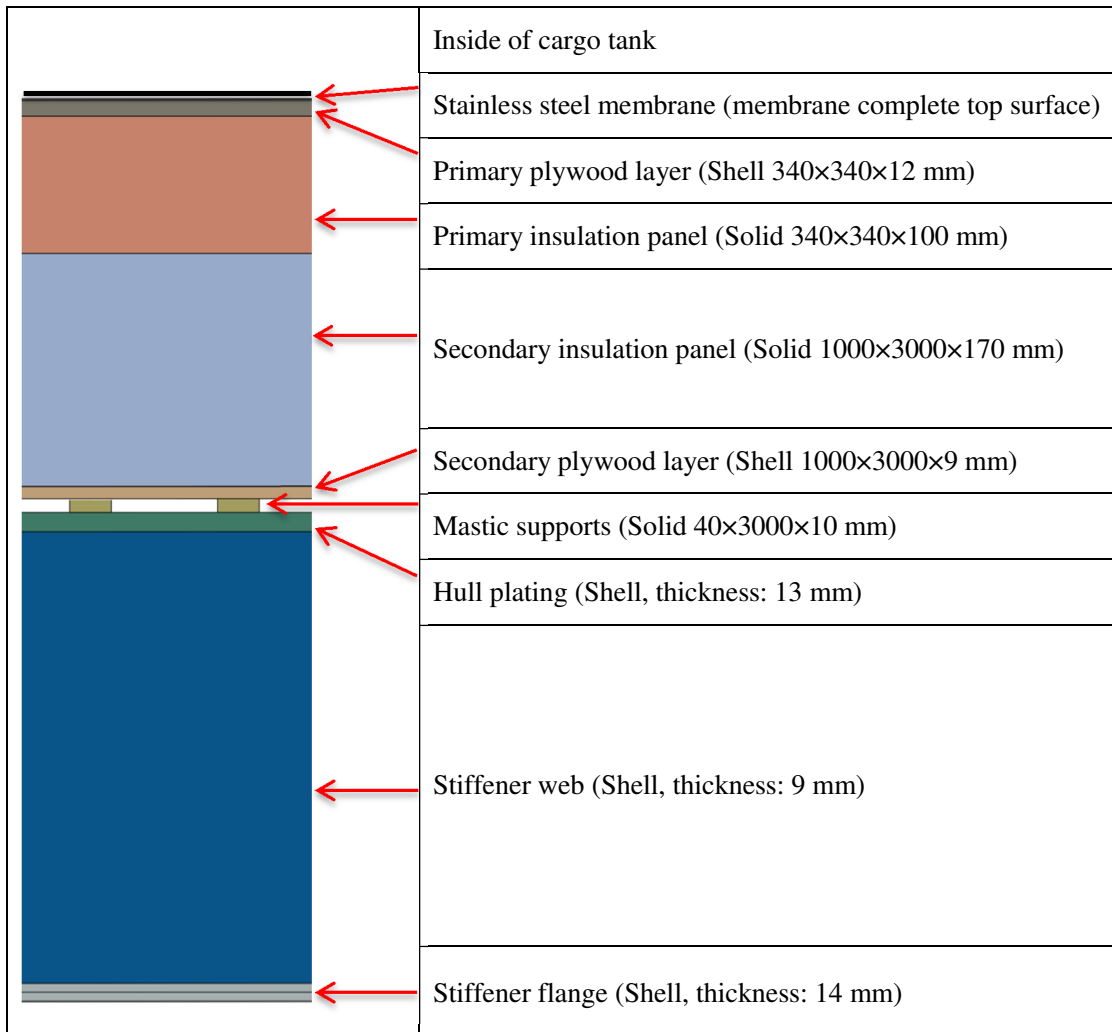

| Inside of cargo tank |
| Stainless steel membrane (membrane complete top surface) |
| Primary plywood layer (Shell 340×340×12 mm) |
| Primary insulation panel (Solid 340×340×100 mm) |
| Secondary insulation panel (Solid 1000×3000×170 mm) |
| Secondary plywood layer (Shell 1000×3000×9 mm) |
| Mastic supports (Solid 40×3000×10 mm) |
| Hull plating (Shell, thickness: 13 mm) |
| Stiffener web (Shell, thickness: 9 mm) |
| Stiffener flange (Shell, thickness: 14 mm) |

Figure 4.3   Detailed view of insulation system cross section.

Material properties for the different layers are assigned according to the recommended practice described in DNV GL classification note No. 30.9 (DNV, 2014). The element types and layer connections are also assigned in accordance with the classification note. A summary of the used material properties is given in Appendix D. Insulation panels and plywood plates are modelled with a homogenous linear elastic orthotropic material behaviour and the mastic supports with homogenous linear elastic isotropic behaviour. Since the stiffness parameters for both plywood and insulation foam is temperature-dependent two sets of parameters need to be considered. The ambient temperature inside the tank during operation is approximately -163 ºC, which is why

the primary plywood layer and insulation panel are modelled with material stiffness parameters corresponding to this temperature. The secondary plywood layer and insulation panel are assumed to experience a temperature of 20 ºC and are thus assigned with material properties accordingly. Finally, the choice of discretizing the stainless steel membrane with membrane elements allows for a simplified geometry. By doing this, the layer's bending stiffness is omitted and thus provides a representation of the membrane's multidirectional corrugations while still maintaining its inertial effects on the structural dynamics (DNV, 2014).

4.2 Mesh

Figure 4.4 illustrates the degree of discretization in the small model. The seemingly dense mesh is a consequence of the large amount of part connections. In order to assure that the modelled joints between parts in the different layers of the CCS is behaving in a desired way, nodes in joining surfaces are made sure to coincide to as large a degree as possible. In the current model and the scope of this thesis the most effective approach to realize this is found to be limiting the mesh element size. This allows for having the same degree of discretization within each part and, in turn, the possibility of a good node coincident, see Figure 4.4. Therefore, the average element size is set to 20 mm throughout the model.
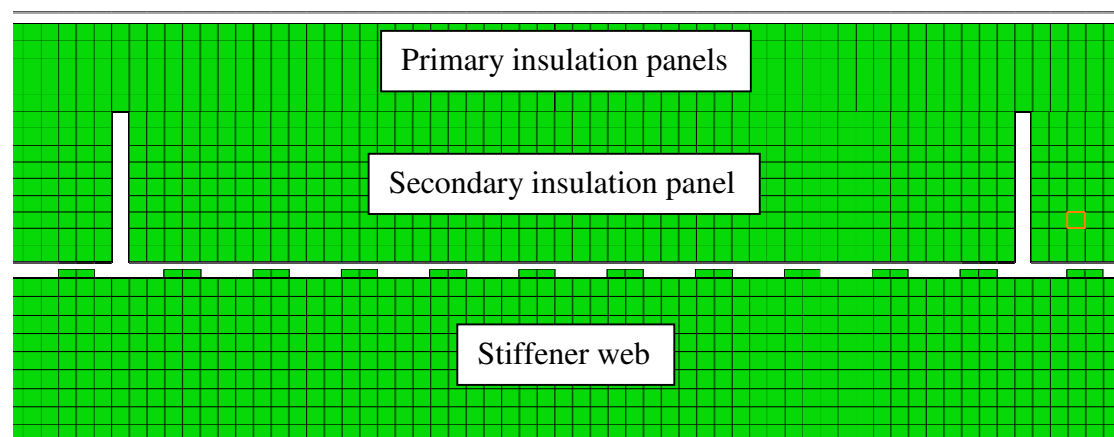

Figure 4.4   Mesh of small model.

The hull structure is discretized with the same warping compensated small-strain shell elements (S4RSW) as in the full model in order to solve the warping of the stiffeners in an accurate manner. Standard small-strain shell elements (S4R) are used for the plywood layers in the CCS. The reinforced foam in the insulation panels is modelled with first-order reduced integration solid elements (C3D8R). Finally, general membrane elements (M3D4R) are used to represent steel membrane. For further information with regard to the element types, one may refer to ABAQUS manual (Dassault Systèmes, 2014b).

4.3 Boundary conditions and contact formulations

The coinciding surfaces between the layers in the CCS are tied together by constraining the nodes in adjacent surfaces to each other. Since a tied constraint in ABAQUS Explicit is not interpreted as a contact formulation, no contact pressure output is provided in the simulation results. The contact pressure in the interaction between the CCS and the underlying hull structure is, however, considered as a desirable output for the current study. Therefore, the joint between adjacent surfaces

of the mastic supports and inner deck plate are modelled with a cohesive contact formulation. Other surfaces subjected to contact are assigned with frictionless contact behaviour to assure that no penetration will occur.

In Figure 4.5 the chosen boundary condition is presented. All the outer boundaries of inner deck and transverse bulkhead plates (highlighted in white) are pinned in all translation directions but free to rotate. The webs of the longitudinal stiffeners are pinned in transvers translation at web frame and transvers bulkhead locations; as indicated in Figure 4.5 (highlighted in red). This allows for a representation of the interaction between stiffeners and structural elements omitted in this model. Furthermore, a pinned boundary condition in the vertical direction is assigned in order to take the limitation in translational motion due the first web frame into account (location highlighted in blue). Finally, the vertical surface closest to the transverse bulkhead in the secondary insulation panels are limited in longitudinal translation. This is meant to represent the interaction with the left-out corner panels and to avoid undesired contact with the transverse bulkhead.
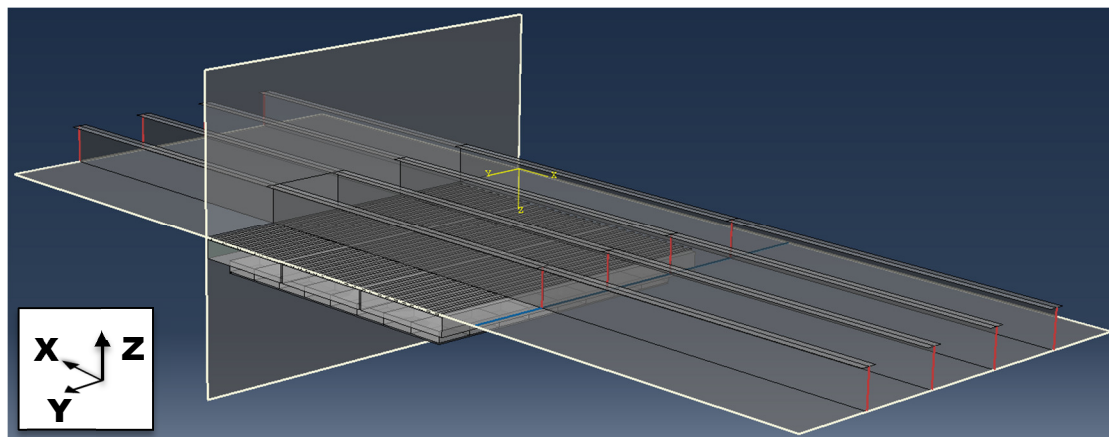

Figure 4.5   Illustration of boundary conditions for the small model.

4.4 Model versions

Three versions of the small model are set up for the comparative study. These are presented in Table 4.1 and described in the following. Comparing the response behaviour from SM v.1 and the large model is not considered possible due to their geometrical differences. Therefore SM v.3 is thought to be a reference case for determining the influence of the CCS. The motivation to also compare the response with SM v.2 is in order to determine if it is possible to get an accurate representation of the CCS by only including the CCS mass.

Table 4.1   Explanation of versions of the small model.

Model version	Description
SM v.1	Hull with modelled CCS mass and stiffness
SM v.2	Hull with CCS mass
SM v.3	Hull

SM v.1 is illustrated to the left in Figure 4.6. It includes discretized representations of both the hull structure and CCS according to specifications given in Chapters 4.1 to 4.3. The modelled CCS contributes with both stiffness and mass to the structure. To reduce computational time the modelled part of the CCS only covers part of the inner deck corresponding to the roof of the tank. Therefore, in order to account for the inertial effects from the excluded parts of the CCS an adjustment in material density is made on the steel plates on the inner deck and transvers bulkhead. The plate regions, where this adjustment is made, are coloured red as presented in the figure. Based on the separate layer thicknesses (see Figure 4.3) and their corresponding densities (see Appendix D) the average distributed weight of the CCS can be calculated to approximately 65.4 kg/m^2. By increasing the density of the 13 mm steel plates from 7850 kg/m^3 to 12880 kg/m^3 the mass of non-modelled parts of the insulation system is accounted for.

In the two other versions of the small model the geometric representation of the CCS is excluded. This gives models where the CCS stiffness is not accounted for. The geometry of these models is presented to the right in Figure 4.6. SM v.3 only accounts for the hull structure whilst SM v.2 includes the mass of the omitted insulation panels in the same manner as in the full model version. The steel plates with adjusted density are again illustrated in red in the figure. Mesh density and hull boundary conditions are kept identical for these versions as for SM v.1.
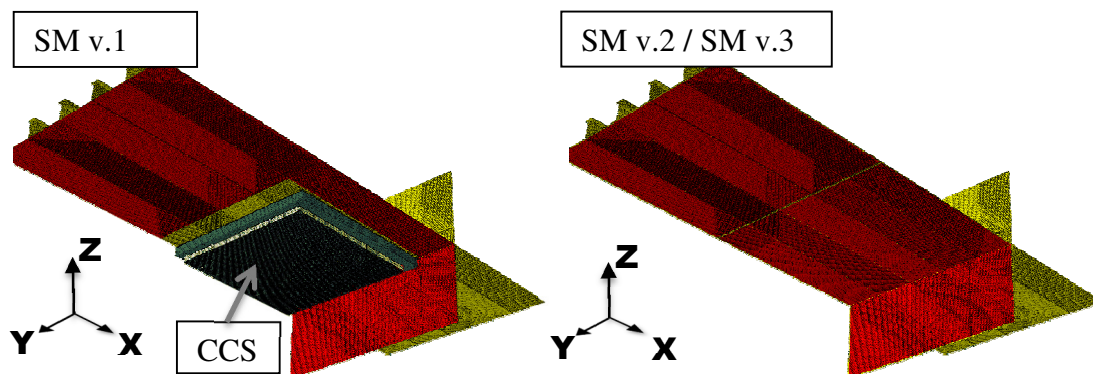

Figure 4.6   Comparison of the model versions, red faces indicate plates with increased density for SM v.1 and SM v.2.

4.5 Load cases

The load cases set up in the analyses of the small model are limited to only one area extent and two different load locations. The geometrical locations are applied in similar locations as for the full model, see Table 3.2, where one corresponds to a position centred under a stiffener and the other one in between two stiffeners. The distance from the transverse bulkhead is in this case taken as 350 mm. Rise times, ratio between rise time and total load duration and simulation durations are kept the same as the previous analyses with the full model. The motivation behind the chosen load parameters is discussed in Chapter 3.4.

The load case where the load is applied in between two stiffeners is presented in Figure 4.7. The size of the area corresponds to 400×400 mm. The position of the load cases for the small model without the hull is projected though the CCS and applied on the hull, but with the same horizontal coordinates. Principal sketches and descriptions of the load cases are outlined in Table 4.2.
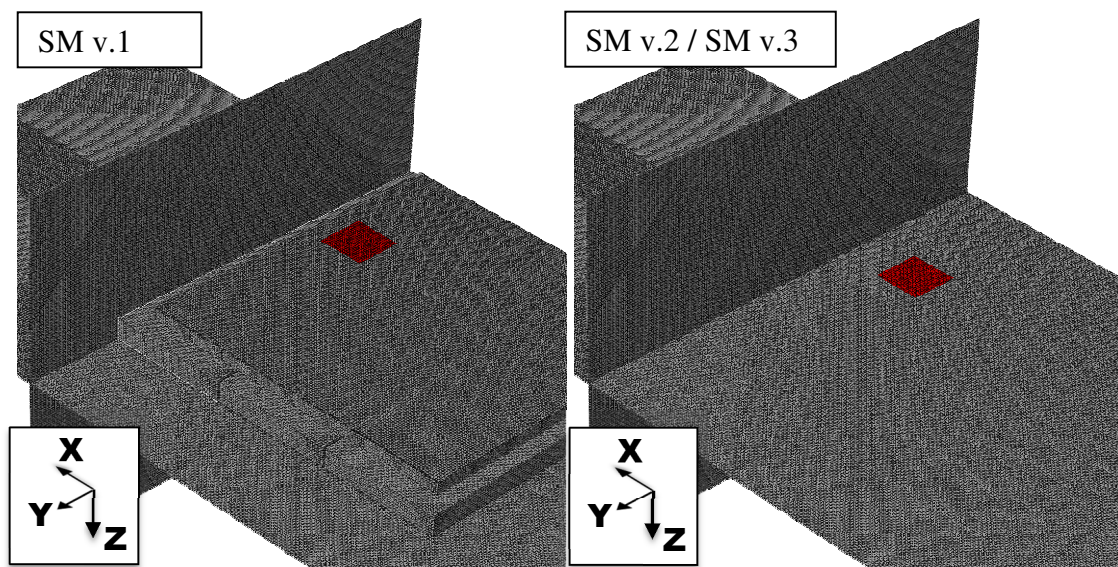

Figure 4.7   *Structural members subjected to the applied loads for the different versions of the small model. The red rectangles indicate the loaded areas to one of the load cases.*

Table 4.2 Load cases for small model.

Load case number	Load area [mm × mm]	Load location	Comment
LC SM Plate 400	400×400	In between stiffeners	The cargo containment system is only present for *SM v.1*

Load case number	Load area [mm × mm]	Load location	Comment
LC SM Stiffener 400	400×400	Underneath stiffener	The cargo containment system is only present for *SM v.1*

5 Results and discussion

In this chapter, the results from the FE analyses are presented and discussed. It outlines the most relevant findings regarding how the structural response is affected by variations of impact load parameters. Each parameter influence is dealt with separately in the following. Results from the investigation on how the *cargo containment system* (CCS) influences the studied response behaviours are presented in Chapter 5.4.

The major part of the results is presented in terms of *dynamic amplification factor* (DAF) versus rise time charts. They are based upon extracted values of the maximum observed response variables from the FE analyses outputs at specific structural members, described in Chapter 5.1. The response variables under consideration are von Mises effective stress and vertical deflection. Von Mises stress is strongly connected to the strength capacity of the structure under consideration and is therefore a key measure for design criteria of marine structures (DNV, 2015). For some of the considered structural members the deflection components give a clearer representation of the structural dynamic behaviour, which is why also the vertical deflections are evaluated. Deflections in the inner hull structure are furthermore relevant for the design criteria of the CCS membranes in terms of allowable strain (DNV, 2008). The considered stresses are based on calculated stress at the element integration point, having the largest stress value. The vertical deflection corresponds to nodal deflections.

Static values for the studied response variables are obtained from static analyses for all of the investigated load cases as described in Chapter 3.4 and Chapter 4.5. These static values are then used for normalizing the maximum stress or deflection acquired from the dynamic analyses with a different load rise time for each corresponding load case. This gives sets of DAF values, corresponding to the studied range of load rise times, for the stress or deflection response depending on what is sought for. These sets of DAF values allow for comparison between the different load cases.

As mentioned in the preface, the information regarding absolute values of the studied responses cannot be presented. This implies the following:

- The static reference values used for obtaining the presented DAF charts are not disclosed in this thesis.
- All contour plots showing stress and deflection profiles in the structure are normalized against the maximum response value for each case, respectively. Contours are thus presented in a scale from 0 to ±1.
- Charts showing the relative difference in response magnitudes between separate load cases are normalized against a common reference value for the compared load cases. This reference value is taken as the largest observed response value for the compared responses. These normalized charts are thus presented in a scale 0 to 1 or -1 to 1. Response variables corresponding to these results are referred to as normalized stress and normalized deflection, respectively.

A discussion regarding observed levels of stress and deflection and what this implies for the outcome of this thesis is provided in Chapter 5.5.4.

5.1 Output locations

According to DNV (2014) the design criteria for the hull structure with regards to sloshing impacts only covers the structural properties of the plate in the inner tank shell and its corresponding stiffening members. Therefore, a focus in the output extraction is put to these structural members. Since the sought structural responses correspond to maximums of von Mises stress and vertical deflection, the output locations are required to be in close proximity to the applied loads. The localized nature of the applied loads gives reason to believe that the maximum response will occur close to the load location. Furthermore, for the case of the stiffener the maximum normal stresses from lateral bending loads will occur in the flange. This can be explained by the location of the neutral axis for stiffener and plate system. The studied stiffener response is thus limited to the response in the flange. This also allows for a more fair distinction between plate and stiffener response.

In accordance with the previous discussion the output locations under consideration are located in the inner deck structure at the region subjected to mesh refinement, see Chapter 3.3. They are represented by a stiffener flange and a plate field limited by the natural boundaries of two adjacent stiffeners. The output locations correspond to the structural members subjected to the applied loads for the two analysed load locations, as described in Chapters 3.4 and 4.5. In the following text the two output locations are referred to as stiffener flange and plate, respectively. The geometries corresponding to the studied locations in the full model are presented in Figure 5.1 and for the small model in Figure 5.2.
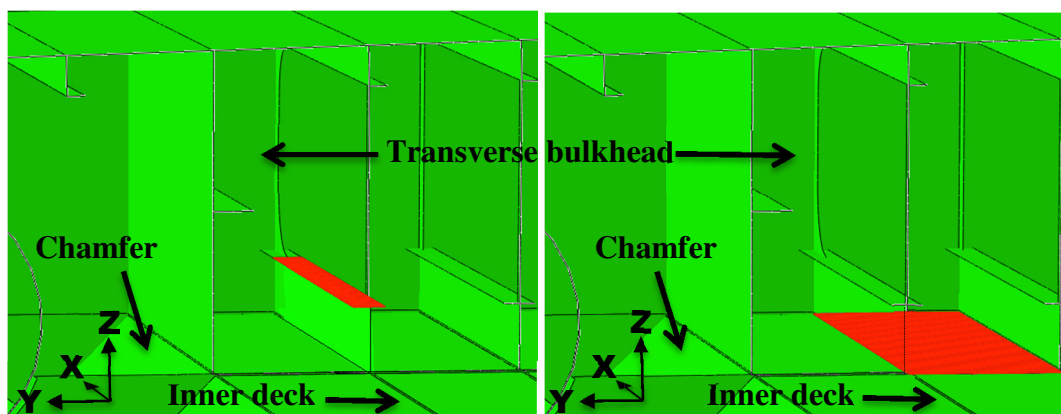

Figure 5.1   Area under consideration for response evaluations in the full model (highlighted in red).
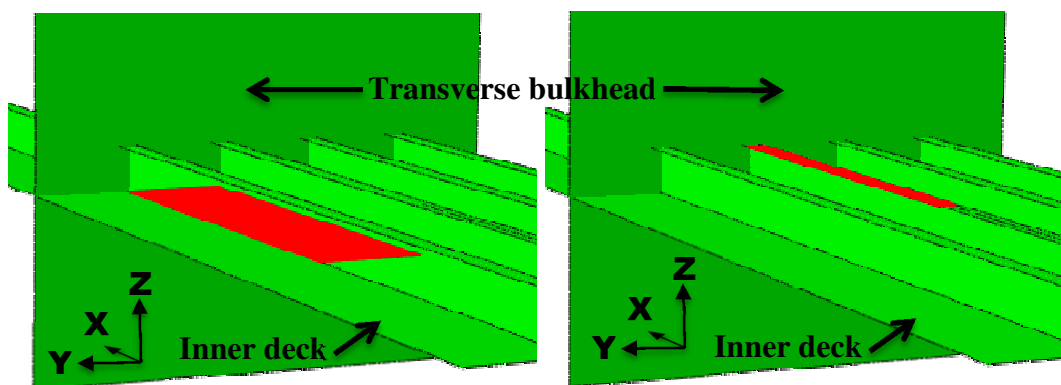

Figure 5.2   Area under consideration for response evaluations in the small model (highlighted in red).

Since the analyses are dynamic the specific element or node where the maximum response appears within a structural member can vary depending on the rise time of the applied load. Unless otherwise stated, the extracted response value is taken from the local position that experiences the highest stress or largest deflection.

5.2 Effect of load location

In order to determine the influence on the structural response behaviour from the location where the load is applied, it is preferred to study the load cases with smaller load area extents; LC Plate 400 and LC Stiffener 400, respectively. A load with a smaller area extent is more localized and therefore allows for better distinction between the two loaded locations. The specifics regarding these load cases are presented in Table 3.2 in Chapter 3.4.

Figure 5.3 presents the DAF with regard to the vertical deflection of the plate for the studied set of load rise times and load locations. It is shown that the plate experiences a dynamic amplification with a maximum DAF value around 1.3 for both of the load cases under consideration. The curves representing the dynamic deflection behaviour of the studied inner deck plate for the two different load cases coincide well, only showing slight deviations in maximum DAF. This suggests that the load location has a minor influence on the dynamic behaviour of the plate. The explanation behind this observation is further elaborated in Chapter 5.3.
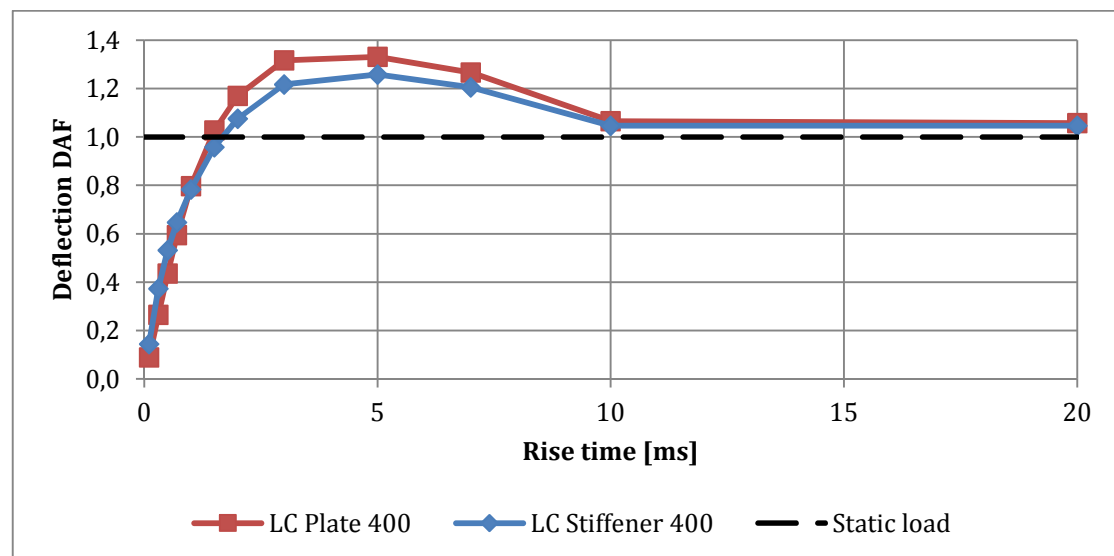

Figure 5.3   DAF corresponding to the maximum vertical deflection of the plate for two different load locations.

LC Plate 400 gives a significantly higher dynamic amplification of the maximum von Mises stress in the stiffener flange compared to LC Stiffener 400, see Figure 5.4. The maximum dynamic amplification also occurs at a lower rise time for this load case. Worth noting are also the rather steady DAF values occurring for LC Plate 400 for rise times of 2-5 ms. These large differences in dynamic behaviour for the stress in the stiffener flange due to change in load location are interpreted and discussed in the following.
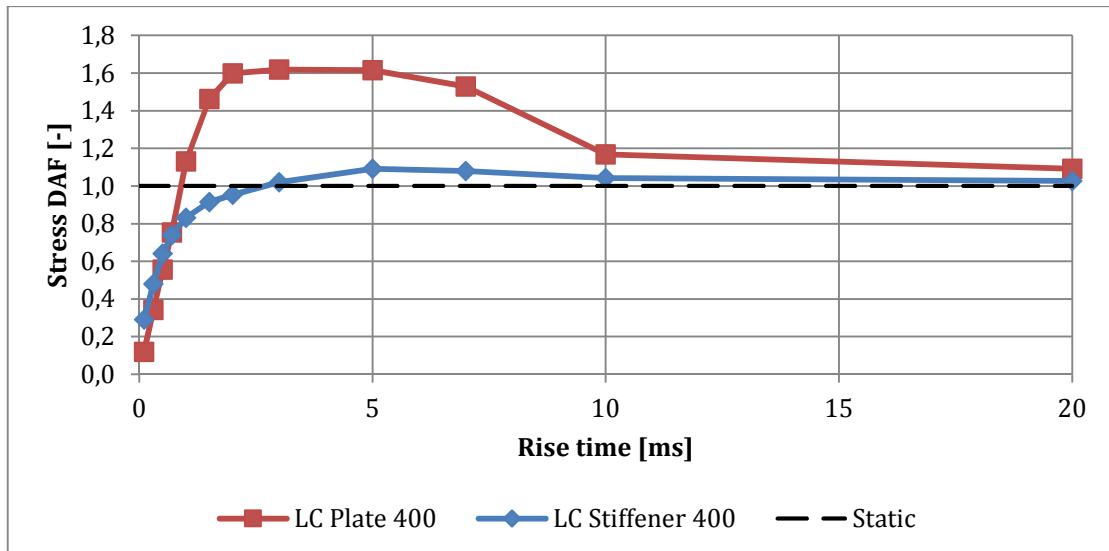
Figure 5.4   DAF for von Mises stress for the stiffener flange for two different load locations.

The relative difference in actual stiffener response between LC Plate 400 and LC Stiffener 400 are presented in Figure 5.5. Also, the static values for this structural response are significantly larger for LC Plate 400. This could be considered as being unexpected by just looking at the location of the applied load. The reason behind this behaviour of the structure is that the load acting on the plate generates a torsional moment in the stiffener. The design of the stiffeners with a high web and relatively narrow flange implies that their stiffness towards pure bending, in the vertical direction, is great. It does, however, make them susceptible to horizontal deformations due to torsional moments. The stress contributions from these horizontal deformations are therefore several times larger than the contributions from pure bending when the load is applied between the stiffeners. When the load is centred under the stiffeners no torsional moment is generated for the stiffener under consideration and the von Mises stress is thus dominated by contributions from pure bending.
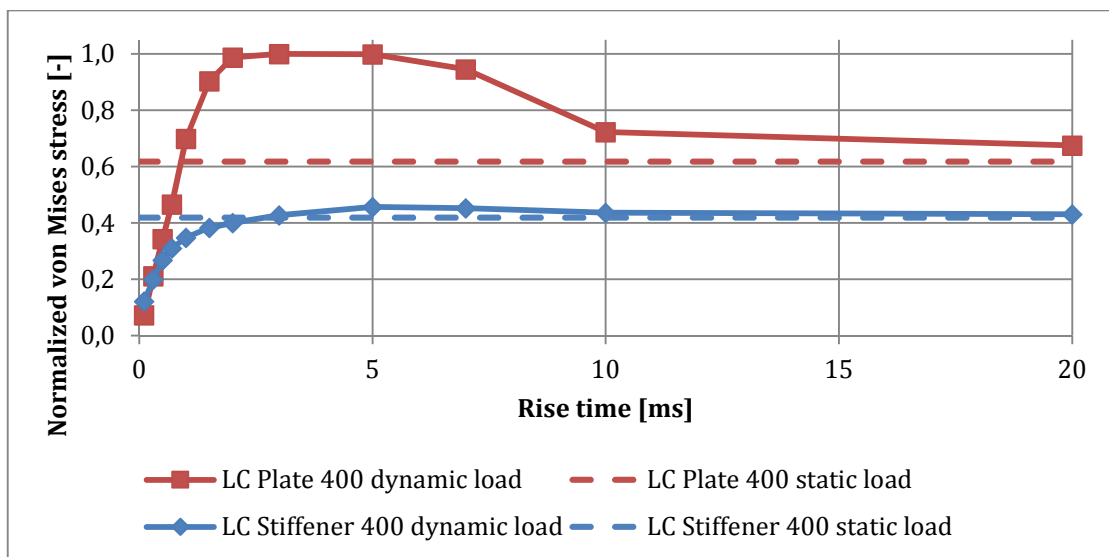

Figure 5.5   Normalized von Mises stress for the stiffener flange for two different load locations.

Figure 5.6 presents the von Mises stress contours in the inner deck structure as a result of an impact load corresponding to LC Plate 400. The figure shows the previously discussed horizontal deflections of the stiffeners as a result of the load location and how these influence the stress profile in the flange. The deflection behaviour produces in-plane bending moments in the flanges of the stiffeners, which results in high normal stresses in their edges. It should be noted that the stress contours in Figure 5.6 correspond to a time of 9 ms after the applied load has reached its peak and that the maximum von Mises stress occurs at a location far from the point of load application. The reason for this is that the load induces an oscillation where the stiffener oscillates in a specific deflection pattern. The maximum stress then occurs at the location where the amplitude of these oscillations is largest. For the presented case this location is approximately ¾ of the stiffener span from the transverse bulkhead.
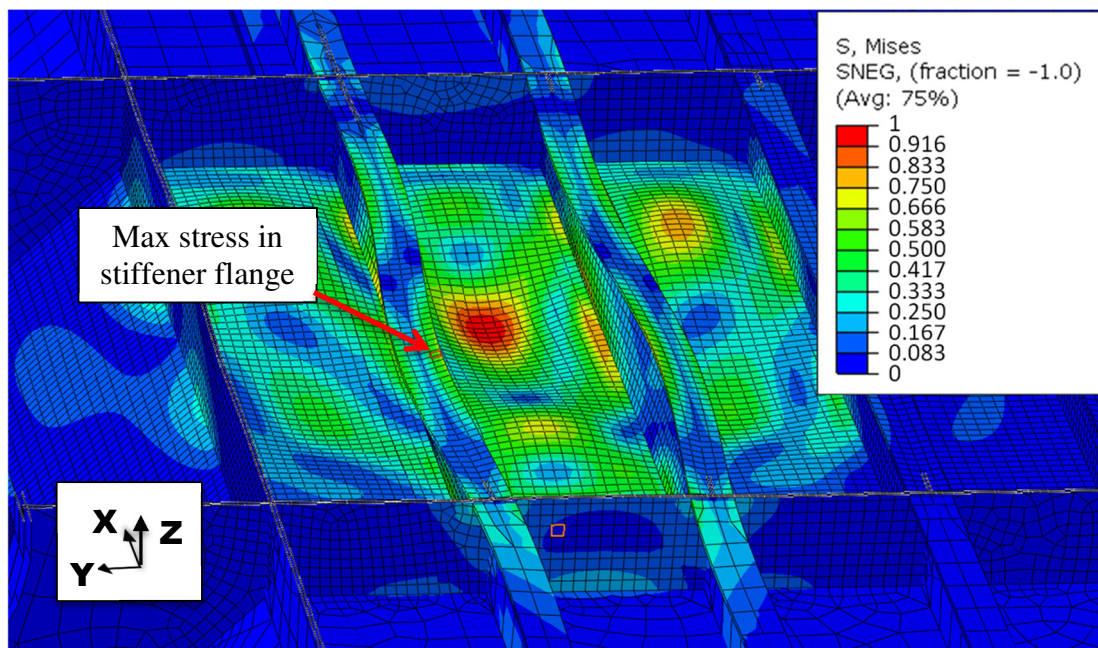

Figure 5.6   Von Mises stress profile for the stiffener flange corresponding to LC Plate 400 with a load rise time of 3 ms. Scale of deformation: ×20.

The previously discussed dynamic deflection pattern of the stiffener is highly dependent on the load rise time, which is shown in Figure 5.7. The contours represent horizontal deflections and deformations are scaled up by a factor of 40. These results show that different rise times result in different torsional deflection modes. Rise times around 3 ms excite the stiffener in a deflection pattern corresponding to a full sine wave. A rise time of around 5 ms, on the other hand, excites the stiffener in a deflection pattern corresponding to a half sine wave. As described by Fadini (2014) all structures can vibrate in several different ways. These vibration modes have their own corresponding natural frequency. If the structure is forced into an oscillation with a frequency close to one of the natural frequencies its corresponding vibration mode will become dominating. It is therefore reasonable to assume that the applied loads with a rise time of 3 ms and 5 ms excite the structure in oscillatory motions with frequencies close to two such resonance frequencies, respectively. This can explain the high levels of dynamic amplification for a wide span of rise times, corresponding to the flat part of the curve in Figure 5.4.
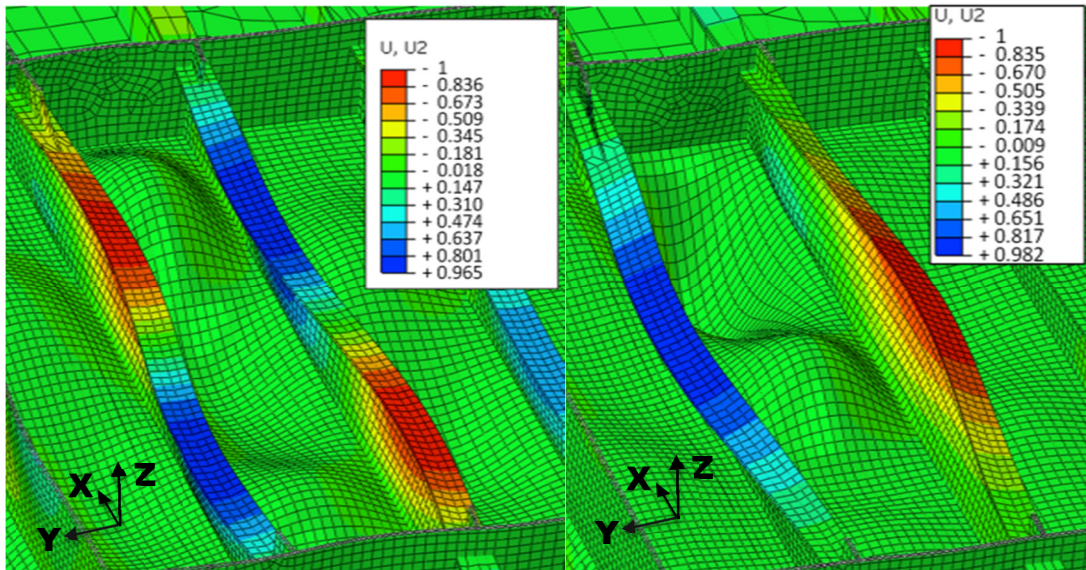
Figure 5.7   Torsional deflection modes of stiffeners. The left-hand side represents a load rise time of 3 ms and the right-hand side represents a load rise time of 5 ms. Scale of deformation: ×40.

The periods corresponding to the frequency of the excited vibrations can be estimated by studying the time series of the horizontal deflections of the stiffener. The horizontal deflection throughout the analysis time for the two different rise times under consideration are shown in Figure 5.8. These are extracted at specific longitudinal positions on the stiffener flange corresponding to the largest oscillation amplitude. The figure indicates that the oscillation period is approximately 11.4 ms for the 3 ms load rise time and 16.9 ms for the 5 ms load rise time. These rough estimations are based on trough-to-peak values for the first oscillation. They confirm that the two different load rise times induce vibratory motions with a different frequency of oscillation.
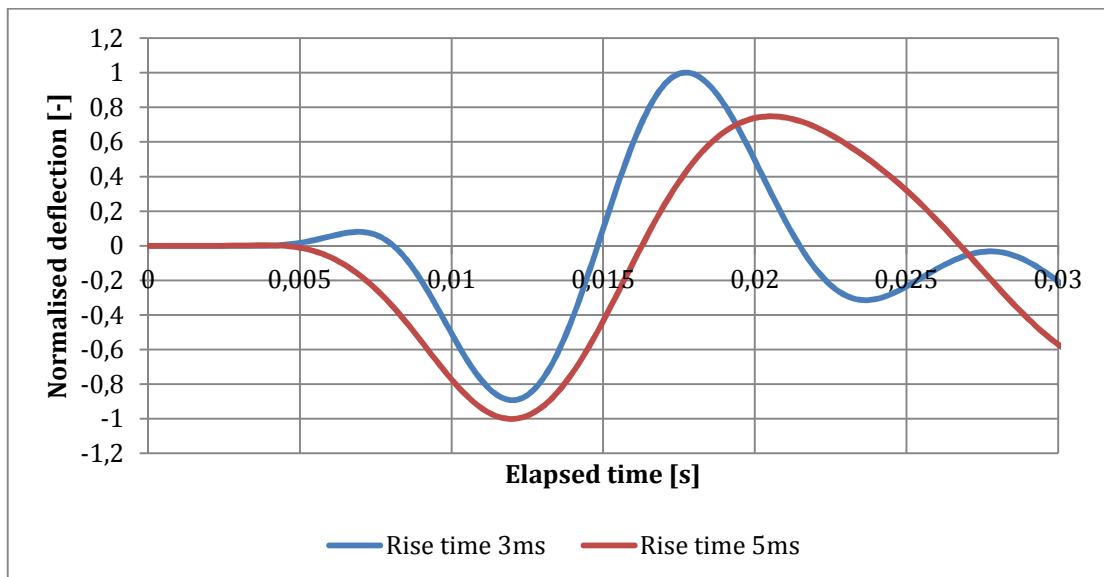

Figure 5.8   Normalised horizontal deflection of stiffener for two different load rise times.

5.3 Effect of load area extent

In order to determine the influence of the load area extent all load cases have to be compared. The load cases are described in Table 3.2 in Chapter 3.4. The response DAF for von Mises stress in the stiffener flange is presented in Figure 5.9. The load rise times that result in dynamic amplification range from 1.5 ms to 10 ms. For the load cases where the load is applied underneath the stiffener the larger load extent gives a higher dynamic amplification. The reason for this behaviour is that the load is distributed to a greater extent in the direction of the stiffener further away from the transverse bulkhead. Since the stiffness of the structure is lower in this direction the dynamic response is also more sensitive to dynamic amplification.

For the case when the load is applied in between two stiffeners the smaller load extent gives the higher dynamic load amplification. The main reason for this behaviour is related to the torsional deflections and their susceptibility to dynamic amplification as described in Chapter 5.2. The larger area, see the green line in Figure 5.9, results in a more distributed load and thus acting closer to the stiffeners. This reduces the torsional dynamic effects on the stiffeners, which in turn reduces the dynamic amplification of the maximum stress in the flange.
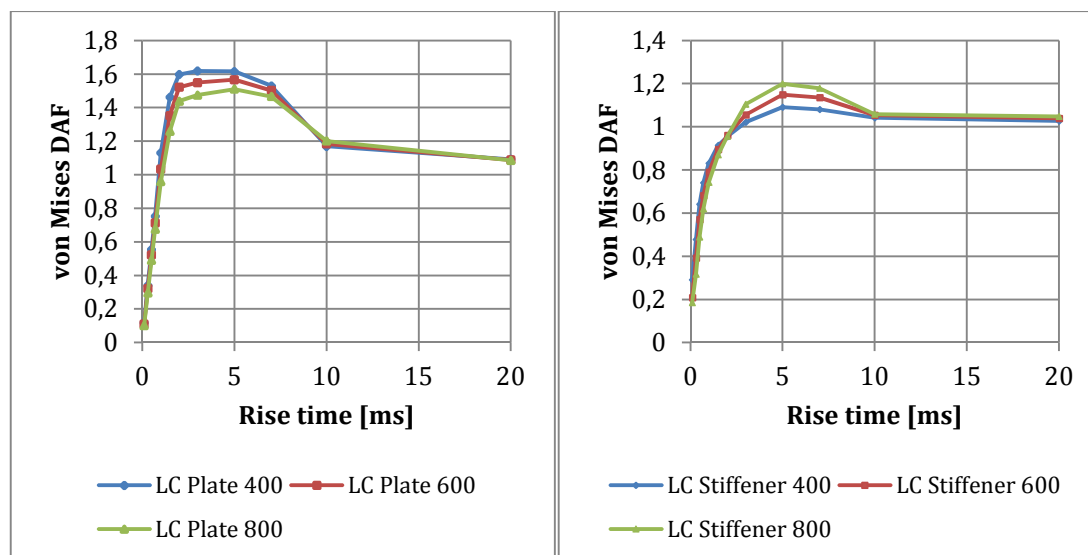

Figure 5.9   DAF for von Mises stress in the stiffener flange.

The comparison of DAF for the maximum vertical deflection of the plate is presented for all load cases in Figure 5.10. The dynamic amplification behaviour of this response is very similar for the analysed load area extents when the load is applied in between the stiffeners. On the other hand, for the load cases when the load is applied under the stiffeners the DAF curves for the different load area extents deviates for high DAF values. The vertical deflection of the plate for LC Stiffener 400-800 is to a greater extent dependent on the deflection behaviour of the stiffener than for LC Plate 400-800. Based on these results it is reasonable to assume that the dynamic amplification behaviour of the plate is non-dependent on the load area extent. Deviations observed in DAF values for the plate deflection for the load cases with the load applied underneath the stiffener can be explained by the dynamic behaviour of the stiffeners. This is based on the similarity between the stiffeners DAF of von Mises stress and DAF values of the plate deflection observed for these load cases.
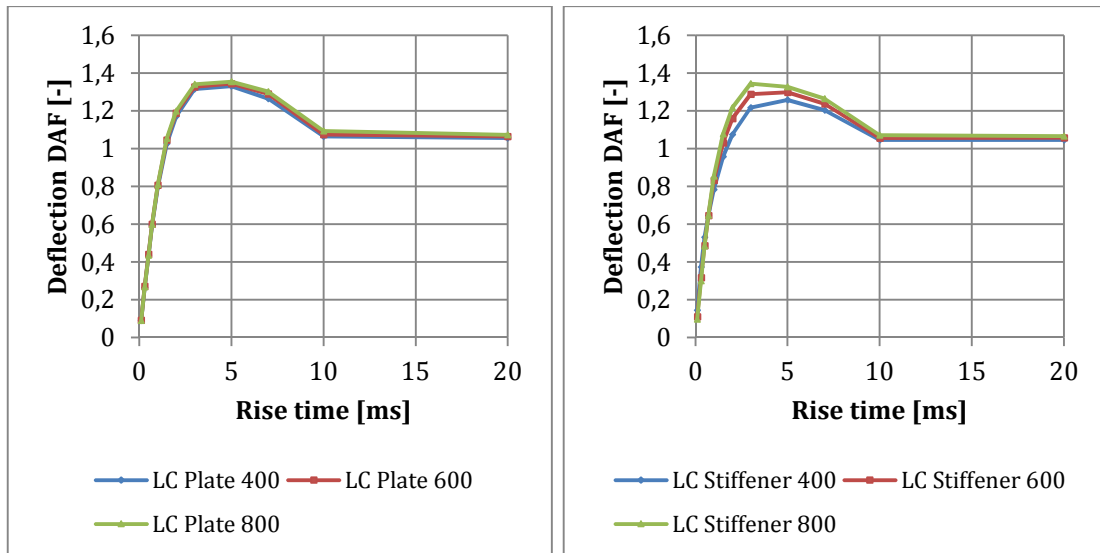
Figure 5.10   DAF for vertical deflection of the plate.

Although the dynamic amplification can be of great importance from a design perspective the relative stress magnitude should also be taken into consideration for the structural members. Figure 5.11 presents normalized magnitudes for the studied responses for all load cases. The response values for the different load area extents are normalized against the corresponding load footprint area. In practice this means that the absolute values of the response are divided by the load area extent of the applied load. The values are then normalized against the highest response value for all of the three load cases under consideration in order to obtain an easy comparison of their relative difference. The reason for normalizing against the load area is that it allows for a more accurate estimation of the pure influence of the load area extent. A larger area would otherwise mean that a higher amount of energy is introduced into the hull structure if the load magnitude is maintained. Since the analyses are linear the introduced energy is directly proportional to the load area this normalization approach is considered feasible.

Both the relative von Mises stresses and deflection presented in Figure 5.11 show a higher response for the smaller load area extent. This means that the larger area extent gives lower values of the actual responses compared to the smaller areas, based on that the same amount of energy is induced into the structure. This can be explained by the fact that the pressure load is distributed to the stiffening elements in the structure, which contributes to decreased stress and deflection levels.

The motivation to compare the normalized responses for the von Mises stress and deflection is that in the case of sloshing impact loads with the same amount of energy, the DAF values show an independency of load area extent. However, by looking at the normalized values the load cases with a smaller area extent gives considerably higher levels of stress and deflection in the structural members, which is worth taking into consideration when studying the dynamic behaviour.
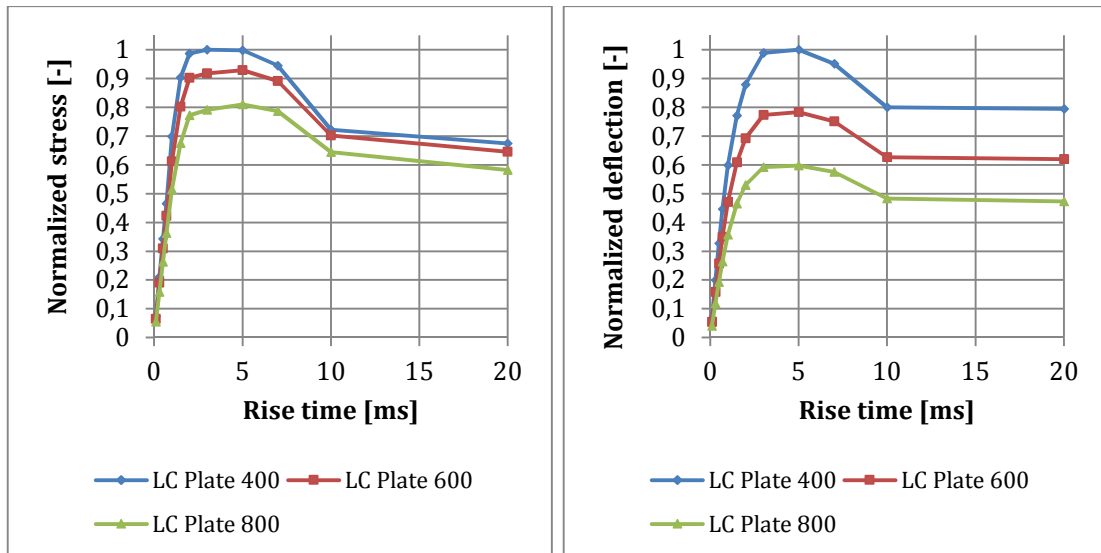
Figure 5.11   Normalized von Mises stress in the stiffener flange (left) and vertical deflection of the plate (right).

5.4 Effect of cargo containment system

Results and discussions from the performed comparative response study aimed at investigating the influence of the CCS are presented in the following. The compared structural responses are von Mises stress in the stiffener flange and vertical deflection in the plate. The studied locations are described in Chapter 5.1.

Figures 5.12 and 5.13 present the DAF for the studied responses for a range of load rise times corresponding to LC SM Plate 400 as defined in Table 4.2 in Chapter 4.5. The figures show that the largest DAF for both studied responses are higher for the small model with the containment system included. The relative difference is especially pronounced for the maximum von Mises stress in the stiffener flange. DAF values of up to 2.04 are observed for this structural response for the SM v.1 case. It can also be seen that the introduction of the CCS shifts the point of largest DAF towards lower rise times. This is an interesting observation since the introduction of only the CCS mass in SM v.2 shows the opposite trend compared to SM v.3. Adding the mass of the CCS without accounting for its stiffness increases the inertia of the system, which in turn increases the natural periods of the system (Biggs, 1964). The fact that the DAF peak for SM v.1 is present for lower rise times indicates that the stiffness of the CCS plays a more significant role for the dynamic behaviour of the studied hull responses than the CCS mass.
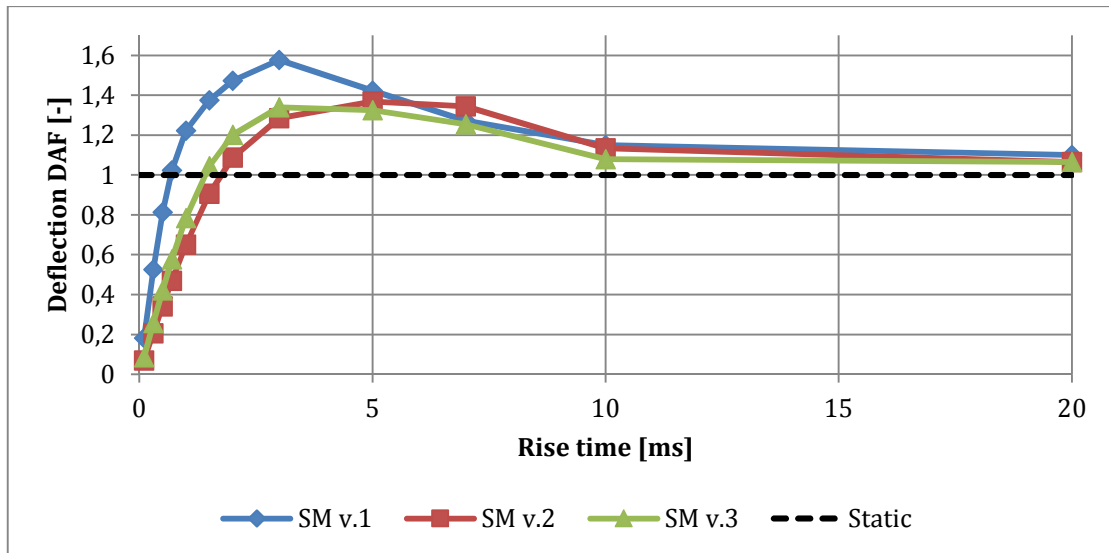
Figure 5.12   DAF for the vertical deflection of the plate for versions of the small model, LC SM Plate 400.
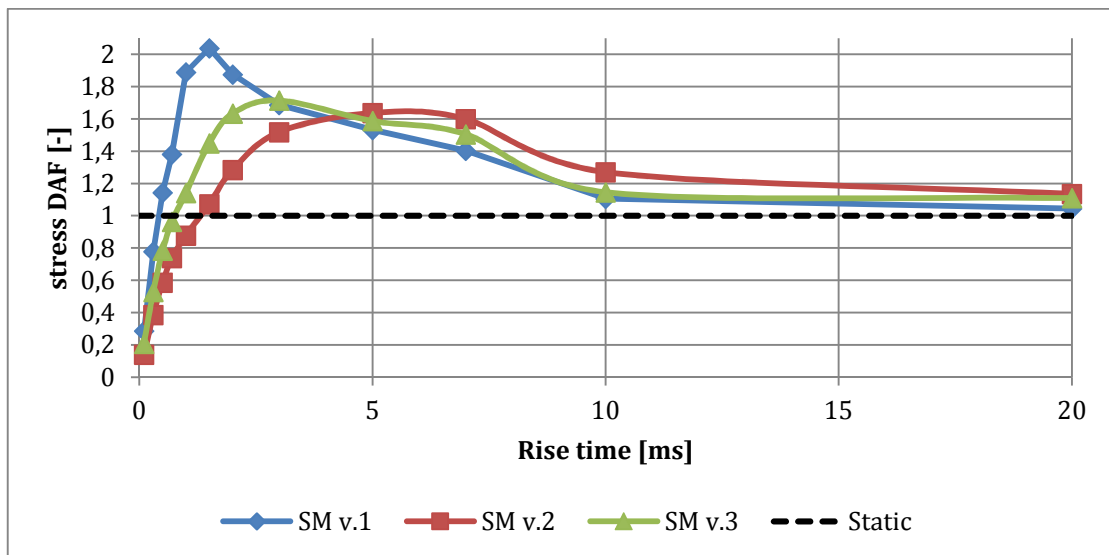

Figure 5.13   DAF for the von Mises stress of stiffener flange for versions of the small model, LC SM Plate 400.

The relative difference in actual response between the versions of the small model is presented in Figure 5.14. The magnitude of both plate deflection and stiffener flange stress is a lot lower for SM v.1 than for the other two versions of the small model. This can to a great extent be explained by the load-distributing effect of the CCS. The translated load acts on a larger area on the hull compared to the applied load. As presented in Figure 5.15, the load footprint indicated in the figure has a much smaller extent than the contact pressure between the CCS and the hull. The contact pressure can be considered as the filtered load acting on the hull and is represented by the contours in Figure 5.15. The contour of the contact pressure naturally follows the contact area between the mastic supports and the hull. This significantly reduces the torsional moments on the stiffeners. Furthermore, it should be said that the modelled CCS together with the cohesive connection between to the hull adds stiffness to the inner deck. This restrains the deflection of the plate, which in turn also contributes to less torsion of the stiffener.
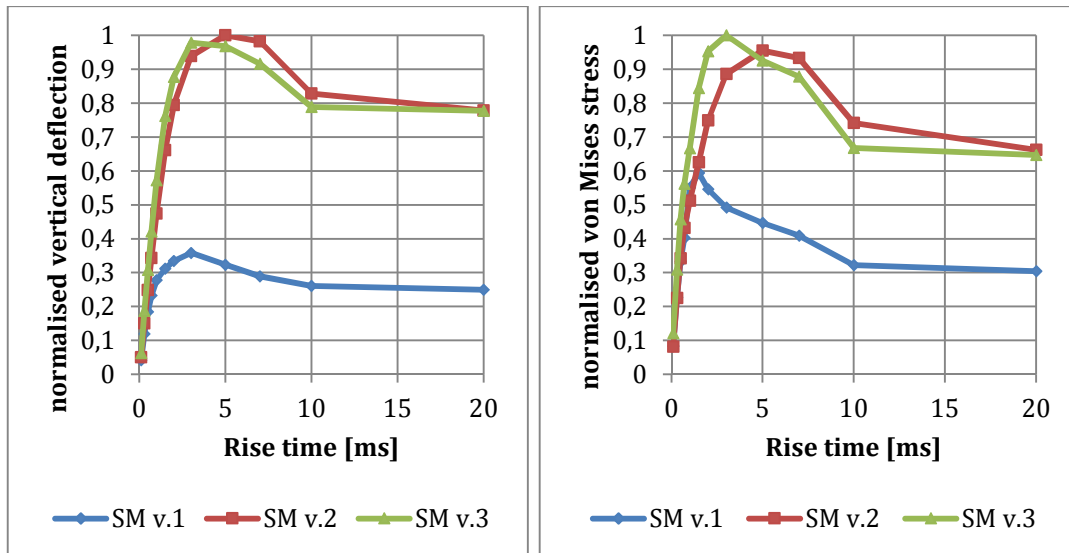
Figure 5.14   Normalized maximum plate deflection and stiffener flange von Mises stress for versions of the small model, LC SM Plate 400.
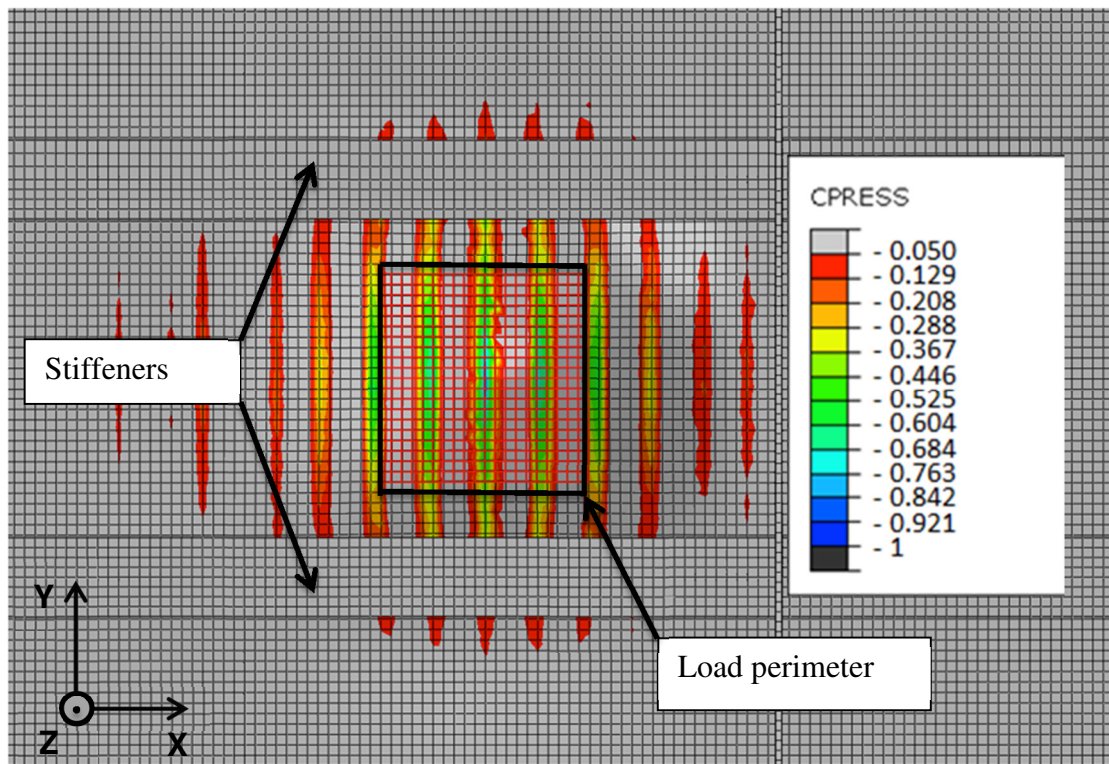
Figure 5.15   Example of the contact pressure field between the CCS and hull structure for LC SM Plate 400 (1.5ms).

Even though the above results indicate that the CCS limits the magnitudes of the torsional deflection behaviour of the stiffeners the phenomenon is still present. Figure 5.16 presents the deflection mode of the stiffener and the location of the maximum stress in the stiffener for the rise time corresponding to the maximum dynamic amplification. The explanation behind this behaviour and its impact on the dynamic behaviour of the stiffeners is discussed in Chapter 5.2. For this case the maximum stress in the stiffener flange occurs 13 ms after the peak of the applied pressure, in

contrast to the case discussed in Chapter 5.2 where the maximum stress occurs after 9 ms.
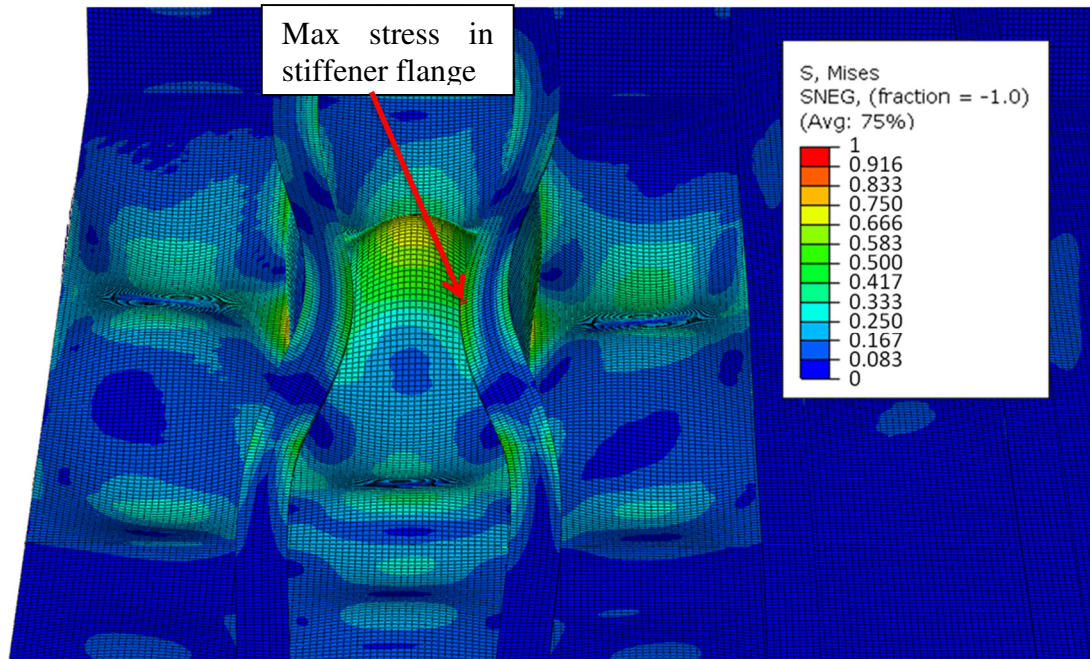

Figure 5.16   Von Mises stress due to the torsional deflection of the stiffener for SM v.1 due to 1.5ms rise time impact. Scale of deformation: ×100.

In Figure 5.17 the DAF for von Mises stress in the stiffener flange corresponding to LC SM Stiffener 400 is presented. Similar to the previously discussed load case the largest DAF for the response is higher for SM v.1 than for SM v.2 and SM v.3. This confirms that the introduction of the CCS increases the dynamic amplification of the response in the structural members. Also, the shift of the maximum dynamic amplification towards rise times around 1 ms is even more pronounced compared to Figure 5.13. This verifies that the CCS contributes to a dynamic amplification for a range of rise times close to 1 ms.
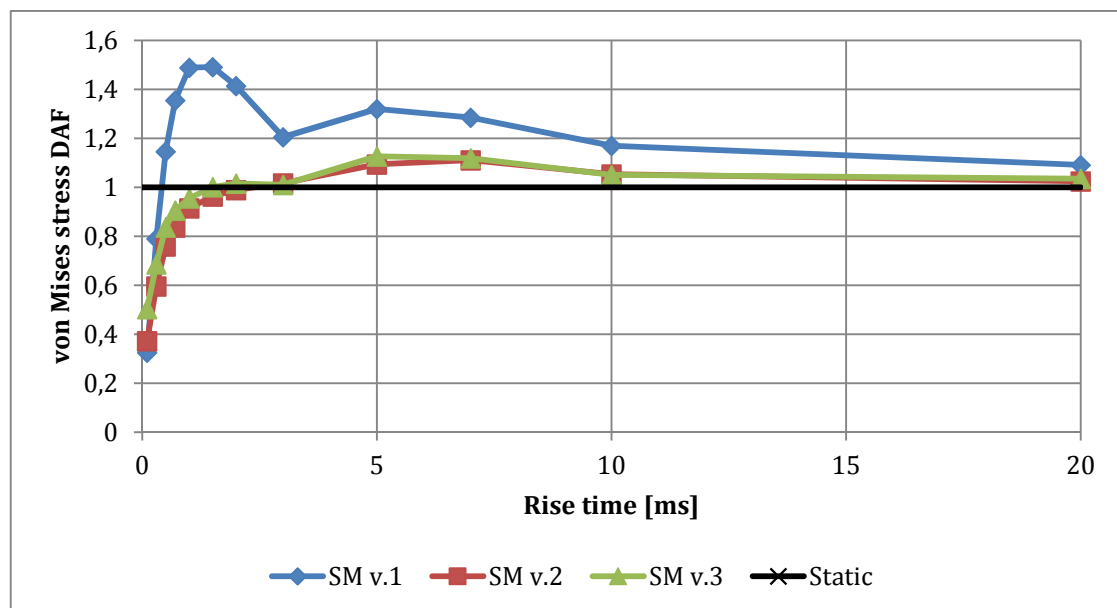

Figure 5.17   DAF for the maximum von Mises stress of stiffener flange for versions of the small model, LC SM Stiffener 400.

The relative difference in actual response between the versions of the small model is very different for LC SM Stiffener 400 compared to LC SM Plate 400. In Figure 5.18, the normalized von Mises stresses in the stiffener flange is presented for the three versions of the small model. The figure shows that the actual response is significantly higher for SM v.1 than for the two other cases at rise times from 0.7 to 2ms. This phenomenon is discussed further in the following.
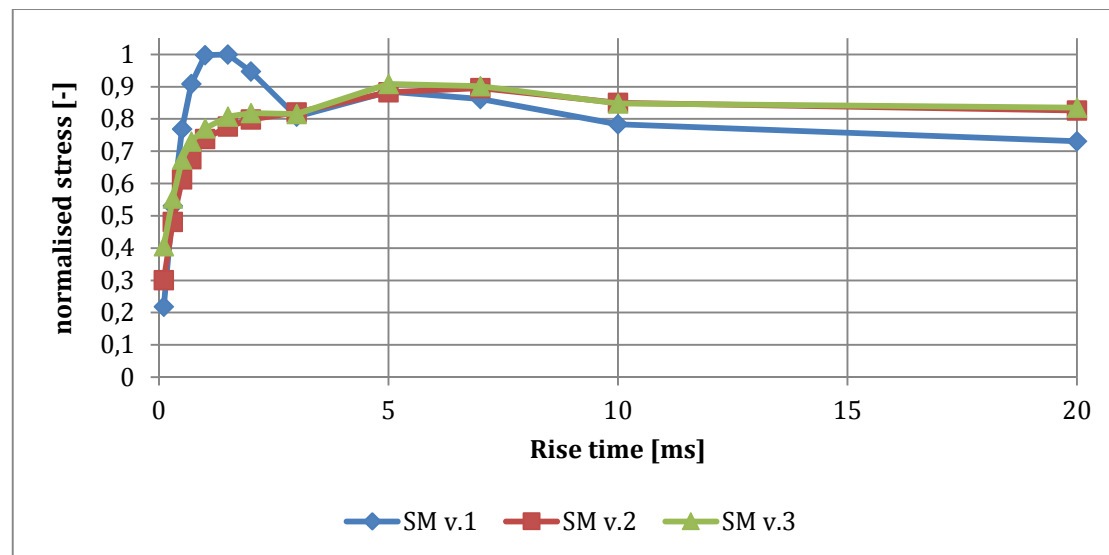
Figure 5.18   Normalized maximum von Mises stress in the stiffener flange for versions of the small model, load case LC SM Stiffener 400.

The contact pressure for two locations between the mastic supports and the inner deck plate is evaluated in terms of dynamic amplification. This is done in order to identify the relationship between the dynamic behaviour of the CCS and the dynamic response in the stiffener flange. The mesh nodes evaluated with regard to contact pressure are located as presented in Figure 5.19. The reason for evaluating the contact pressure in the intersection between the stiffener web and the plate is that these locations experience the highest level of contact pressure, see contours in Figure 5.19. Node 1 corresponds to the point of the maximum contact pressure centred under the applied load. Node 2 is evaluated in order to investigate if the same dynamic behaviour is present for more than just one location.

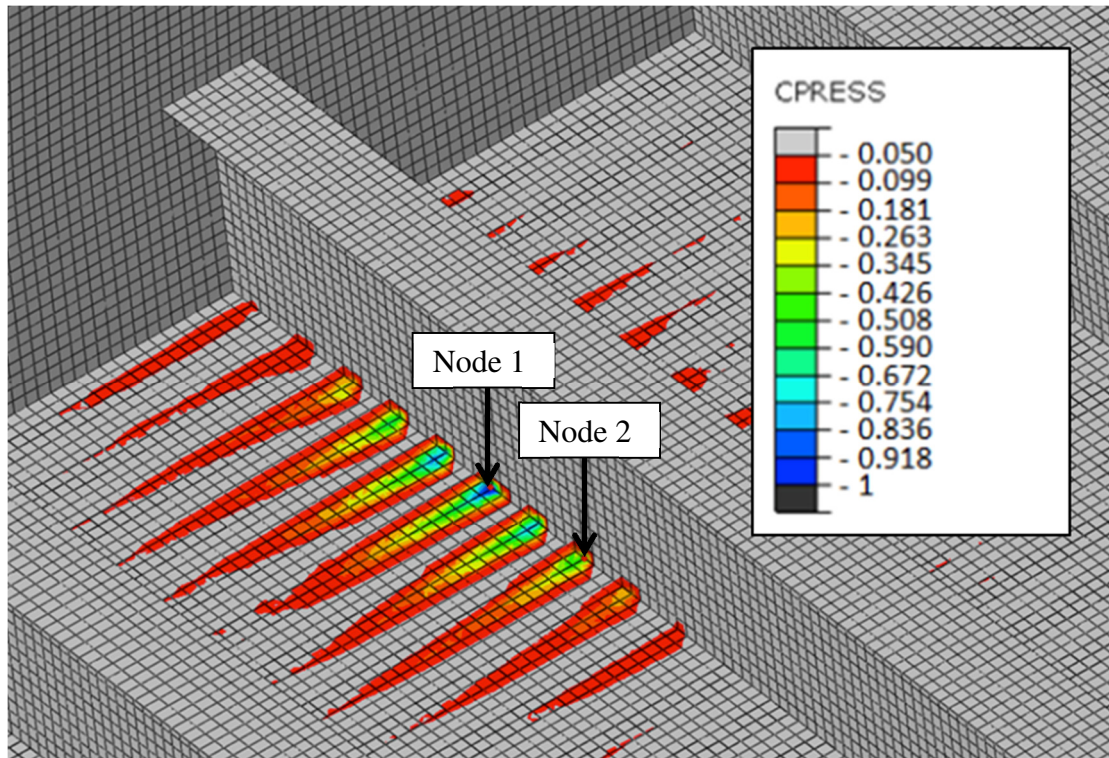*Figure 5.19   Evaluated nodes for contact pressure between the mastic supports of the insulation system and the hull.*

Figure 5.20 shows the DAF of the contact pressure for the two evaluated node locations. Load pulses corresponding to 0.7-2 ms rise times result in high DAF values. This indicates that the transferred load through the CCS onto the hull structure is to a great degree dependent on the dynamic behaviour of the CCS. A resonance period in the CCS would explain the large relative difference in response magnitudes between the versions of the small model that is presented in Figure 5.18 for the set of rise times around 1 to 1.5 ms. This hypothesis is supported by numerical analyses on a MARK III FE-model that have been performed by the R&D structural department at GTT (Pillon, 2009). Here it was found that rise times around 1 ms for uniform pressure impacts resulted in DAF values around 1.5 for normal and shear stresses in the bottom plywood layer of the CCS. The relationship between the shear force and the contact pressure is elaborated further in the following.
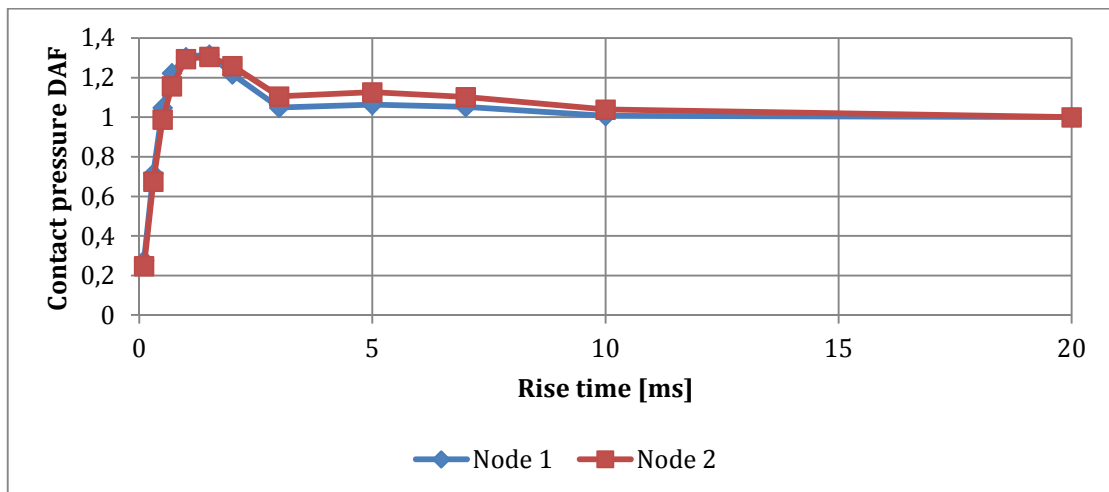
Figure 5.20   DAF for the Contact pressure in two locations, LC SM Stiffener 400.

A principle illustration of the region of interaction between the CCS and hull is presented in Figure 5.21. It indicates the principal location where Pillon (2009) evaluated the shear stresses. A dynamic increase of the shear force at this location will give a simultaneous increase in the reaction force acting on the mastic support. This will in turn result in an increase of the contact pressure, as has been shown in this study.
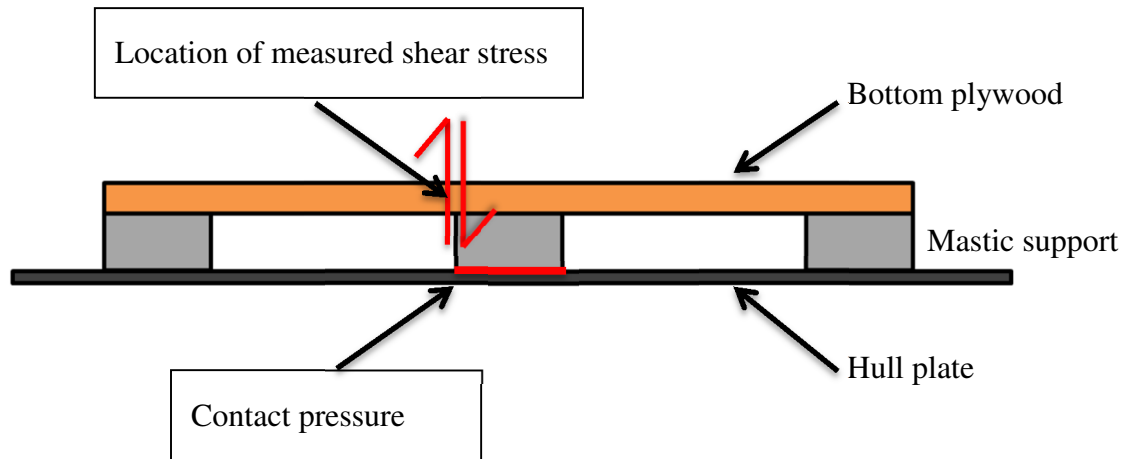
Figure 5.21   Principle outline of the interaction region between the CCS and the hull.

5.5 General observations and concluding remarks

The following aims at outlining general observations made throughout the study. It also covers a comparison between the obtained dynamic amplification values and measured data from previously conducted model tests and full-scale measurements. Furthermore, a discussion regarding limitations in the used method and how these influence the outcome are provided. Finally, a remark is included about the absolute values observed with respect to the material yield limit.

5.5.1 Dynamic behaviour of the structure for short rise times

The applied loads with shorter rise time have for most cases given a very low DAF on the studied responses. A general trend in the results is also the steep increase in DAF values as the rise time approach approximately 1 ms. The main reason for this is that the inertia forces counteract the pressure force when the load duration is a lot shorter than the natural period of the structure. This causes the maximum strain to occur first after the load has decayed, which in turn leads to that the structural response becomes less dependent on the load magnitude (Graczyk et al., 2007). In Figure 5.22 a time series of the von Mises stress is seen, where the response pulse travels in the longitudinal direction and decreases as the vibrations are decaying. The left-hand picture (a) in the figure represents the time instance when the stress is at its maximum, which approximately occurs 1 ms after the load has decayed. Worth noting are the very small deformations.
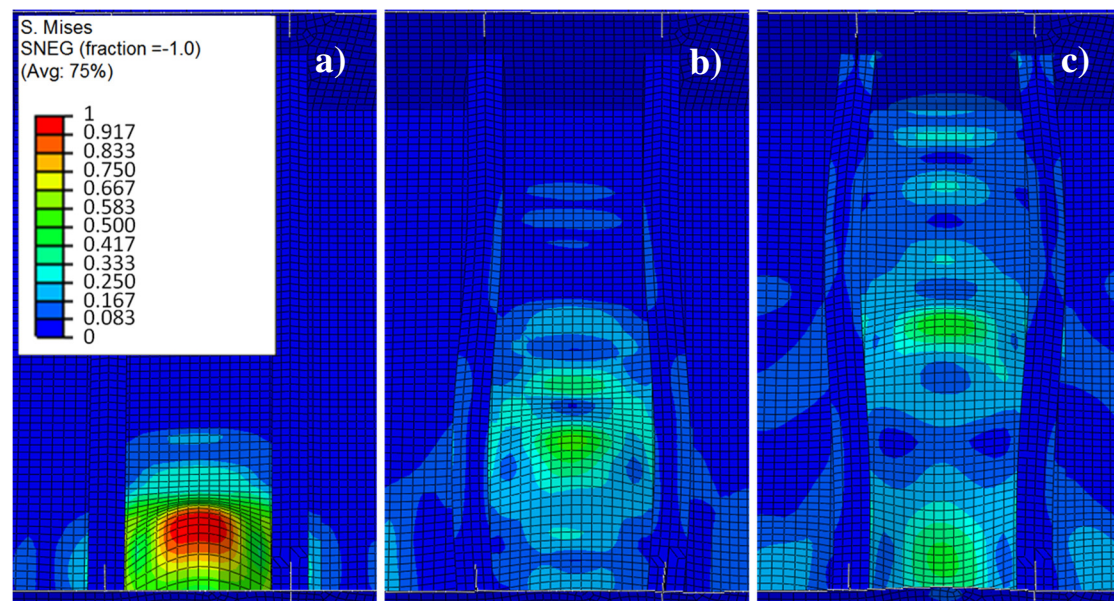
Figure 5.22   A time series of the von Mises stress of for LC Plate 400 rise time 0.1 ms, output taken at three sequential times represented by a), b) and c), respectively. Scale of deformation ×200.

5.5.2 Dynamic amplification compared to measurements

In order to put the results of the study in perspective to what is likely to occur in a vessel in operation, they must be compared with what has been established through model tests and full-scale measurements from DNV GL (2015). The range of rise times that have been seen to commonly occur for the sloshing impact loads are indicated in Figure 5.23. The orange area in the chart indicates the rise times that are most likely to occur and the blue area indicates the range of rise times that also are

present although at a much lower event rates. The figure shows that the higher values for the DAF coincide with a range of rise times that have a high probability of occurrence. This indicates that there is a high probability that the hull structure will experience these levels of dynamic amplification. Therefore this should be considered in the further development of class rules.

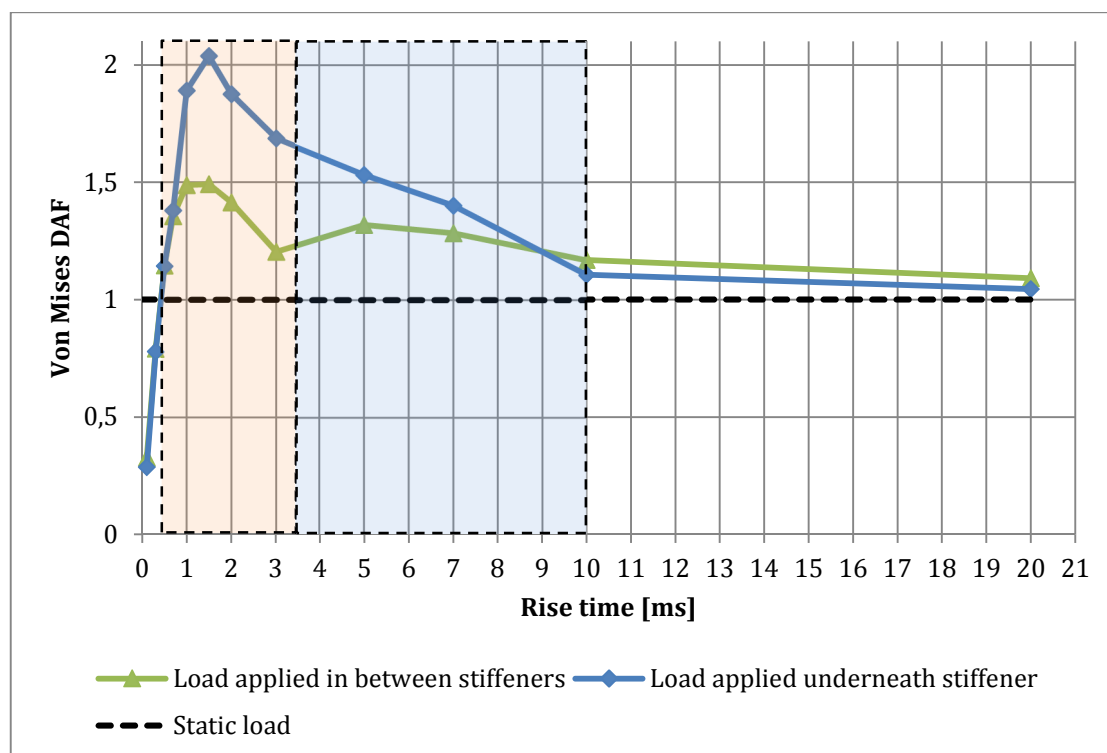*Figure 5.23   Comparison between DAF for the von Mises stress in the stiffener and ranges frequently occurring for sloshing impact in SM v.1. Load cases under consideration are LC SM Plate 400 and LC SM Stiffener 400.*

5.5.3 Concluding remarks

The following provides a discussion regarding the methodology used and the archived results. Limitations and other possible factors that might influence the results are presented in the following.

As the study is limited to one reference vessel it should be said that the results presented are to be treated as trends in the dynamic response behaviour of the hull structure. It is reasonable to assume that the possible presence of brackets or other additional structural members in other vessels that alter the stiffness profile of the structure will influence the dynamic response behaviour. Since class rules do not require any additional elements it is likely that the structural arrangement is similar for other LNG membrane carriers. It is therefore believed that the trends in dynamic response could be considered as being representative.

The studied location in the tank is limited to the upper tank corner. This means that the observed results can only be considered valid for this region. The main reason for this is that the loads acting in other regions are considerably different in their characteristics. An example of this is the lower filling level phenomena, such as hydraulic jump and travelling bore mentioned in Chapter 2.2.1.

Throughout the study, deformations are assumed to be small so that geometric nonlinearity in the applied loads can be neglected. The magnitude and geometric

extents of the applied loads have been based on findings from previously performed model tests and result in small deformations. Therefore, the effects of geometric non-linearity should be small.

The load cases have been limited to the sloshing impact phenomena. Stresses due to global loads like still water bending moment, etc., are thus not considered. The presence of such loads would influence the absolute values of the structural response. Whether or not they influence the dynamic behaviour of the structural response has not been evaluated in this study.

In the FE-models, cut-outs for the longitudinal stiffeners in the web frames and bulkheads have been excluded. It has been observed that stress concentrations occur in the intersection between stiffener and web frame, see Figure 5.24. These effects have been excluded from the results. The simplification in the model could, however, also influence the dynamic behaviour of the stiffeners due to the fact that they are more rigidly fixed in the FE-model compared to the actual vessel. It should, however, be mentioned that the intersection between the stiffener and the web frame in the small model are modelled with a boundary condition that allows for free rotation. The two different boundary conditions do show similar dynamic behaviour, which indicates that the effects most likely are of minor importance to the overall dynamic behaviour of the system.
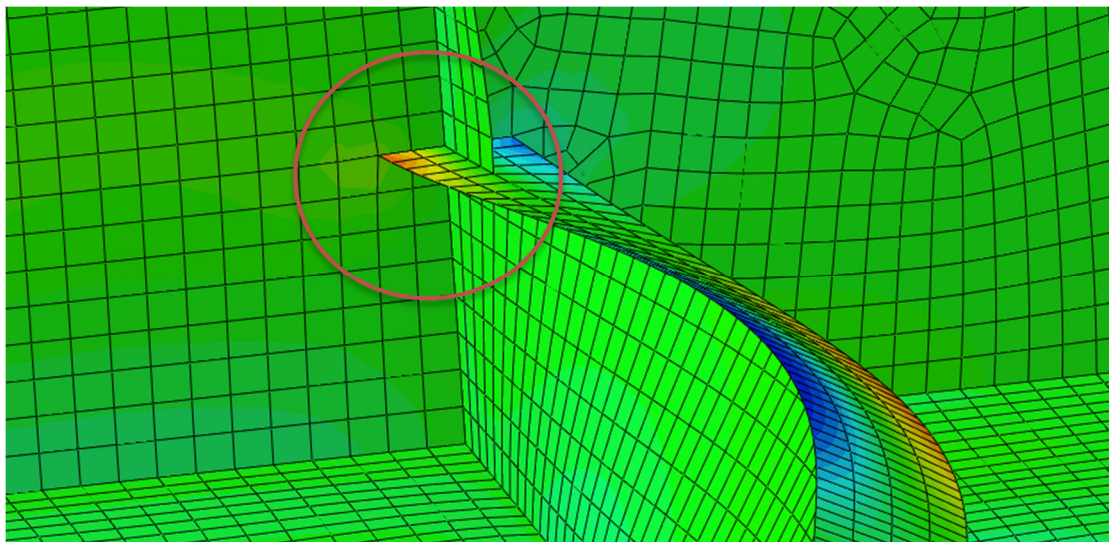
Figure 5.24   Stress concentrations in the intersection between stiffener and web frame.

5.5.4 Discussion regarding absolute values and yield stress

The results presented in this thesis do not cover any absolute values as discussed in the preface. It should, however, be mentioned that for some of the analyses the von Mises stresses have exceeded the material yield stress. The influence on the method and how the results most likely are affected by this is discussed further in the following.

In general it can be concluded that the highest levels of von Mises stresses are observed in the plate segment in the full FE model used for investigating the influence of load parameter variations. When the largest load extent is applied in between two stiffeners the plate segment experiences maximum stresses that are several times greater than the yield limit of the material, which for the studied case is 235 MPa. For

the stiffener, the studied von Mises stresses have much lower magnitudes and the most severe load case results in values that are in the order of the yield stress limit. Exceeding yield in a real structure will influence the dynamic behaviour due to several factors. The method used, however, is based on fully linear analyses, which do not take any post-yield effects into account. This allows for linear scaling of the achieved results making the observed dynamic stress and deflection behaviours also representable for lower response magnitudes. The results regarding the dynamic amplification behaviour of the studied stresses and deflections obtained from the FE analyses throughout this study can thus be considered valid for the linear elastic region.

Considering the results from analyses performed on the small model, the stress levels are shown to be significantly reduced when introducing the structural properties of the CCS. When the insulation system's stiffness and mass is included in the analyses the maximum observed von Mises stress lies on the limit of the yield stress for the plate segment for the most severe load case. For the stresses in the stiffener flange there is quite a large margin to the yield limit. It should, however, be mentioned that the analyses performed on the small model are based on load cases corresponding to the smallest load footprint. Increasing the load area extent whilst maintaining the load magnitude will most likely increase the stress levels in the hull structure, which has been the case for the full model. On the other hand, the load-distributing effect of the CCS might limit this effect to some degree.

The applied load magnitudes are chosen to represent levels of pressure magnitudes that have been measured in model tests and full-scale measurements. As described in Chapter 2.2.2, full-scale measurements have indicated that pressures of up to 1 MPa can be expected in the corner region studied in this thesis. Design pressures from a model test that is based on extreme predictions with an annual exceedance probability of 10^{-3} shows even higher pressure magnitudes, especially for smaller load area extents (DNV GL, 2015). The method used in this thesis thus indicates that local stresses in the hull structure may exceed the yield limit as a result of sloshing impact loads. Therefore, it should be discussed what effects the exceedance of the material yield limit could have on the dynamic behaviour of the structure or more specifically the dynamic amplification of the responses analysed.

One effect from exceeding the yield limit is that local plasticity in the structural members would redistribute the stresses. This limits the maximum stress by spreading the stresses across a larger area extent in the structural members. The results in this thesis regarding dynamic amplification in maximum stress would most likely to some degree be impacted by this phenomenon. The largest DAF values in stress would probably be reduced due to a larger amount of stress redistribution compared to static conditions. This is something that is accounted for in guidance from classification societies when considering linear FE analyses.

Strain hardening is also an effect that is likely to occur when approaching the yield limit when high strain rates in the structure are present. Due to the short duration of the sloshing impact pressures, the strain rate is likely to be high and thereby also the strain hardening effects. This phenomenon can lead to a significant increase in the materials yield limit, which would expand the range of stress levels for where the material can be treated as linear elastic.

Another example where yield might have a great influence on the results is the high DAF values observed for the von Mises stress in the stiffener flange due to excited

torsional deflection behaviours. A small amount of plastic strains occurring in the initial stages of the oscillation motions would most likely limit this resonance phenomenon.

As a final remark, the results obtained in this thesis, regarding the trends in dynamic behaviour should be considered representative. However, the values of the DAF of the studied responses might, in some cases, be influenced by previously mentioned nonlinear material effects when the yield limit is exceeded. As discussed, all results are linearly scalable and thereby considered valid for the linear elastic region. Furthermore, it should be noted that the yield effects discussed in this chapter would most likely result in lower levels of the dynamic amplification. The results from this study are therefore considered conservative in that aspect.

6 Conclusions

The objective with this study has been to quantify the dynamic amplification in structural response expected to occur from sloshing impact loadings in the cargo tanks of LNG membrane carriers. In the following, conclusions from the study are presented.

For the load rise times and load cases under consideration the presence of a dynamic amplification has been shown. The rise times that experience this phenomenon lie within the range of 0.7 to 10ms. For these rise times, observed values of *dynamic amplification factor* (DAF), of stress and deflection, range between 1.05 and 2 depending on load case and whether or not the insulation system is present in the model. These values are valid for the linear elastic material region.

This conclusion together with previously conducted sloshing model tests and full-scale measurements points out that sloshing impact loads are likely to generate high levels of dynamic amplification of the response in the hull. The highest levels of dynamic amplification have been shown to be present for a range of load rise times that have a high probability of occurring in LNG membrane tanks, see Figure 6.1. The orange area indicates the frequently occurring rise times and the blue area represents less frequent, but still occurring rise times. It is therefore recommended that dynamic amplification from sloshing impact is taken into consideration in the continued development of classification rules.
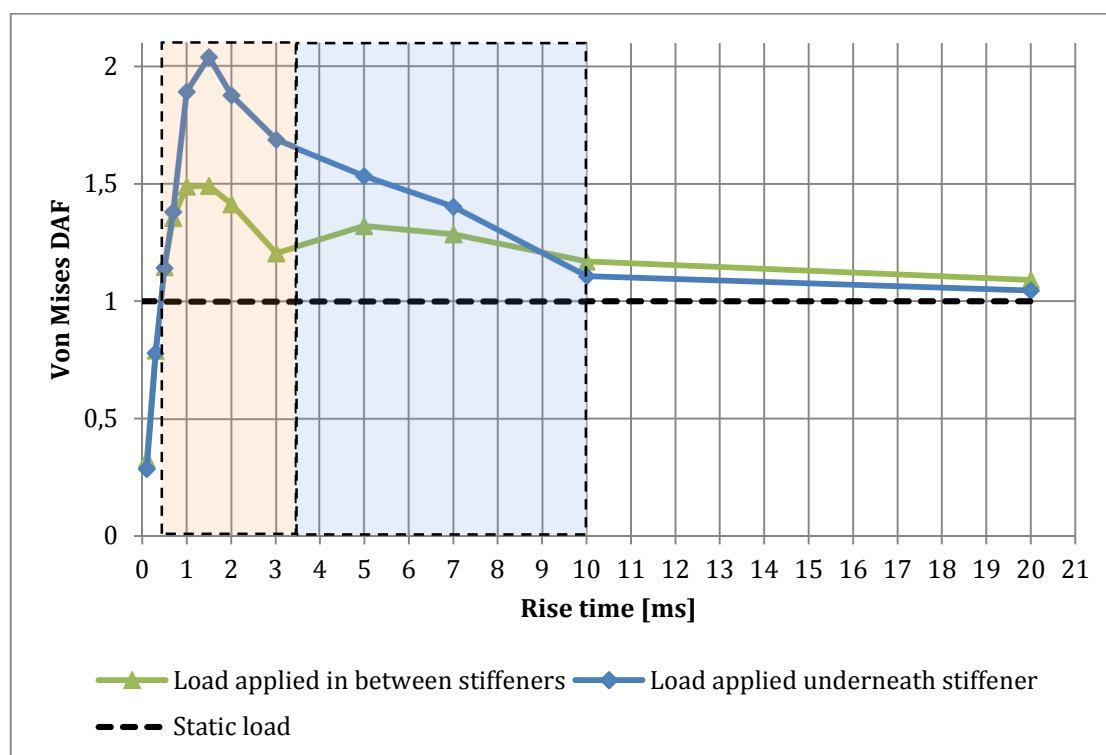

Figure 6.1   A comparison between DAF for the von Mises stress in the stiffener and ranges frequently occurring for sloshing impact in SM v.1. Load cases under consideration are LC SM Plate 400 and LC SM Stiffener 400.

The influence of temporal and spatial properties of the impact loads are as follows:

- It is concluded that the load location has a great influence on the dynamic response of the stiffeners in the inner deck. It has been shown that the torsional deflection of the stiffeners, when the load is applied in between two stiffeners, gives high levels of dynamic amplification of stresses in the stiffeners.
- In general, the increased area has been found to increase the maximum DAF of the structural members under consideration. An exception is, however, when considering the stiffener and the load cases where the load is applied in between two stiffeners. For these load cases the increased area extent gives lower maximum values of dynamic amplification of the stiffener stress.
- Two different excitation modes have been identified for several load cases for key structural elements under consideration. It has been shown that there is a strong connection between the highest levels of dynamic amplification and the occurrence of these deflection modes.

The *cargo containment system* (CCS) has been concluded to have the following influence:

- The cargo containment system filters the load applied before it reaches the hull. The impact load area that reaches the hull is more widely spread compared to the load applied to the cargo containment system.
- It has been observed that the translated pressure through the CCS is amplified for rise times in the range of 0.7 to 2 ms, resulting in a high DAF for the studied responses. The actual values of the response has been observed to be higher when the CCS is included compared to when it is not for certain load cases.
- The most critical load case has been found to have a DAF of magnitude 2. It is close to the maximum theoretical value as discussed by Biggs (1964). It should be noted that the reason for the high DAF value is due to torsional moments acting on the stiffeners. In order to increase the resistance against these amplified loads, stiffening by increasing the web height is not recommended since this would increase the torsional behaviour. Instead, torsional limiting members such as tripping brackets are a better option.
- It has been concluded that the stiffness of the CCS has been found more significant than the mass of the CCS in terms of dynamic behaviour of the hull. Therefore it is not recommended to model the CCS only by its mass in order to give a good representation of the dynamic behaviour.

7 Recommendations for future work

This study has investigated the influence of a number of load parameters and load cases. In order to give a more extensive knowledge of the dynamic behaviour of the structure, the following is recommended as future work:

- Determine how the results and conclusions from this study could be used for the continued development of requirements from classification societies.
- Expand the study to cover tank parts that are likely to experience sloshing impact loads for lower filling levels since they are quite different in their characteristics.
- Evaluate how non-linear material properties influence the dynamic response of the structure. This could be important information in order to determine whether or not the high levels of dynamic amplifications found in this study should be considered as a concern when designing against sloshing impact loads.
- Evaluate if local stress concentrations could be a concern for the design of the structure in areas such as cut-outs or brackets.
- Consider to implement actual pressure magnitudes and load footprints that are measured in sloshing model tests and full-scale measurements.
- Investigate the influence of the ratio between rise time and total load duration. It has been observed in the study that the load can act as a dampener when the structural response oscillates with periods shorter than the load duration.
- Consider the possibility of applying global loads to the model in order to determine if this has an influence on the dynamic behaviour of the hull.

8 References

ABS (2006): *Guidance Notes on Strength Assessment of Membrane-Type LNG Containment Systems under Sloshing Loads*, American Bureau of Shipping, Huston, USA.

Belytschko, T., Wong, B. L, Chiang, H. Y. (1991): Advances in One-Point Quadrature Shell Elements. *Computer Methods in Applied Mechanics and Engineering*, Vol. 96, No. 1, 1992, pp. 93-107.

Biggs, J. M. (1964): *Introduction to Structural Dynamics*. McGraw-Hill, USA.

Bogaert, H., Brosset, L., Kaminski, M. L. (2010b): Interaction Between Wave Impacts and Corrugations of MarkIII Containment System for LNG Carriers: Findings From the Sloshel Project. In *Proceedings of the Twentieth International Offshore and Polar Engineering Conference*, 20-25 June 2010, Beijing, China.

Bogaert, H., Léonard, S., Brosset, L., Kaminski, M. L. (2010a): Sloshing and Scaling: Results from the Sloshel Project. In *Proceedings of the Twentieth International Offshore and Polar Engineering Conference*, 20-25 June 2010, Beijing, China.

Dassault Systèmes (2014a): ABAQUS (Version 6.14). [Computer software]. Providence, USA: Dassault Systèmes Simulia Corp.

Dassault Systèmes (2014b): *ABAQUS 6.14 Documentation*, Dassault Systèmes Simulia Corp., Providence, USA.

DNV (2008): *Classification Notes No. 31.9: Strength Analysis of Hull Structure in Liquefied Gas Carriers with Membrane Tanks,* Det Norske Veritas, Høvik, Norway.

DNV (2011): *Offshore Technical Guidance OTG-02: Floating Liquified Gas Terminals,* Det Norske Veritas, Høvik, Norway.

DNV (2013): *Rules for Classification of Ships Part 5 Chapter 5,* Det Norske Veritas, Høvik, Norway

DNV (2014): *Classification Notes No. 30.9: Sloshing Analysis of LNG Membrane Tanks,* Det Norske Veritas, Høvik, Norway.

DNV (2015): *Rules for Classification of Ships Part 3 Chapter 1,* Det Norske Veritas, Høvik, Norway.

DNV GL (2015): Documentation on sloshing model tests and full-scale measurements, Documents have restricted access due to confidentiality.

Fadini, G. C. (2014): *Crack Identification Method for Mechanical Structures* (Master thesis, Politecnico di Milano, Department of Mechatronics and Robotics).

Graczyk, M. (2008): *Experimental Investigation of Sloshing Loading and Load Effects in Membrane LNG Tanks Subjected to Random Excitation* (Doctoral thesis, Norwegian University of Science and Technology, Department of Marine Technology).

Graczyk, M., Moan, T. (2008): A Probabilistic Assessment of Design Sloshing Pressure Time Histories in LNG Tanks. *Ocean Engineering, Ocean Engineering,* Vol. 35, No. 8-9, 2008, pp. 834-855.

Graczyk, M., Moan, T., MingKang, W. (2007): Extreme Sloshing and Whipping-Induced Pressures and Structural Response in Membrane LNG Tanks. *Ships and Offshore Structures*, Vol. 2, No. 3, 2007, pp. 201-216.

GTT (2012a): *Products: Mark III System.* Retrieved from http://www.gtt.fr/product/mark-iii-system/.

GTT (2012b): *Products: NO 96 System.* Retrieved from http://www.gtt.fr/product/no96-system/.

Lafeber, W., Brosset, L., Bogaert, H. (2012): Comparison of Wave Impact Tests at Large and Full Scale: Results from the Sloshel Project. In *Proceedings of the Twenty Second International Offshore and Polar Engineering Conference*, June 17-22 2012, Rhodes, Greece.

Lee, D. H., Kim, M. H., Kwon, S. H., Kim, J. W., Lee, Y. B (2006): A Parametric Sensitivity Study on LNG Tank Sloshing Loads by Numerical Simulations. *Ocean Engineering,* Vol. 34, No. 1, 2007, pp. 3-9.

Liu, G. R., Quek, S. S. (2013): *The Finite Element Method: A practical course*. Elsevier, Oxford, UK.

Malencia, Š., Kwon, S. H. (2013): An Overview of the Hydro-Structure Interactions During Sloshing Impacts in the Tanks of LNG Carriers. *Brodo Gradnja*, Vol. 64, No. 1, January 2013, pp. 22-30.

Pastoor, W., Østvold, T. K., Byklum, E., Valsgård, S. (2005) Sloshing Load and Response in LNG carriers for New Designs, New Operations and New Trades. In *Proceedings of Gastech*, 14–17 March 2005, Bilbao.

Pillon, B., Marhem, M., Leclère, G., Canler, G. (2009): Numerical Approach for Structural Assessment of LNG Containment Systems. In *Proceedings of the Nineteenth International Offshore and Polar Engineering Conference*, 21-26 July 2009, Osaka, Japan.

Tavakoli, H. R., Kiakojouri, F. (2013): Numerical Dynamic Analysis of Stiffened Plates under Blast Loading. *Latin American Journal of Solids and Structures,* No. 11, 2013, pp. 185-199.

Appendix A – Parametric analysis on sloshing impact loads

Before fitting a cargo tank with a membrane-type containment system model tests are performed in order to estimate the loads acting on the system. The output data of a sample of model test reports are analysed in order to investigate if any relationship between the design loads and basic parameters of the vessel and/or the tank dimensions can be found.

The data sample under consideration consists of 8 model test reports where 5 of them have differences in dimensions both for vessel and tanks. The redundant vessels are left out of the study. The capacity of the vessels ranges from approximately 160 000 to 174 000 m^3.

The reports contain information of sloshing impact pressures of high (95%) and low (10%) filling level of the tanks for different levels of exceedance probability. The pressures are meant to serve as validation that the expected loads fall within the CCS strength. They are based on long-term distributions of measured sloshing impacts acquired from model tests. The methodology behind sloshing model tests and treatment of the measured data are described in DNV GL's classification note No. 30.9 (DNV, 2014). The tank closest to the bow has a different shape compared to tank number 2, 3 and 4 due to a different hull cross section for all studied vessel. The reports therefore take tank number 1 and 4 under consideration.

Study of ship specific parameters

The goal with this study is to conclude whether or not any simple relationship between the design pressures given from the model tests and ship particulars could be found. The parameters evaluated are the basic geometrical dimensions such as length and breadth of both the ship and tank under consideration. Chamfer angles in the tank's sides, tank height, the ships *metacentric height* (GM) and period of roll are also parameters that are included in the study.

In order to investigate any possible relationship, scatter diagrams are used to plot each vessel's design pressure against the corresponding parameter under investigation. This is performed for all the abovementioned ship specific parameters and at three different impact areas; 0.04, 0.48 and 0.96 m^2, respectively. Both tank number 1 and tank number 4 at high and low fillings are evaluated in this study.

The main conclusion from this parametric study is that the amount of relevant data contained within the available test reports has proved insufficient to say if any direct relationship is present. The limited sample size and the relatively small variations in the studied dimensions (within 10%) are the main contributing factors to this issue. GM is, however, a parameter that poses as an exception to the above stated and are thus treated further in the following.

The variation in GM for the vessels under consideration should be considered as significant since the values varies from approximately 1 to 4 m when sailing at design draught (DNV GL, 2015). Furthermore, the results from the parameter study show that a potential correlation between the design pressure and GM is present, at least for vessels with GM > 2 m, see Figure A.1. The figure illustrates normalized values of model test design pressures expected to occur in tank number 4 during high fillings plotted against the GM for the corresponding vessels. The values are normalized

against the highest presented pressure. This result can be considered as reasonable since GM is proportional to the ship motion accelerations, which in turn is believed to be a driving factor for sloshing occurrences (DNV, 2015). It should be noted that the GM values used in this study are based on available stability data from the vessels as operational, whilst the pressure data are based on model tests performed during the design stage of the vessel. This implies that the GM values used in this study may vary from the ones used in the seakeeping calculations during the model tests. It is, however, considered as negligible in the current study, since such variations are believed to be consistent for all studied cases and thus not effecting potential trends.

Figure A.1 also presents a set of data points corresponding to sloshing impact design pressures that are calculated in accordance to the class rules. These are based on the averaged dimensions and geometric specifications of the investigated vessels and are scaled up in order to be comparable with the local design loads as given from the model tests. Even though the available data is outside of the valid range of GM according to (DNV, 2015) the results suggests that there is a strong correlation in trend between model tests and class rules for the vessels with GM exceeding 2 m. This holds true for all studied impact areas. For the two vessels corresponding to the GM values lower than 2 m the trend in relation towards the pressure is inconsistent.
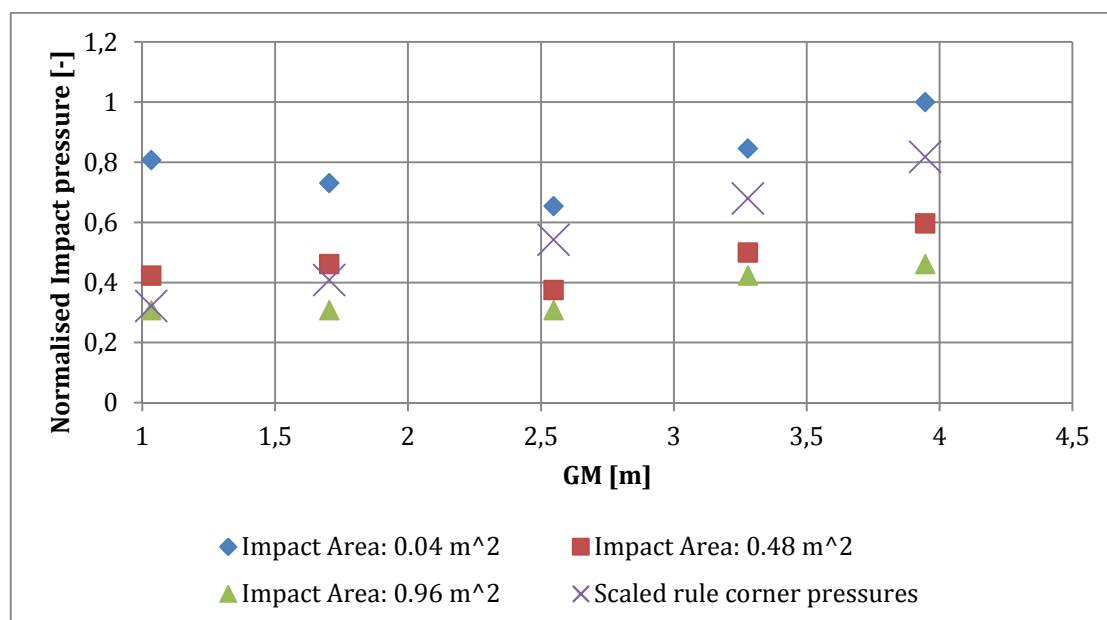

Figure A.1   Scatter plot illustrating trends between model test design impact pressure and GM for tank no. 4 at high fillings.

An observation worth noting is that the spread in the evaluated design pressures increases for a decreasing impact area. The standard deviation in available samples of design pressure has been calculated and shows a decreasing trend with an increasing impact area. This supports the fact that the high impact pressures during sloshing is a highly localized phenomenon.

A study of heading and liquid period relationship

A simple relationship between basic parameters such as tank length or breadth compared to sloshing impact pressure is hard to find. One of the theories discussed early in the project is the possibility that the amplitude of the pressures is highly dependent on the tank breadth-to-length ratio, although this correlation could not be shown from the data extracted from the model test reports. Developing this concept, a hypothesis concerning the impact of heading direction compared to tank fluid Eigen period is considered, where the aspect ratio of the tank length to breadth has a contribution. From the output data in the model test reports the liquid Eigen period can be extracted for different filling levels. The hypothesis can also be supported by DNV GL classification note NO. 30.9 (DNV, 2014). The note states that the most severe cases of sloshing impact takes place when the motion of the vessel is close to the resonance period of the fluid in the tanks.

Due to limitations of input data in some of the reports and also a limitation in the output data for filling levels, the hypothesis was evaluated by only considering tank number 4 and with a 95% filling level. The shape of this tank was most consistent and data was available for all studied vessels, which made it the most suitable to use. Only one of the reports contains the *response amplitude operator* (RAO) of the tank motions with regard to the heading angle and sea state, though the comparison between Eigen period and sloshing event rate could be made for all 6 of the reports under consideration.

Available data is given as a transverse and longitudinal fluid period for the different tanks of the vessel. In order to estimate the period in other directions than transverse and longitudinal direction, assumptions were made that they could be approximated with Pythagoras theorem. This assumption was considered to be more valid for heading angles of the vessel, which was close to the ratio between length and breadth of the tank under consideration.

The investigated correlation between the liquid period and the magnitude of the sloshing impact pressures could not be found and therefore these parameters cannot be used in order to evaluate the expected impact pressures that will act on the hull structure.

In general no simple correlation between the sloshing impact load magnitudes and ship-specific parameters could be found, except from the GM of the vessels. With more extensive data and possibly a larger interval of parameters it could be advantageous to establish such relations, if they exist.

Appendix B – Size-dependency study

The initial FE-model that was produced for the sensitivity analysis presented in this master thesis covered the full breadth of the tank, see Figure B.1. This requires a significant amount of computational effort to be analysed dynamically. The extent of this model was based on the assumption that the sloshing impact loads are a highly localized phenomenon. In order to save computation time a size-dependency study was therefore performed. Here the model is reduced by half the beam and thus only covers the port side of the tank partition and then compared against the initial model.
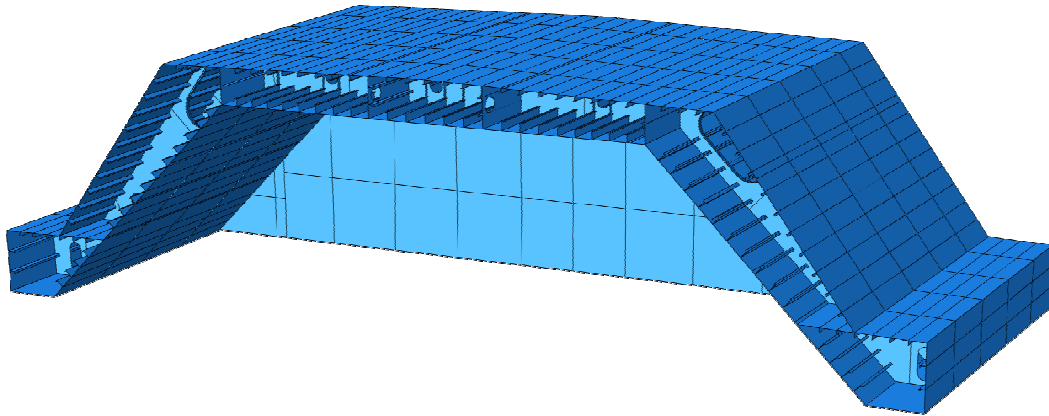

Figure B.1   Overview of initial FE model.

The reduced model is taken as half of the breadth of the initial model. In the centre line there is a need to introduce boundary conditions that represent the stiffness of the tank side that is taken away in the reduced model. The boundary conditions that are introduced in two versions of the reduced model are set to represent two extreme cases with regards to structural stiffness. In one case the centre line boundaries are fixed, in the other one they are simply supported in the boundaries of the inner deck plate and the plates of the transverse bulkheads. All other boundary conditions are set as fixed for both the initial model and the reduced models. Figure B.2 illustrates the reduced model and location of the boundary conditions.
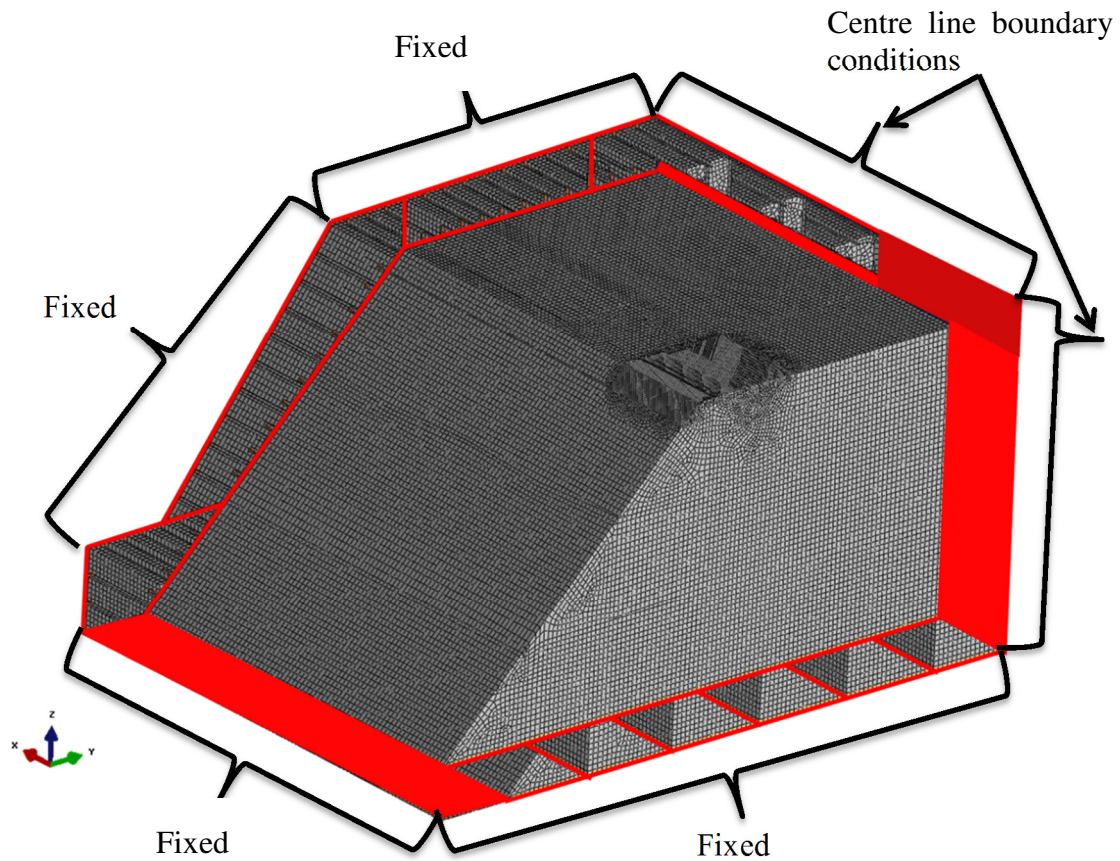
Figure B.2   Overview of the reduced FE model including locations for applied boundary conditions. The centre line boundary conditions are altered between the two versions of the reduced model.

In order to get a fair comparison between the models, the mesh is identical for both cases. The full beam model is discretized with ABAQUS Explicit default mesh with specifics as presented in Table B.1. In the half-beam model the calculation domain is simply reduced by removing the mesh elements on the starboard side of the tank symmetry line. This procedure assures an identical mesh, in the area of interest, for both models.

Table B.1   Mesh specifics used in the size-dependency study.

Element type:	S4R/S3R (standard shell elements)
Element shape:	Quad Dominated
App. element side length:	170 mm

To evaluate if the reduced model is of sufficient size with regard to capturing similar dynamic response behaviour compared to the initial model, four analyses are performed. Two different load cases for each model (see Table B.2) are analysed using an explicit solver. The load cases represent an impact load with two different rise times and are meant to cover the span of load dynamics that is of interests for the main study.

Table B.2   *Evaluated load cases in the size-dependency study*

Model	Rise Time [ms]	Decay time [ms]
Initial model	1	2
Reduced model	1	2
Initial model	10	20
Reduced model	10	20

The load amplitude and loaded area extent are taken as arbitrary values, which are kept constant throughout this comparative analysis. The full corner plate field is used for load application as presented in Figure B.3. The loaded area thus spans from the transverse bulkhead to the first web frame in the longitudinal direction and from the chamfer to the first girder in the transverse direction. This is significantly larger than the exposed area during a typical sloshing event. The load amplitude is set to 1 MPa.
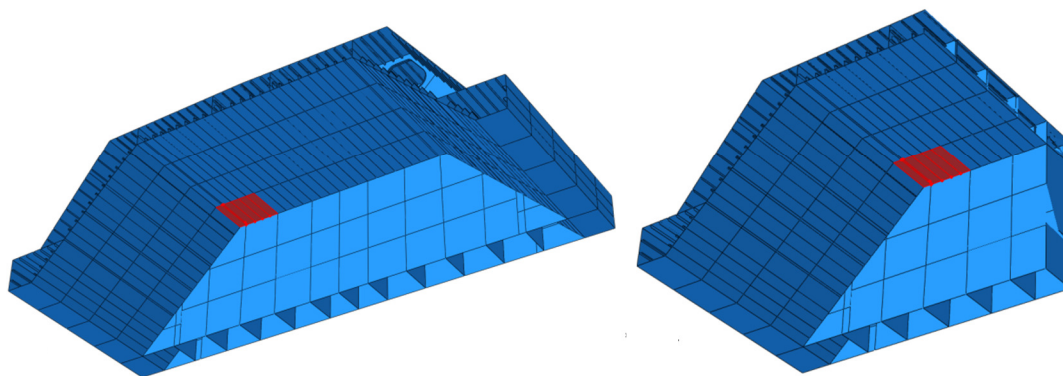

Figure B.3   *Loaded areas for the comparative study indicated in red for both model extents.*

The compared responses are the deflection in the *vertical direction* (U3) and the *first principle stress* (S11). U3 is recorded from a specific node in the plate field and S11 in a specific element on a stiffener flange. The exact locations are the same for both models and are indicated in Figure B.4.

The motivation behind these responses and their locations is that they represent areas that will experience high response levels. Therefore, they can be seen as a good indication to whether or not the response behaviour is similar for the two models. Furthermore, the stiffener flanges and the plates are the structural members under consideration in the main study, and therefore it is crucial that the model can accurately describe the response in these. The reason that stress and deflection components are evaluated instead of effective stress and multiaxial deflection is that these give a more representative description of the dynamic behaviour.
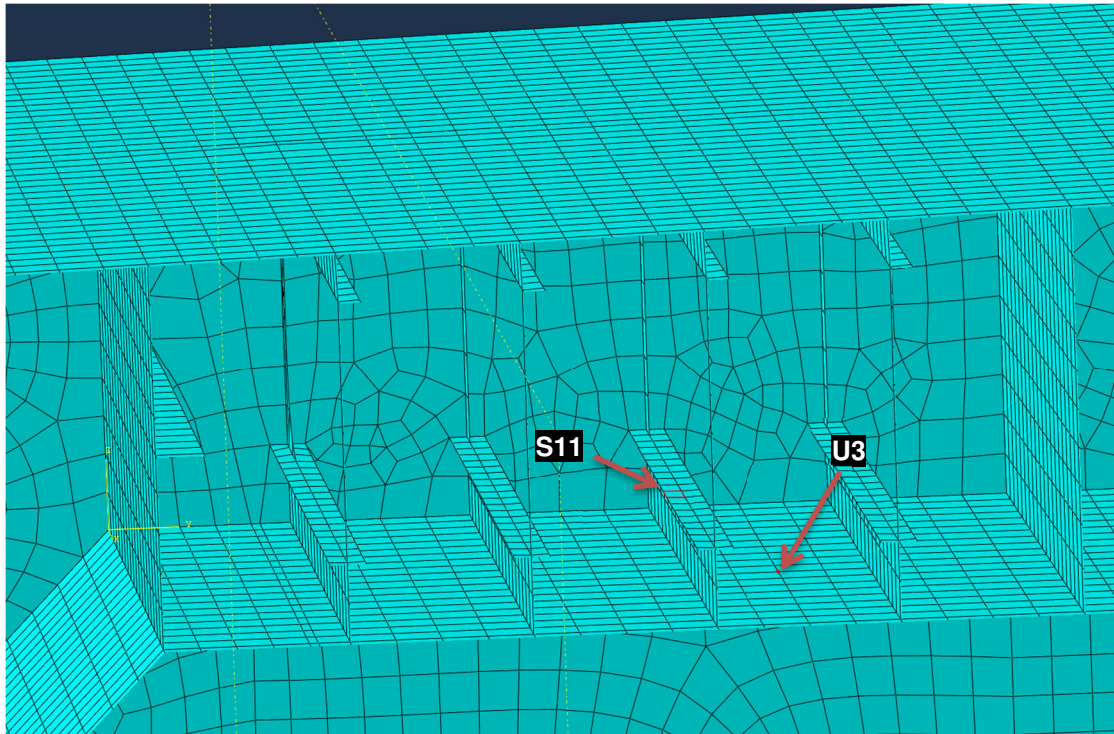
*Figure B.4   An illustration of the locations for response extractions.*

Table B.3 presents the relative difference of the maximum values for the investigated responses between the reduced models and the initial model. The results from the analyses with a load rise time of 1 ms are identical for the compared model whilst for the case with a load rise time of 10 ms the results show a minor difference in peak value. The effect of the boundary condition cannot be totally neglected but the differences in the results are not more than 1.5 %, which is considered as being sufficiently accurate.

Table B.3   Relative difference in maximum response compared to the full model from investigated time series.

Model	Rise time [ms]	Relative difference in maximum deformation U3 from full model
Fixed boundaries	10	0,60 %
Simply supported boundaries	10	-0,40 %
Fixed boundaries	1	0,01 %
Simply supported boundaries	1	-0,01 %
Model	Rise time [ms]	Relative difference in maximum stress S11 from full model
Fixed boundaries	10	-0,40 %
Simply supported boundaries	10	-0,2 %
Fixed boundaries	1	0,008 %
Simply supported boundaries	1	0,006 %

Table B.4 illustrates the full time series of the response during the analyses. The table shows that difference in response behaviour is in most cases very small between the models. A significant difference can, however, be distinguished in the later parts of the studied time series, especially for the analyses of 10 ms load rise times. This is of minor importance for the main study, since it is the maximum response (initial peak) that is of interest.

Table B.4   A comparison of response time series between the different model cases for the studied loadings.
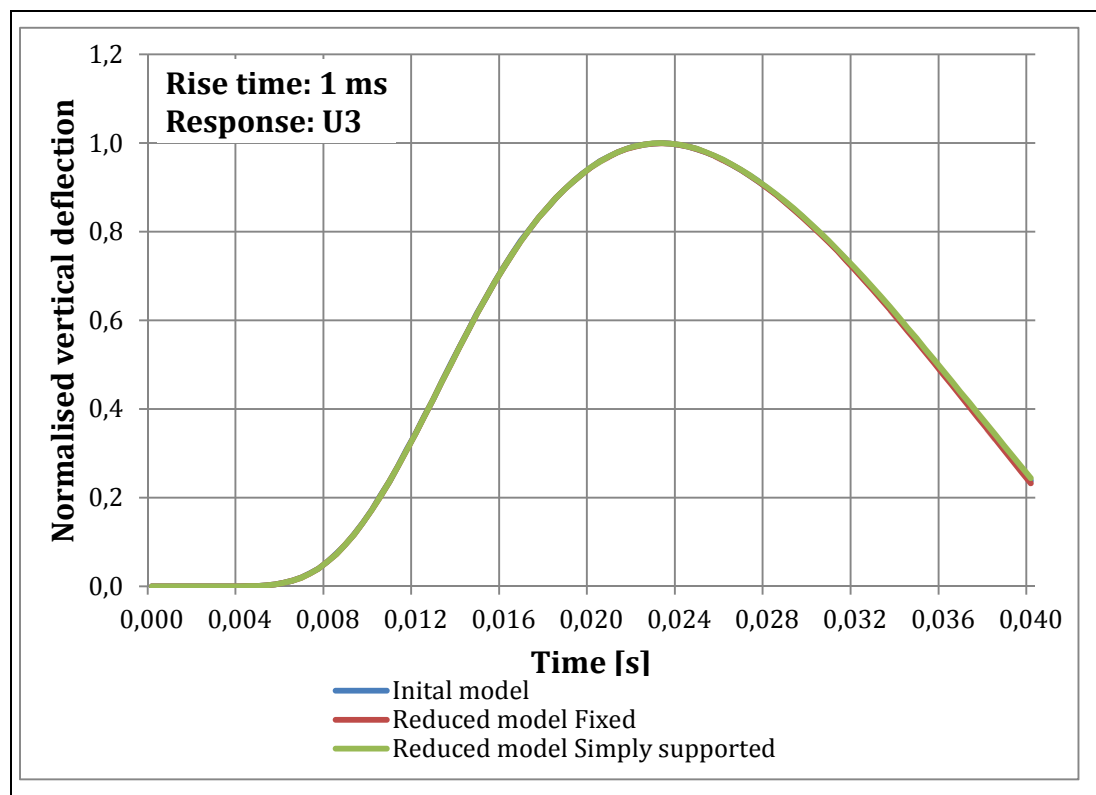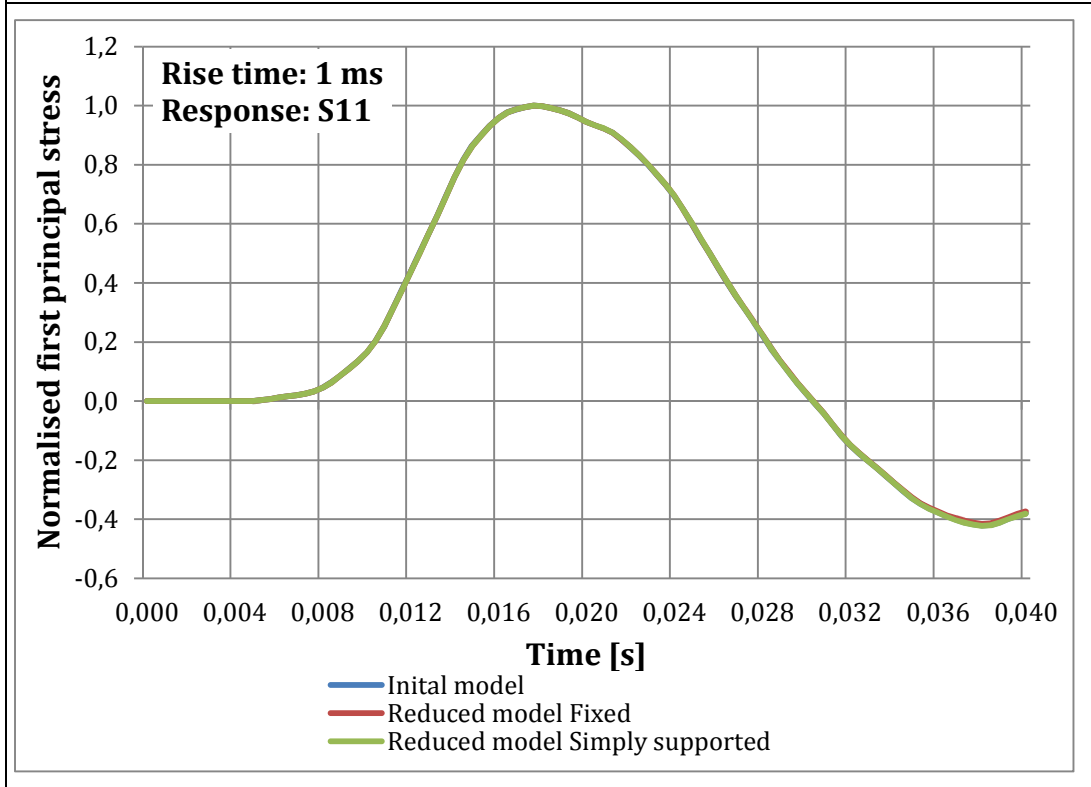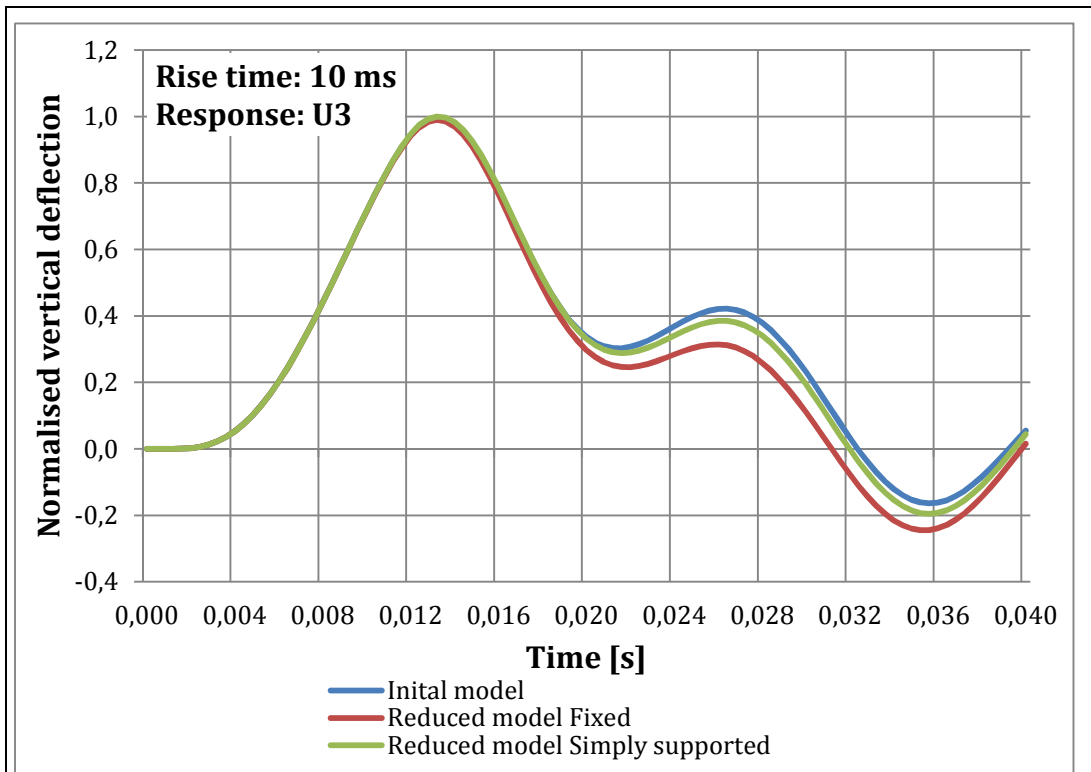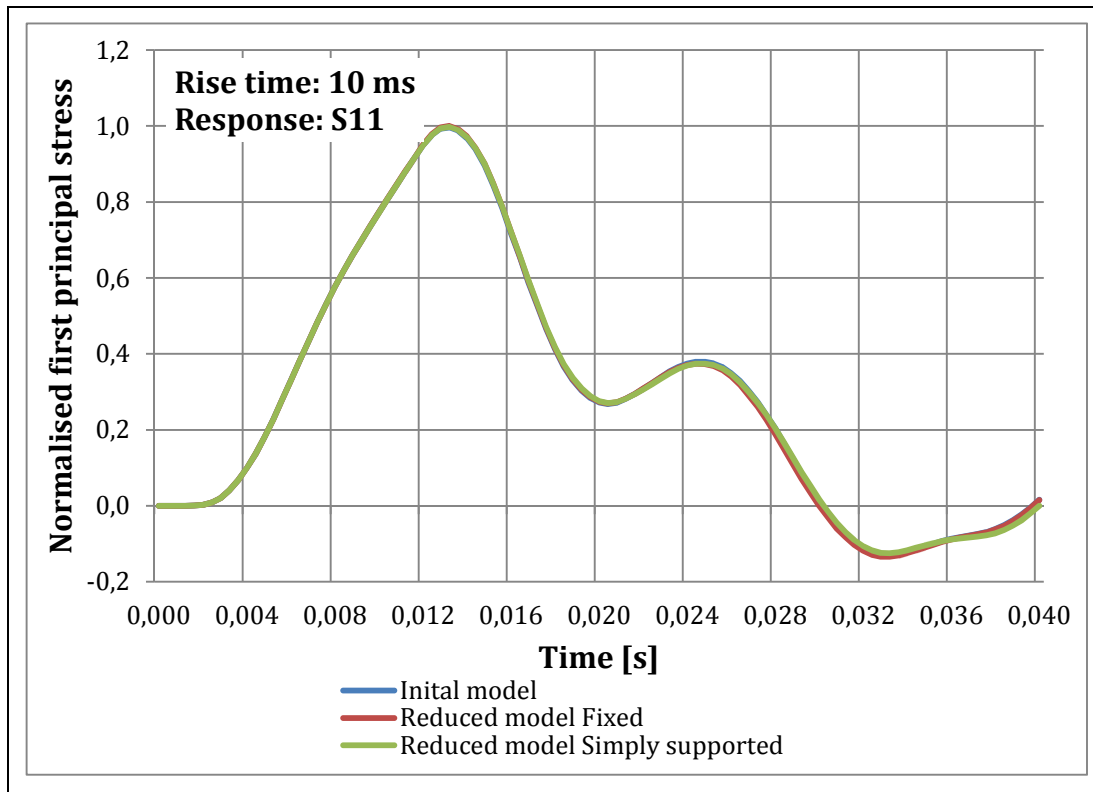
From this we can conclude that the half breadth model will be sufficient to give an accurate description of the structural response. The computation time is approximately linear to the number of elements which is halved by the change to half breadth model. Unless stated otherwise, the reduced model will be used in the main study. The boundary conditions are found to play a minor role for the studied response behaviours.

Appendix C – Mesh dependency study

The solution accuracy that an FE model can provide is highly dependent on its degree of element discretization. Therefore, the mesh density plays a vital role for achieving acceptable solutions. A denser mesh contains more and closer allocated calculation points than a coarse one, generally yielding more accurate results; see Liu (2013). A mesh convergence study is therefore performed in order to assure acceptable solutions for the main analyses. This is done by iteratively increasing the mesh density by a factor of 4 on structural members in the area of interest, which is highlighted in Figure C.1. Each refinement is analysed and compared with regard to structural response. The mesh density outside the refined area is kept unaltered from the automatically generated mesh according to ABAQUS default settings, which for this case has an average element side length of approximately 170 mm. Figure C.2 illustrates two of the different meshes.
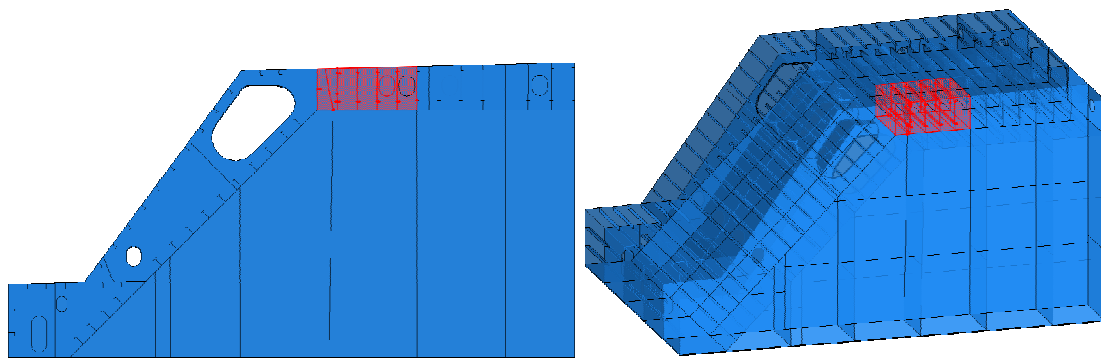

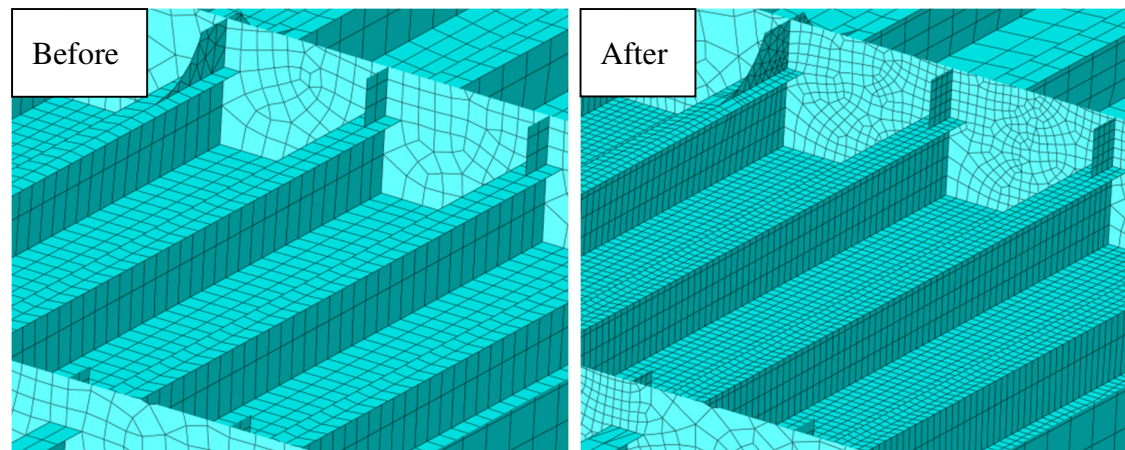Figure C.1   An illustration of the tank region subjected to mesh refinement (highlighted in red).

Figure C.2   A comparison between mesh densities for one refinement step

The convergence study is limited to one load case only, which is represented by an applied impact pressure. The load shape is idealized as a triangular load pulse with characteristics matching the loads intended for the main sensitivity analysis, see Chapter 3.4. The considered load rise time is 1ms. The pressure field is applied on the full corner plate field. The loaded area thus spans from the transverse bulkhead to the first web frame in the longitudinal direction and from the chamfer to the first girder in the transverse direction as presented in Figure C.3. This is significantly larger than the

exposed area for a typical sloshing event. For the scope of this project it is, however, assumed that the load area used for the convergence study is adequate for verifying the mesh in the area of interest. The load amplitude is set to 1 MPa.
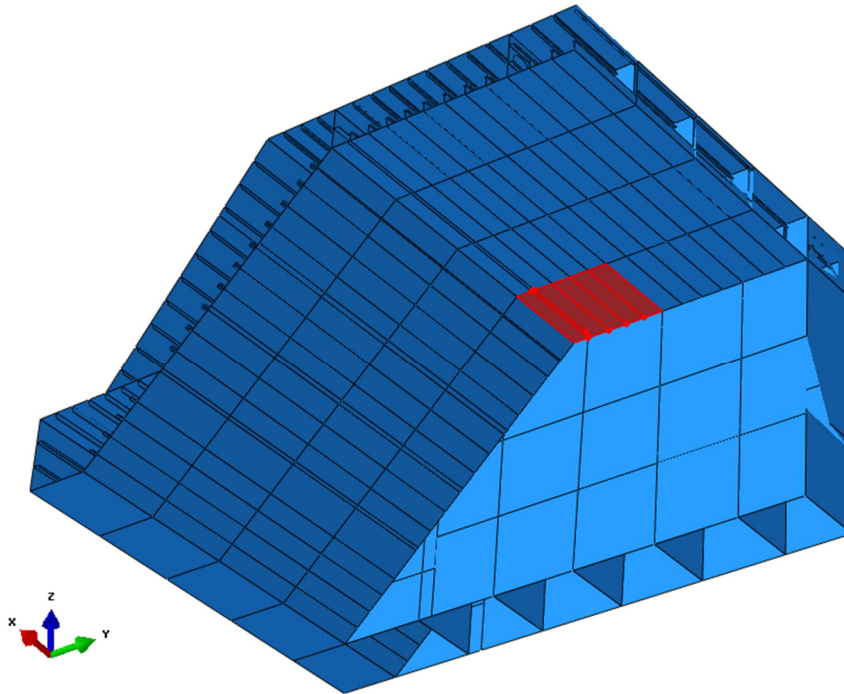

Figure C.3   Loaded area for the mesh dependency study indicated in red.

The dynamic response behaviour of two geometric locations in the stiffened plate field corresponding to the inner deck structure forms the criteria for the desired convergence in dynamic behaviour. In order to study the dynamic response behaviour, time series of the studied responses are considered for the comparison. The locations under consideration represent the nodal coordinates with the greatest response values for the model with the initial mesh density at two different structural members. The studied responses are the first principal stress component in one of the stiffeners (S11) and the vertical deflection in one of the plate fields (U3). An overview of the approximate response locations are presented in Figure C.4. Due to the localized nature of sloshing impacts, the inner deck plate and its stiffeners are assumed to be the structural members most affected and thus more sensitive towards these loads. This is a reasonable assumption since the surrounding members, such as girders, web frame and transverse bulkhead, are a lot stiffer than the inner deck structure. The desired convergence in response is considered to be achieved when both studied response behaviours show insignificant deviations between two mesh refinement steps.
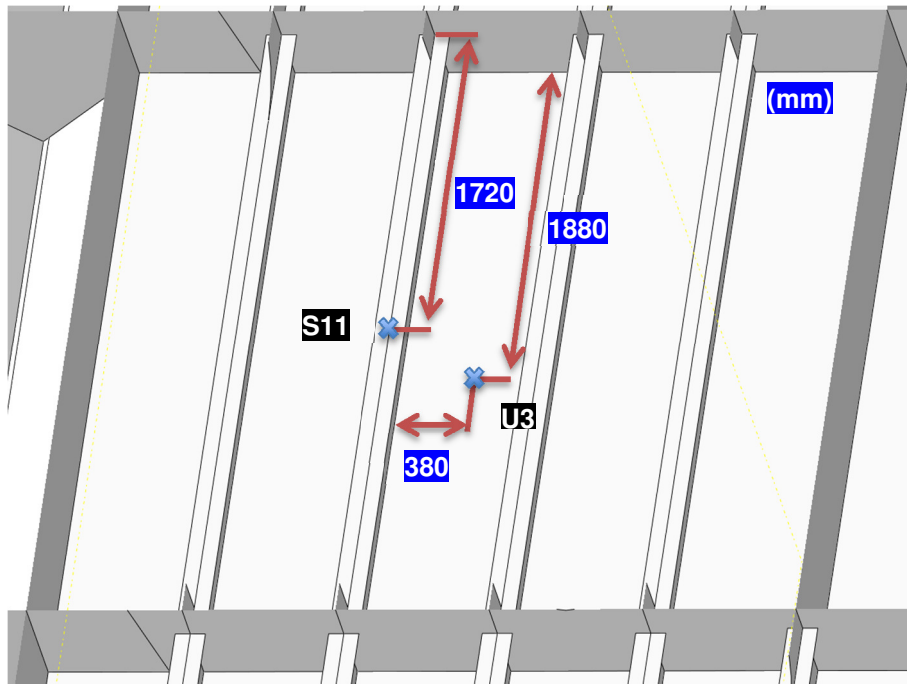
Figure C.4   An illustration of the locations for response extractions in the mesh convergence study.

The time series of the studied responses are plotted for all mesh cases in Figure C.5 and Figure C.6, respectively. Both of the presented time series correspond to the load case with 1ms rise time. Mesh 1 represents the original mesh, Mesh 2 a factor 4 in mesh density increase, Mesh 3 a factor 16, etc. The figures show that the response curves coincide very well for the three finest meshes. The greatest relative difference in both stress and deflection amplitude between these meshes is 0.6 % and 0.7 %, respectively. Hence the model with a local mesh density 16 times higher than the ABAQUS standard mesh is considered to yield solutions with an acceptable accuracy. The average element side length for this mesh density is approximately 40-50 mm depending on the meshed geometry.
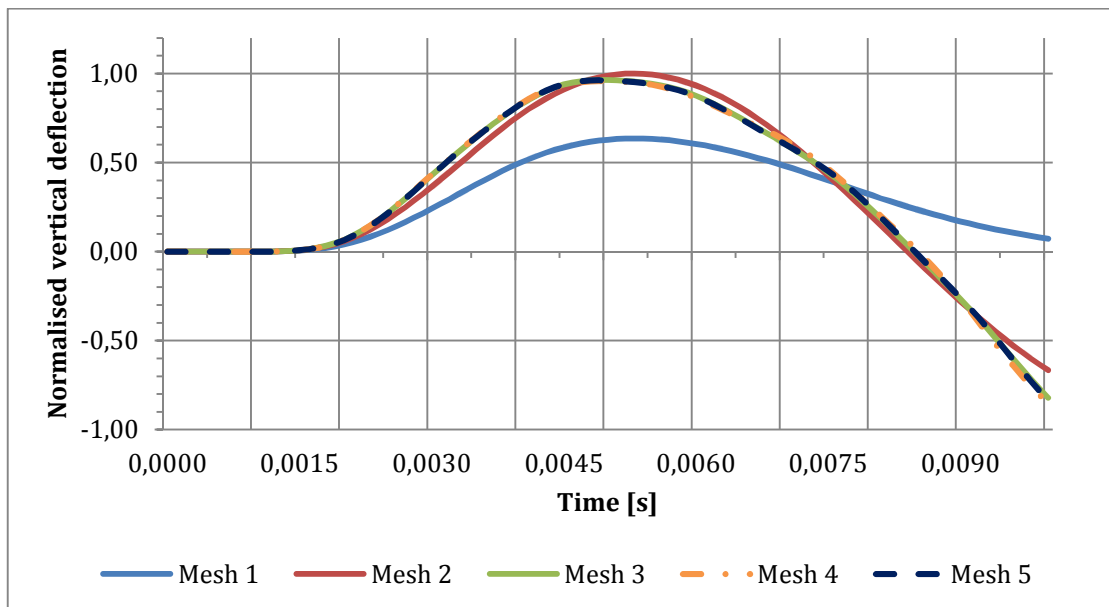

Figure C.5   A comparison of the time series for the vertical deflection at studied plate location for the different meshes. Rise time 1 ms.
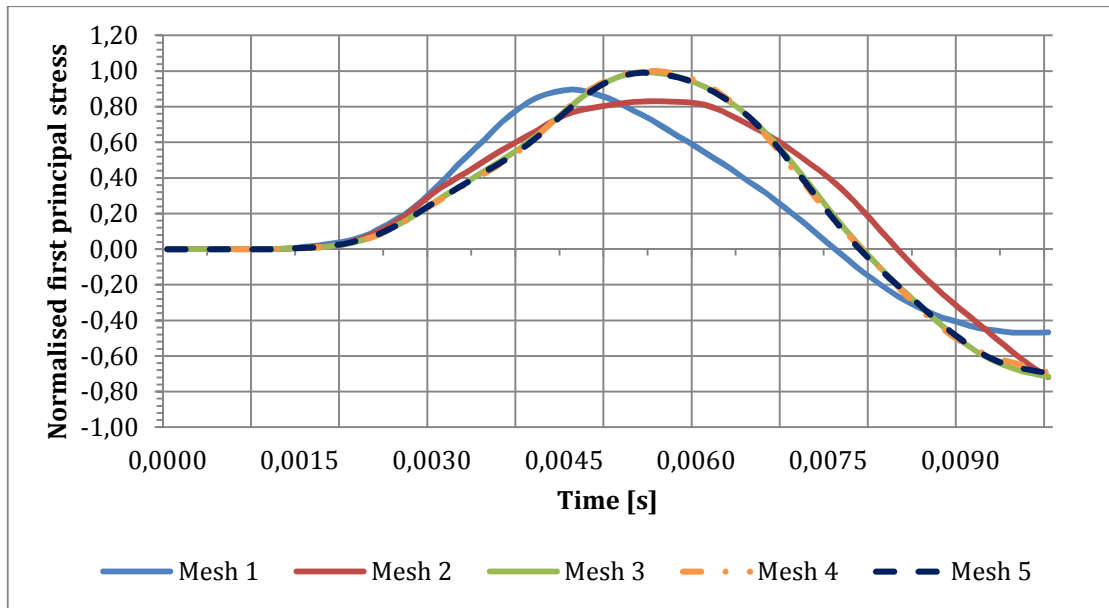
Figure C.6   A comparison of the time series for the first principal stress at studied stiffener location for the mesh refinement cases. Rise time 1 ms.

In order to assure that the convergence is valid also for longer rise times, the three finest mesh cases are analysed with a rise time of 10 ms. These analyses show that a slightly greater difference in response is evident for longer pulse times. A maximum deviation of 2.6 % in peak deflection for the three finest mesh cases is observed. These deviations are considered to be within acceptable limits

The results from this mesh convergence study have shown that deviations in the studied peak stresses and deflections become negligible for finer mesh densities than that corresponding to Mesh 3. The differences also do not show any clear increase or decrease for the peak values for finer meshes. A model with a local mesh density corresponding to Mesh 3 or finer is therefore considered mesh-independent for stresses in the stiffeners and deflections in the inner deck plates in the area of interest. In order to limit the computational effort mesh, Number 3 is thus chosen for the analyses discussed in the thesis.

Appendix D – CCS material data

Material properties for the MARK III cargo containment system in accordance with DNV classification note No. 30.9. For material orientation, refer to the classification note.

Integrated orthotropic material stiffness properties for plywood plates		
Parameter	**20°C**	**-163°C**
$E_{m,1}$ [MPa]	9450	13 200
$E_{m,2}$ [MPa]	8000	11 200
$E_{m,3}$ [MPa]	820	1800
$G_{m,12}$ [MPa]	790	2900
$G_{m,13}$ [MPa]	325	700
$G_{m,23}$ [MPa]	260	550
v_{12}	0,1	0,1
v_{13}	0,1	0,1
v_{23}	0,1	0,1
$E_{b,1}$ 9mm [MPa]	10 950	15 350
$E_{b,2}$ 9mm [MPa]	6550	9150
$E_{b,1}$ 12mm [MPa]	10 450	14 650
$E_{b,2}$ 12mm [MPa]	7000	9800
Density [kg/m^3]	680	680

Material stiffness properties for reinforced polyurethane foam		
Parameter	**20°C**	**-163°C**
E1 [MPa]	135	170
E2 [MPa]	180	215
E3 [MPa]	65	95
G12 [MPa]	7	11
G13 [MPa]	7	11
G23 [MPa]	7	11
v12	0,4	0,4
v13	0,2	0,2
v23	0,2	0,2
Density [kg/m^3]	125	125
Material stiffness properties for mastic		
Parameter	**20°C**	**-163°C**
E [MPa]	2900	Not applicable
v	0,3	Not applicable
Density [kg/m^3]	1600	Not applicable